A Thesis for the Doctor of Philosophy

Molecular mechanisms underlying anti-leukemic activities of stemphol and 6-acetylmonodethiogliotoxin

항 백혈병 효능을 가진 Stemphol 과 6-acetylmonodethiogliotoxin 의 분자 기전

February, 2018

Seungwon Ji

College of Pharmacy

Seoul National University

Molecular mechanisms underlying anti-leukemic activities of stemphol and 6-acetylmonodethiogliotoxin

by

Seungwon Ji

A thesis submitted in partial fulfillment of the requirements

for the degree of

DOCTOR OF PHILOSOPHY

(Pharmacy: Pharmaceutical bioscience major)

Under the supervision of

Professor Marc Francois Diederich

College of Pharmacy

Seoul National University

February, 2018

Table of Contents

List of Tables

CHAPTER 1. Literature review

CHAPTER 2. Epipolythiodiketopiperazines from the marine derived fungus Dichotomomyces cejpii with NF-κB inhibitory potential

CHAPTER 3. The dialkyl resorcinol stemphol disrupts calcium homeostasis to trigger programmed immunogenic necrosis in leukemia

List of Figures

CHAPTER 1. Literature review

CHAPTER 2. Epipolythiodiketopiperazines from the marine derived fungus Dichotomomyces cejpii with NF-κB inhibitory potential

CHAPTER 3. The dialkyl resorcinol stemphol disrupts calcium homeostasis to trigger programmed immunogenic necrosis in leukemia

List of Abbreviations

TNF-α: Tumor Necrosis Factor-α

NF-κB: Nuclear factor kappa-light-chain-enhancer of activated B cells

NEMO: NF-kappa-B essential modulator

Ικκ: I Kappa B Kinase

IκB-α: nuclear factor of kappa light polypeptide gene enhancer in B-cells inhibitor, alpha

NIK: NF-kappa B inducing kinase

NBD: NEMO binding domain

PMCA: Plasma membrane Ca^{2+} ATPase

PBMCs: peripheral blood mononuclear cells

ER: Endoplasmic Reticulum

SERCA: Sarco/endoplasmic reticulum (ER) Ca^{2+}-ATPase

HMGB1: High mobility group box

RIPK1: Receptor interacting serine/threonine kinase 1

MLKL: Mixed lineage kinase domain like pseudokinase

MCU: Mitochondrial Ca2+ uniporter

CsA: Cyclosporine A

Nec-1: Necrostatin-1

NSA: Necrosulfonamide

2-APB: 2-aminoethoxydiphenyl borate

IP_3R: Inositol 1,4,5-trisphosphate receptor

RyR: Ryanodine receptor

CHAPTER 1

LITERATURE REVIEW

1.1. Cancer

1.1.1. Definition

Cancer is an extremely complex and hard-to-cure disease even though many scientists have expended tremendous efforts and research funding for a long time. Cancer is distinguished by several characteristics, and these traits were well classified as hallmarks of cancer by Drs. Hanahan and Weinberg. Recently, they added 4 new hallmarks to the previous 6 and these total 10 hallmarks are useful for understanding of cancer [1]. Among these newly added hallmarks, tumor-promoting inflammation and genome instability/mutation are already widely recognized as important targets for cancer treatment, whereas deregulation of cellular energetics and avoidance of immune destruction are attracting many scientists' interest (Fig 1.1).

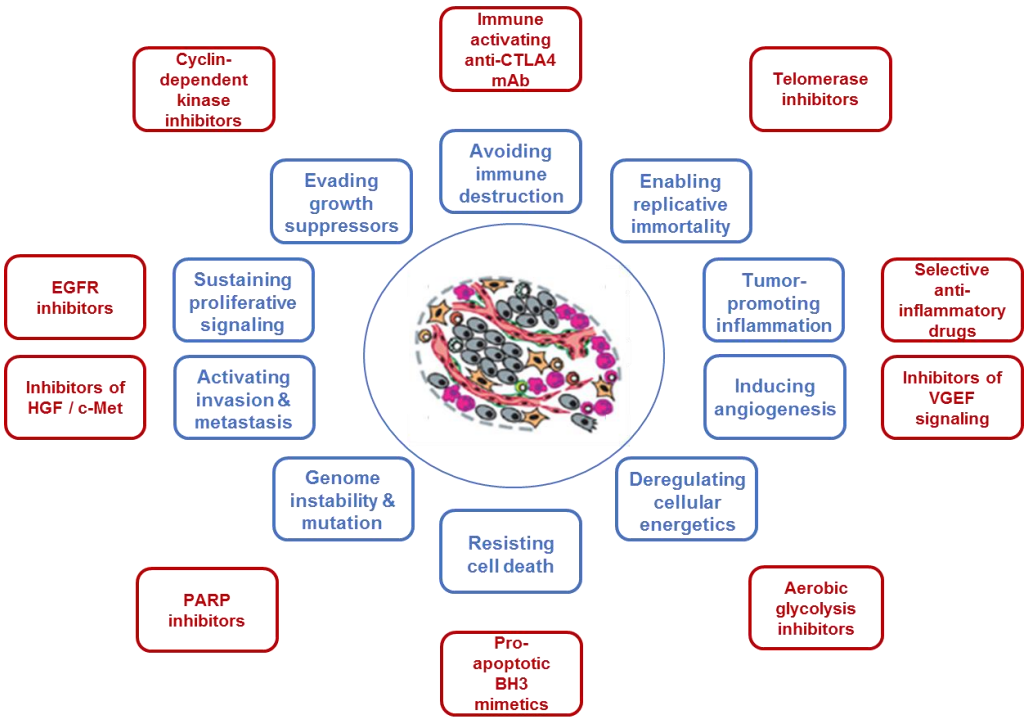

Figure 1.1. Hallmarks of cancer and therapeutic targeting of these hallmarks. Four new hallmarks were added to the previous list of hallmarks of cancer and these hallmarks provide important targets for cancer treatment. Adapted from ref. [1].

Cancer is a complicated disease, and there are ~100 different types of cancer. Most cancers are named after the origin: an organ or a type of cells. According to the National Cancer Institute, cancer can be subdivided into 5 broad categories (Dictionary of Cancer Terms, National Cancer Institute, USA):

1) Carcinoma: Cancer that develops in the skin or in tissues that cover internal organs. Carcinoma has a number of subtypes including

adenocarcinoma, basal cell carcinoma, squamous cell carcinoma, and transitional cell carcinoma.

2) Sarcoma: Cancer that originates in bone, cartilage, fat, muscle, blood vessels, or other connective or supportive tissue.

3) Leukemia: Cancer that originates in blood-forming tissue like bone marrow and generates large numbers of abnormal blood cells.

4) Lymphoma and myeloma: Cancer that occurs in the cells of the immune system.

5) Central nervous system cancer: Cancer that develops in the tissues of the brain and spinal cord.

1.1.2. Status of cancer occurrence

According to the report of World Cancer Research Fund International, 14.1 million cancer cases were estimated worldwide in 2012; 7.4 million cases occurred in men and 6.7 million cases in women. Based on these statistics, it is estimated that the number will increase to 24 million by 2035. Lung cancer is the most common type of cancer, contributing 13% of the total number of cases; breast and colorectal cancer were the second and third most common cancers worldwide in 2012 (Table 1.1).

Table 1.1. Estimated cancer incidence worldwide in 2012: Both sexes. Lung cancer is the most common cancer, whereas breast and colorectal cancers rank second and third, respectively, with respect to incidence.

Rank	Cancer	New cases diagnosed in 2012 (1,000s)	Percentage of all cancer cases (excluding nonmelanoma skin cancer)
1	Lung	1,825	13.0
2	Breast	1,677	11.9
3	Colorectal	1,361	9.7
4	Prostate	1,112	7.9
5	Stomach	952	6.8
6	Liver	782	5.6
7	Cervix uteri	528	3.7
8	Esophagus	456	3.2
9	Bladder	430	3.1
10	Non-Hodgkin lymphoma	386	2.7
11	Leukemia	352	2.5
12	Pancreas	338	2.4
13	Kidney	338	2.4

14	Corpus uteri (endometrium)	320	2.3
15	Lip, oral cavity	300	2.1
16	Thyroid	298	2.1
17	Brain, nervous system	256	1.8
18	Ovary	239	1.7
19	Melanoma of skin	232	1.6
20	Gallbladder	178	1.3
21	Larynx	157	1.1
22	Other pharynx	142	1.0
23	Multiple myeloma	114	0.8
24	Nasopharynx	87	0.6
25	Hodgkin lymphoma	66	0.5
26	Testis	55	0.4
27	Kaposi sarcoma	44	0.3

1.1.3. Developmental stages

Carcinogenesis is a multistep process. One of the most predominant multistep modes for carcinogenesis is that a large number of independent genetic or epigenetic alterations help cancer to develop and broadly can be subdivided into three stages: initiation, promotion, and progression [2].

Initiation involves the induction of irreversibly mutated or altered genes and continuous accumulation of subsequent mutational events. Mutational activation of proto-oncogenes and inhibition of tumor suppressor genes support this conclusion. Promotion is the stage that expands the clonally mutated cells into a visible tumor. In this process, epigenetic regulation processes selectively influence the proliferation of the initiated transformed cells. The final products of tumor promotion are normally benign lesions or foci of preneoplastic cells. These cells must undergo one or more subset of mutations, which lead to a malignant neoplasm. This process is called progression and is clearly distinct from promotion (Fig 1.2).

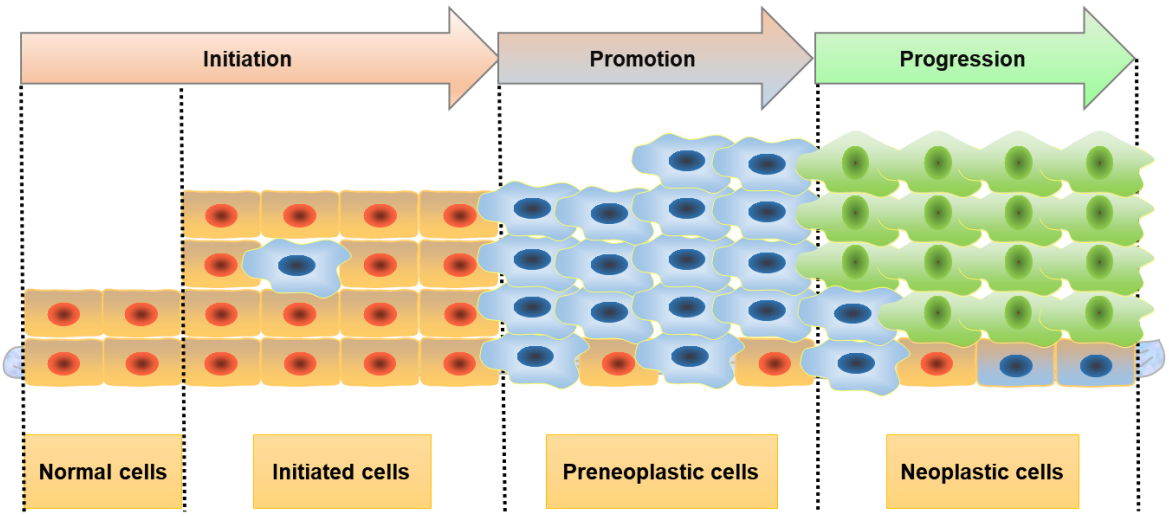

Figure 1.2. The multistep process of carcinogenesis. Carcinogenesis consists of multiple steps (events) and usually can be divided into three stages: initiation, promotion and progression. Adapted from ref. [3].

1.1.4. Treatment

Cancer caused 8.2 million deaths in 2008, and it is estimated that cancer will cause 13.1 million deaths in 2030 (Ferlay J., GLOBOCAN 2012 v1.0 (2013)). Accordingly, the anticancer drug market is rapidly evolving to keep up with the increasing numbers of cancer patients. Of note, 18% of all global sales of the top 100 drugs, which totaled $51 billion, involved the sale of 20 cancer drugs in 2009 (22nd Annual Cancer Progress Conference 2011, KANTAR HEALTH).

Natural products serve as a novel source for the development of anticancer drugs because of their unique structural diversity. The current sources of natural products are more diversified than they have been in the past and include plants, marine organisms, and microorganisms. Recently, natural compounds from marine organisms were actively studied and have already improved cancer treatment [3]. According to Drs. Newman and Cragg, approximately 80% of cancer drugs that were approved from 1940 to 2010 have a natural origin, and this observation indicates that natural-source compounds have a good anticancer potential [4] (Fig 1.3).

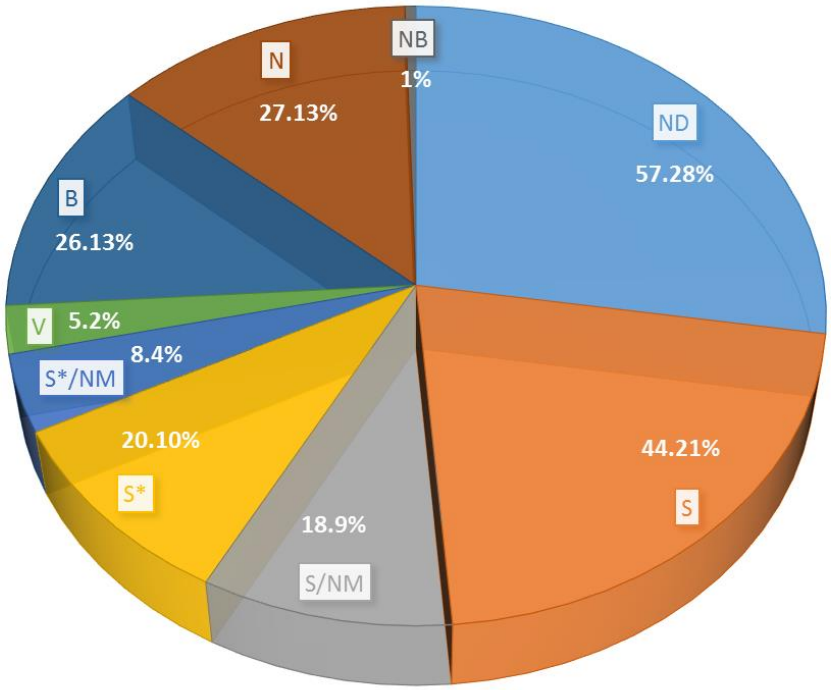

Figure 1.3. All anticancer drugs from 1940s to 2010 by source. Natural-source products are widely used for the development of anticancer drugs, and this situation indicates that natural products have potential as effective anticancer drugs. **Abbreviations:** B, Biological: usually a large (>45 residues) peptide or protein either isolated from an organism/cell line or produced by biotechnological means in a surrogate host; N, natural product; NB, natural product "Botanical" (in general, these were approved recently); ND, derived from a natural product and is usually a semisynthetic modification; S, a totally synthetic drug, often found by random screening/modification of an existing agent; S*, derived by total synthesis, but the pharmacophore is/was from a natural product; V, vaccine; NM, Natural Product Mimic. Adapted from ref. [3].

1.2. Inflammation

1.2.1. Inflammation and cancer

In response to a physiological or pathological situation such as infection or wound healing, the multifactorial network of chemokines and cytokines activates and enables migration of leukocytes from the venous system to infected or damaged sites [5]. Even though this inflammatory response is required for protection of the human body from an invader or damage, it paradoxically promotes neoplasia. Inflammation can contribute to diverse hallmarks of a tumor microenvironment by inducing growth factors, antiapoptotic factors, and extracellular-matrix–modifying enzymes that can enable sustainable proliferation, avoidance of cell death, and strong angiogenesis, invasion, and metastasis. Thus, tumor-promoting inflammation is now widely accepted as an additional hallmark of cancer [1].

1.2.2. NF-κB signaling

Interleukin-1 (IL-1), TNF receptor families, and Toll-like microbial pattern recognition receptors (TLRs) strongly contribute to the progression of knowledge about inflammation signaling. Even though all these receptors have different structures, they activate signal transduction similarly, including IκB

kinase (IKK) and NF-κB [6]. NF-κB is a key regulator of signaling for inflammation and has been investigated intensively in the canonical and alternative signaling pathways, or both. The "canonical" and "alternative" NF-κB pathways are triggered by different stimuli, leading to distinct mediators and products (Fig 1.4). The canonical pathway is triggered by an infection-associated microbial product and proinflammatory cytokines such as IL-1 or TNFα, usually inducing activating p65 (RelA) or cRel complexes [7]. TNFα is not involved in triggering the alternative pathway; instead, lymphotoxin b (TNFSF3), CD40 ligand (CD40L and TNFSF5), cell activating factor (BAFF and TNFSF13B), and receptor activator of the NF-κB ligand (RANKL and TNFSF11) strongly contribute to activation of the alternative signaling pathway, leading to activation of RelB–p52 complexes [8]. Moreover, IKK subunits are differentially recruited by two NF-κB pathways. In the canonical pathway, the IKK complex (consists of α and β catalytic subunits and two molecules of the regulatory scaffold NEMO) phosphorylates IκB, leading to the proteasomal degradation of IκB. Next, the released p65 (RelA)–p50 complex relocates into the nucleus. In the alternative pathway, NIK (NF-κB–inducing kinase) phosphorylates the IKKα complex, which in turn phosphorylates p100 to form the p52–RelB complex. In addition to the two representative NF-κB pathways, another distinct pathway exists. For example, in pathway 3, the p105–p50 complex is converted to p50 homodimers by proteolytic processing of p105. The p50 homodimeric complex

can enter the nucleus and acquire transcriptional activity by forming a complex with IkB-like coactivator Bcl-3 (or IkBζ) [9].

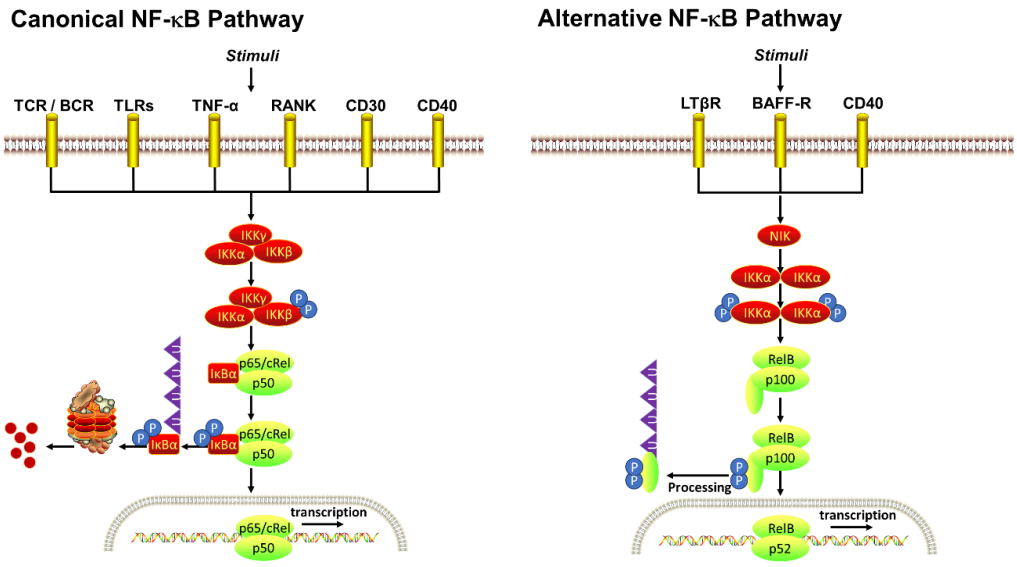

Figure 1.4. Activation of the canonical and alternative NF-κB pathways. Different modes of NF-κB pathway are activated depending on kinds of stimuli. Once activated, P65/p50 complex triggers gene transcription in canonical mode and RelB/p52 complex stimulates gene transcription in alternative mode. Adapted from ref. [10].

1.2.3. Pharmacological NF-κB inhibitors

So far, no drugs are approved as specific NF-κB inhibitors. Nevertheless, many groups try to develop an NF-κB inhibitor because NF-κB has an important role in chronic inflammation and cancer. Among the NF-κB inhibitors, TNFα

antagonists are clinically used for the treatment of rheumatoid arthritis (RA), and some of them are being tested in clinical trials in patients with advanced cancer [11]. Of note, these kinds of TNFα antagonists definitely have off-target effects on all TNFα-related downstream factors, such as c-Jun N-terminal kinase (JNK) [12], and for this reason, it is necessary to develop NF-κB–specific inhibitors. As mentioned above, the canonical NF-κB signaling pathway mostly can be divided into four steps; receptor activation, IKK activation, IκBα degradation, and transcription activation by NF-κB. Accordingly, compounds exerting an inhibitory effect on each step can be potential NF-κB inhibitors. Many groups try to categorize the NF-κB inhibitors depending on the point of action [13, 14]. Among those inhibitors, here I describe some compounds with high target specificity (Table 1.2). IκB kinase inhibitors mostly target the β-subunit of the kinase complex. SPC 839 (from Celgene) showed an inhibitory effect on IKKβ with an IC_{50} of 62 nM and is effective at reducing paw edema in an arthritis model [15]. BMS345541, another IKKβ inhibitor, also showed efficacy in a mouse model of collagen-induced arthritis, without major toxicity [16]. Degradation of IκBα in a proteasome is a critical step for the NF-κB signaling cascade and allows researchers to consider a proteasomal inhibitor as an NF-κB inhibitor. Bortezomib is a representative proteasome inhibitor that is already approved for the treatment of multiple myeloma (MM). The mode of action of bortezomib on MM is related to the inhibitory effect on proteasome activation

in NF-κB signaling [17]. Another emerging potent proteasome inhibitor is PR171 (carfilzomib). PR171 is used to treat patients with bortezomib resistance [3]. SN50 is also an interesting NF-κB inhibitor and acts on a late stage of the signaling cascade. It inhibits transcriptional activation by NF-κB via interfering with NF-κB translocation. In particular, SN50 directly inhibits phosphorylation of p65 at Ser276, Ser529, and Ser536, sites critical for translocation of NF-κB.

Table 1.2. Pharmacological NF-κB inhibitors and the mode of action.

NF-κB signaling event	Target molecule	Name	Structure	Target molecule
IKK activation	Inhibitor of the catalytical subunits	SPC 839	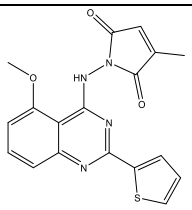	IKKβ
		BMS -345541	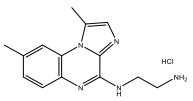	IKKβ
IκBα degradation	Proteasome inhibitor	bortezomib	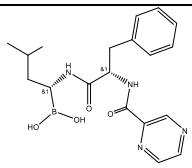	Proteasome
		PR171	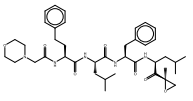	Proteasome

Transcriptional activation by NF-κB	Inhibitor of NF-κB translocation	SN50	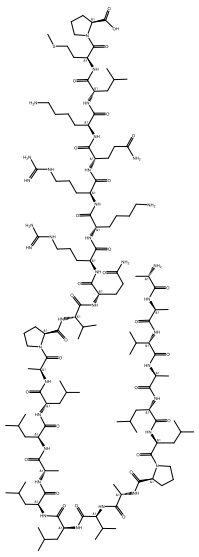	p65 (Ser276, Ser529, and Ser536)

Abbreviations: NBD, NEMO-binding domain

1.3. Calcium regulation

1.3.1. Physiological role

Because calcium ions (Ca^{2+}) are the most common mineral ions in the human body (Robertson W.G., Chemistry and Biochemistry of Calcium (1998)), they play a pivotal role in diverse physiological and biochemical reactions. Ca^{2+} acts as a secondary messenger in diverse cell signal transduction cascades and is involved in muscle contraction, nerve conduction, hormone release, and blood coagulation [18].

For this reason, Ca^{2+} should be tightly regulated and maintained at constant levels. The Ca^{2+} concentration in blood plasma is 2.5 mM, with normal variation

less than 20%. Ca^{2+} in the bloodstream exists as dissolved ions or binds to blood proteins such as serum albumin. Besides blood plasma, Ca^{2+} concentration is closely controlled at approximately 1.2 mM in the extracellular space and typically is between 50 and 100 nM in the intracellular space [19].

The concentration of Ca^{2+} in blood is controlled by three hormones: parathyroid hormone, calcitonin, and the active form of vitamin D (1,25-OH vitamin D3, calcitriol) [20]. The major function of parathyroid hormone is to increase the Ca^{2+} level in blood. Thus, a deficiency in parathyroid hormone causes a decrease of Ca^{2+} by up to 50%, while an excess of this hormone results in hypercalcemia. To maintain the Ca^{2+} concentration in blood plasma, parathyroid hormone acts on the bones, the kidney, and the intestine. In the bone, parathyroid hormone promotes Ca^{2+} outflow from the bone, whereas in the absence of the hormone, it directs a reverse process, resulting in a lower blood Ca^{2+} level. In the kidneys, parathyroid hormone decreases the excretion of Ca^{2+} directly (by stimulating reabsorption of Ca^{2+} from the glomerular filtrate) and indirectly (by promoting the production of calcitriol). Subsequently, this calcitriol accelerates the intestinal absorption of Ca^{2+}. Calcitonin decreases plasma Ca^{2+} by affecting motility and spreading of osteoclasts. It also acts in a way opposite to that of parathyroid hormone in the kidneys and intestines by inhibiting Ca^{2+} reabsorption into kidney tubules and by lowering the intestinal Ca^{2+} absorption. The active form of vitamin D, calcitriol, increases intestinal Ca^{2+} absorption and

participates in proliferation of osteoblasts, thus increasing plasma Ca^{2+} concentration.

1.3.2. Calcium and cancer

Ca^{2+} is highly regulated within cellular compartments via diverse Ca^{2+} pumps and channels. Thus, dysregulation of Ca^{2+} transporters definitely alters cellular characteristics. These days, collected data strongly support the hypothesis that changes in the activity or expression of Ca^{2+} transporters may play a promoting or causal role in cancer [21]. Increased expression of Ca^{2+} channels on the plasma membrane tends to stimulate Ca^{2+} influx and Ca^{2+}-dependent proliferative signaling pathways. For example, an overexpressed α1H subunit of the T-type Ca^{2+} channel on the plasma membrane accelerates the proliferation of human astrocytoma and mouse neuroblastoma cell lines. Moreover, alteration of Ca^{2+} channels or pumps changes the sensitivity to cell death. Overexpression of PMCA (plasma membrane Ca^{2+} ATPase) increases resistance to apoptosis and necrosis induced by staurosporine in CHO cells [22], and BCL2-triggered-alteration of IP_3R activity raises the resistance to apoptosis in many cancer cell lines [23, 24]. In addition to *in vitro* studies, a recent *in vivo* experiment showed that heterozygous SERCA2 knockout mice are easily prone to develop squamous cell carcinomas [25]. This finding strongly supports the notion that alteration of Ca^{2+} regulation is a cause of tumorigenesis. Moreover, the Ricardo Dolmetsch

group identified Ca^{2+} channels and possibly pumps that can directly regulate transcription [26]. Their study showed that CaV1.2, the L-type voltage-gated Ca^{2+} channel was cleaved and translocated to the nucleus. This cleaved form of Ca^{2+} channels is termed *calcium channel–associated transcriptional regulator* (CCAT) and regulates endogenous transcription of diverse genes such as Myc, Bcl-associated death promoter (Bad), and artemin (Artn). This study for the first time revealed that a Ca^{2+} channel can modulate gene expression because it acts as a transcription factor, not via Ca^{2+} transport.

1.3.3. Calcium and cell death

One of the main characteristics of Ca^{2+} is ambivalence. Even though Ca^{2+} is essential for the maintenance and regulation of life-associated phenomena, dysregulation of its level triggers a cellular catastrophe, eventually leading to cell death. Especially, endoplasmic reticulum (ER) and mitochondria are critical organelles for Ca^{2+} regulation and both closely interact and regulate diverse cell death modes. The ER is the largest Ca^{2+}-storing organelle in the cell, and free resting Ca^{2+} within the sarcoplasmic reticulum (SR) or ER is reported to be in the range of 100–500 μM [21]. Disturbances of Ca^{2+} in ER result in protein misfolding and ER stress and induce caspase- or calpain-dependent cell death. In recent studies, dysregulation of Ca^{2+} in the ER was found to affect mitochondrial Ca^{2+} loading and to induce a noncanonical type of cell death.

mPTP (mitochondrial permeability transition pore)-dependent necrosis is a representative mitochondrial-Ca^{2+}-mediated cell death mode. ER stress triggers a transfer of ER-stored Ca^{2+} into mitochondria directly or indirectly, and this continual mitochondrial Ca^{2+} overloading causes opening of mPTP. This phenomenon enables penetration of solutes of 1,500 Da or smaller into mitochondria and physically disrupts mitochondrial structure, eventually leading to programmed necrosis [27]. Besides, paraptosis is another emerging cell death mode where ER and mitochondrial Ca^{2+} regulation are involved. Imbalanced homeostasis of Ca^{2+} in the ER and mitochondria is one of the main causative factors of paraptosis, and this Ca^{2+} dysregulation triggers dilation of the ER and mitochondria and hypervacuolation derived from the ER [28]. Considering the strong resistance of cancer to apoptosis-inducing anticancer drugs, Ca^{2+}-mediated noncanonical cell death is quite an attractive strategy for cancer treatment.

1.3.4. Pharmacological calcium modulators

Because altered expression of Ca^{2+} channels and pumps is important for initiation and maintenance of tumorigenesis, Ca^{2+} transporters are good targets for anticancer drugs. Furthermore, adapted Ca^{2+} channels and pumps in cancer have highly restricted tissue distribution unlike regulators of the cell cycle. For instance, PMCA2 is overexpressed in human breast cancer cell lines [29],

whereas it is normally expressed in the central nervous system. Targeting of factors with a limited tissue distribution enables investigators to prevent general toxicity of a drug and provides a big advantage in the clinical use of compounds. Besides, now it has gone through several trials to ensure more elaborate target specificity to Ca^{2+} channel modulators. One approach is to modify the thapsigargin as a prodrug that is converted into an active form after being cleaved. Two different forms of a prodrug have been developed and named as G-202 (mipsagargin) [30] and G-115 [31]. These are cleaved by prostate-specific membrane antigen membrane antigen (PSMA) and serine protease prostate-specific antigen (PSA), respectively, and this process allows drugs to get activated in advanced solid tumors or prostate cancer specifically.

Both a Ca^{2+} activator and inhibitor can induce cancer cell death, and this feature is also a distinguishing trait of Ca^{2+} channel and pump modulators [21]. Cellular Ca^{2+} overload definitely induces cell demise by physically disrupting organelles or by indirectly activating Ca^{2+}-dependent cell death signaling. On the other hand, cancer maintains higher Ca^{2+} levels than normal cells do because Ca^{2+} is essential for rapid growth and proliferation. A recent study indicates that inhibition of Ca^{2+} transfer from the ER to mitochondria induces cell death, proving Ca^{2+} addiction of cancer [32]. This Ca^{2+} duality in cancer points to a possible wider selection of cancer treatments; thus, Ca^{2+} activators and inhibitors (Table 1.3) have a strong potential as anticancer drugs [21].

Table 1.3. A list of pharmacological Ca^{2+} modulators.

Transporter class	Activators	Inhibitors
Storage Ca^{2+} channels		
IP_3R	Adenophostin A	Heparin, polyvinyl sulfate
RyR	4-chloro-M-cresol, suramin, ryanodine, caffeine	Dantrolene, ruthenium red, ryanodine (high concentrations)
Voltage-gated Ca^{2+} channels		
L-type	(-)-BAY K 8644	Verapamil, diltiazem, nimodipine
P/Q-type	ND	ω-Agatoxin IVA
T-type	ND	Mibefradil, pimozide, penfluridol
Transient receptor potential channels		
TRPM2	H_2O_2, ADP-ribose	N-(p-amylcinnamoyl)anthranilic acid, clotrimazole
TRPM8	Mentho, icilin, geraniol, eucalyptol	BCTC, SB-452533
TRPV1	Capsaicin (hot chili pepper component), anandamide, resiniferatoxin, ethanol	Iodo-resiniferatoxin, capsazepine, BCTC, SB-452533
TRPV3	Camphor, thymol, eugenol	Diphenyltetrahydrofuran
TRPV4	Bisandrographolide A	ND
TRPA1	Allicin (garlic component)	ND
Pumps		
PMCA	ND	Caloxin 2A1
SERCA	ND	Thapsigargin, cyclopiazonic acid

Abbreviations: BCTC, N-(4-tertiarybutylphenyl)-4-(3-chloropyridin-2-yl)tetrahydropyrazine-1(2H)-carboxamide; CaV, voltage-gated Ca^{2+} channel;

H_2O_2, hydrogen peroxide; IP3, inositol 1,4,5-trisphosphate; IP_3R, inositol 1,4,5-trisphosphate receptor; ND, selective pharmacological agents are not available; PMCA, plasmalemmal Ca^{2+}-ATPase; RyR, ryanodine receptor; SERCA, sarcoplasmic/endoplasmic reticulum Ca^{2+}-ATPase; TRPA, transient receptor potential ankyrin; TRPM, transient receptor potential melastatin; TRPV, transient receptor potential vanilloid. Adapted from ref. [21], with permission.

1.4. Non-Edible Source of Compounds with Chemopreventive and Chemotherapeutic Potential

1.4.1. The categorization of natural compounds

We categorized various natural compounds with anti-cancer effects and distinguished edible and non-edible sources. To do this, we first gathered data related to natural compounds from plants containing terrestrial and marine organisms. Next, we divided these natural compounds into two categories, edible or not. The source of each compound was determined from the literature or, when the source was not provided, from well-known databases, such as Super Natural II, NPACT and DrugBank. Edible sources of compounds included fruits, vegetables, teas, or oils, and non-edible sources included various medicinal plants as a whole or their parts, such as the bark, stems and roots. In the past 2 years, 60% of all natural compounds from plants were derived from edible

sources, and the remaining 40% were derived from non-edible sources based upon 165 review papers. Because many of these compounds have been investigated multiple times worldwide, the actual ratio of natural compounds from edible sources to those from non-edible source may, in fact, be much larger. These data demonstrate that many scientists prefer to research with edible plants as a source of natural compounds rather than non-edible plants.

1.4.2. The relationship between approved anti-cancer drugs and the source of the natural compounds

Once anti-cancer compounds have been identified in natural products, an essential final step is to develop the actual drug. Accordingly, we wanted to identify the number of natural compounds with anti-cancer effects that were obtained from edible or non-edible plant sources and that have been approved as an anti-cancer drug. Since David J. Newman and Gordon M. Cragg published an article dealing with natural products and new drugs in 1997, their article has been updated regularly and is currently in the 4th edition [4]. Their paper contains invaluable statistics related to natural products and drugs, making it a valuable paper for many scientists in this field. Additional data were collected from the Food and Drug Administration (FDA) and European Medicines Agency (EMEA). After collecting information from Newman and Cragg's review paper, we searched for the source of each approved drug manually because the authors

simply divided drug sources into B (biological), N (natural product), ND (derived from a natural product), S (synthetic drug) and V (vaccine). We identified the source of each approved anti-cancer drug as an edible or non-edible plant using DrugBank and Drug information portal sites. We finally categorized all approved anti-cancer drugs by dividing them into edible and non-edible sources (Table 1.4). Unlike previous results about the contribution of natural compounds in many articles, approved anti-cancer drugs are derived from 11 non-edible plant sources (65% of all approved anti-cancer drugs from plants) and from only six edible plant sources (35% of all approved anti-cancer drugs from plants). These statistics suggest that natural compounds from non-edible sources have a higher potential of being developed into an anti-cancer drug, indicating that scientists should focus their research on these sources to develop effective cancer therapies.

Table 1.4. The categorization of approved anticancer drugs that are derived from natural compounds based on edible or non-edible sources.

Lead compound	Source	Edible/ Non-edible	Involved stage of cancer	
			Chemo-prevention	Chemo-therapy
Vincristine	*Vinca Rosea.*	Edible		O
Vinblastine	*Vinca rosea.*	Edible		O
Podophyllotoxin	*Podophyllum*	Non-edible		O
Vinblastine	*Vinca Rosea.*	Edible		O

Podophyllotoxin	*Podophyllum peltatum*	Non-edible	O
Ellipticine	*Apocynaceae*	Non-edible	O
Solasodine	*Solanaceae*	Edible	O
Vinblastine	*Catharanthus roseus*	Edible	O
Paclitaxel	*Taxus brevifolia*	Non-edible	O
Taxane	*Taxus brevifolia*	Non-edible	O
Podophyllotoxin	*Podophyllum peltatum*	Non-edible	O
Camptothecin	*Camptotheca acuminata*	Non-edible	O
Camptothecin	*Camptotheca acuminata*	Non-edible	O
Paclitaxel	*Taxus brevifolia*	Non-edible	O
Paclitaxel	*Taxus brevifolia*	Non-edible	O
Paclitaxel	*Taxus baccata*	Non-edible	O
Vinblastine	*Vinca Rosea.*	Edible	O

1.4.3. The effect of natural compounds from non-edible sources on cancer chemoprevention and chemotherapy

The process of tumorigenesis consists of at least three steps: initiation, promotion, and progression [33] suggesting that cancer progresses over a long period of time. Initial efforts of many groups to cure cancer were mainly focused on the terminal stages of cancer. However, this strategy was ineffective because cancer cells have already become wide-spread throughout the body and are very resistant to anti-cancer drugs. Accordingly, the trend in the treatment of cancer is moving from cancer chemotherapy to chemoprevention, which focuses on the initiation or promotion steps of cancer. Cancer chemoprevention may also reverse chemo- and radio-resistance in cancer patients [34]. Therefore, cancer chemoprevention is not only valuable alone but can also be used as an adjuvant for chemotherapy. Table 1 shows that anti-cancer drugs from plant sources have focused on the field of cancer chemotherapy. Thus, natural compounds from non-edible plant sources should be evaluated for their efficacy in chemoprevention (Fig 1.5).

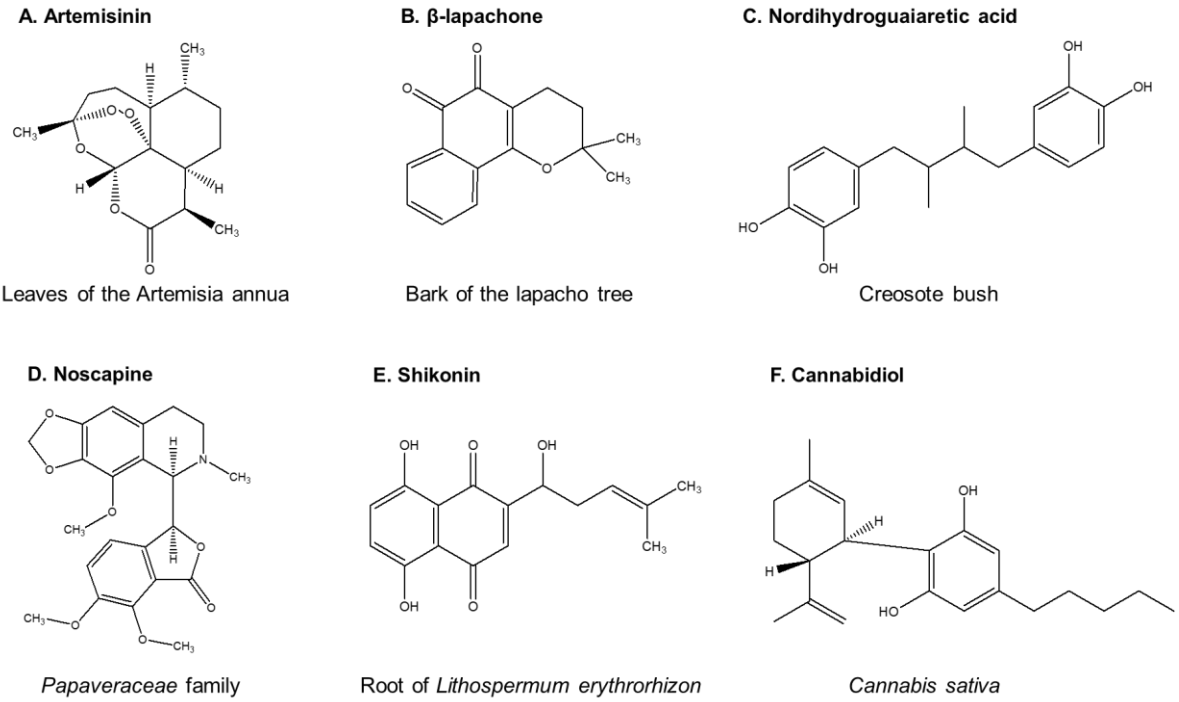

Figure 1.5. Chemical structure of natural compounds with chemopreventive and chemotherapeutic effects from non-edible source. This figure was generated using ChemDraw software.

Artemisinin (Fig 1.5A) is isolated from the leaves of the Artemisia annua, which is a common type of wormwood, and this compound inhibits transferrin receptors in cancer cells. Cancer cells uptake large amounts of ions because of their rapid metabolic rates [35]. Transferrin receptors are expressed at especially high levels in breast cancer and leukemia compared to normal cells. Accordingly, artemisinin may have prominent anticancer effects in the early stages of these types of cancer. An early study showed that artemisinin prevents and delays the

development of breast cancer and leukemia by interrupting ion absorption [36]. In addition, artemisinin has no known side effects at high dose concentrations, so it would be worthwhile to study its effects on the early stages of cancer.

β-lapachone (Fig 1.5B) is found in the bark of the lapacho tree, and it has been shown to inhibit tumor necrosis factor-α (TNF-α)-induced nuclear factor κB (NF-κB) and Activator Protein 1 (AP-1) in U937 leukemic cells [37]. NF-κB is a well-known transcription factor that induces inflammation and inhibits apoptosis. AP-1 is also activated by TNF-α and is involved in growth modulation and apoptosis. Previous data showed that β-lapachone negatively regulates NF-κB by participating in TNF-α-induced NF-κB activation, IκB degradation and p65 translocation. However, β-lapachone does not affect p50-p65 binding to DNA. β-lapachone also attenuated the level of AP1 and its related kinases, c-Jun N-terminal kinase (JNK) and mitogen activated protein kinase (MAPK).

Nordihydroguaiaretic acid (NDGA) (Fig 1.5C) is abundant in the creosote bush and has been shown to epigenetically modify cancer cells to inhibit cancer cell growth. The term “epigenetics” means the modulation of gene expression without gene sequence alteration, and it involves DNA methylation, histone modification and micro RNAs [38]. Because DNA methylation prevents the transcription of target genes, methylation of tumor suppressor genes can lead to cancer. First, previous reports on the effects of NDGA in cancer showed that NDGA reduced global DNA methylation in malignant glioma cells [39].

Subsequently, it was discovered that NDGA lowers the methylation levels of many important tumor suppressor genes including E-cadherin and p16 [39], [40].

Noscapine (Fig 1.5D) is isolated from the Papaveraceae family and has been shown to induce apoptosis by down-regulating survivin expression. Survivin negatively regulates apoptosis or programmed cell death by inhibiting caspase activation [41] In previous studies, noscapine induced apoptosis of neuroblastoma cell lines without affecting p53. Instead, noscapine decreased the expression of survivin sensitizing neuroblastoma cells to apoptosis, suggesting a novel molecular mechanism.

Shikonin (Fig 1.5E) can be purified from root of Lithospermum erythrorhizon, which is native to America. Shikonin affects the “Warburg effect” of cancer, when cancer cells produce energy through increased rates of glycolysis followed by lactic acid fermentation [42]. Pyruvate kinase M2 (PKM2) is one of the most important metabolic enzymes that regulate this pathway. According to a previous study, levels of PKM2 are much higher in skin tumor tissues than in normal tissues [43]. In this research, shikonin inhibited PKM2, which led to cancer cell death and also suppressed the tumor promoter 12-O-tetradecanoylphorbol 13-acetate (TPA), which results in restoring mitochondrial malfunction. This means that shikonin may have a chemopreventive effect by targeting PKM2 involved in the “Warburg effect”.

Cannabidiol (Fig. 1.5F) is found in Cannabis sativa and has a chemopreventive effect in cancer [44]. First, cannabidiol induces fragmentation of caspase-3, which leads to apoptosis of colon cancer cells. Cannabidiol can also down-regulate the expression of Akt, which functions in cell growth, migration and differentiation. Finally, cannabidiol has an anti-inflammatory effect on gut cells by down-regulating inducible nitric oxide synthase (iNOS) but has no anti-inflammatory effect on colon cancer cells.

1.4.4. Conclusion

Using natural compounds as candidates for drugs is advantageous over using synthetic compounds for many reasons. First, the sources of natural compounds are abundant and include plants, marine organisms and microorganisms. Thus, these compounds also have unique structures. Developing drugs from natural compounds takes less time and money, and the drugs also have fewer side effects than synthetic compounds. Because of these features, many laboratories worldwide primarily study natural compounds. Nevertheless, research in this field, which focuses on the specific sources, is limited. Specifically, researchers are focusing on dietary or edible sources such as resveratrol, curcumin and genistein rather than nonedible sources. This field should be widened to focus on diverse sources to find valuable natural compounds. As previously mentioned, natural compounds from non-edible plant sources have been turned into effective

anticancer drugs. Additionally, there are numerous references to medicinal plants, which predict the effects of the natural compounds isolated from those medicinal plants.

Today, researchers in oncology is giving efforts in chemoprevention as well as chemotherapy. Researchers in this field are further encouraged by the success of 10 FDA-approved anti-cancer drugs with chemopreventive effects [45]. Natural compounds from non-edible source have sufficient potential to be developed into chemopreventive drugs. Natural compounds with cancer chemopreventive effects that were obtained from non-edible sources inhibit a variety of pro-tumorigenic pathways. Because of their mechanism of action, cancer chemopreventive drugs function synergistically when administered with chemotherapeutic drugs, providing even more support for the need for continued research in this field (Fig 1.6).

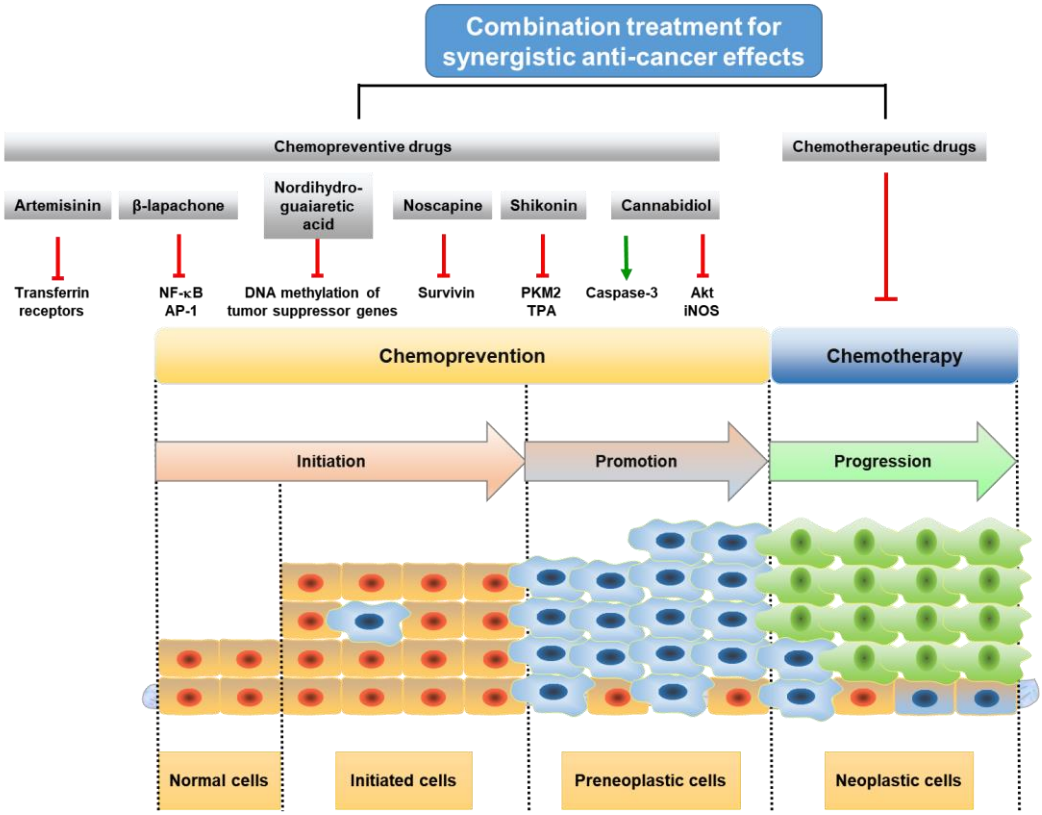

Figure 1.6. Schematic natural compounds for cancer chemoprevention and chemotherapy, acting on multiple stages of carcinogenesis. This figure was generated using Science-Slides software. Adapted from ref. [3].

CHAPTER 2

Epipolythiodiketopiperazines from the marine derived fungus *Dichotomomyces cejpii* with NF-κB inhibitory potential

2.1. Abstract

The Ascomycota *Dichotomomyces cejpii* was isolated from the marine sponge *Callyspongia* cf. *C. flammea.* A new gliotoxin derivative, 6-acetylmonodethiogliotoxin (**1**) was obtained from fungal extracts. Compounds **2** and **3**, methylthio-gliotoxin derivatives were formerly only known as semi-synthetic compounds and are here described as natural products. Additionally the polyketide heveadride (**4**) was isolated. Compounds **1**, **2** and **4** dose-dependently down-regulated TNFα-induced NF-κB activity in human chronic myeloid leukemia cells with IC_{50}s of 38.5 ± 1.2 µM, 65.7 ± 2.0 µM and 82.7 ± 11.3 µM, respectively. The molecular mechanism was studied with the most potent compound **1** and results indicate downstream inhibitory effects targeting binding of NF-κB to DNA. Compound **1 (**6-acetylmonodethiogliotoxin) thus demonstrates potential of epimonothiodiketopiperazine derived compounds for the development of NF-κB inhibitors.

Keywords: Ascomycete; Dichotomomyces; gliotoxin; NF-κB; leukemia

2.2. Introduction

The secondary metabolism of fungi gives rise to chemically most diverse structures, some of which have proven useful in drug development. A promising source for new secondary metabolites are organisms isolated from special habitats, like marine-derived fungi and bacteria [46]. Accordingly, fungal secondary metabolites have gained popularity due to their newly discovered pharmaceutical potential as anti-inflammatory, cytotoxic or cytostatic agents.

A number of gliotoxin derivatives have been isolated inter alia from fungus *Penicillium* sp. strain JMF034, from Japanese deep-sea sediments. These marine-derived drug candidates display epigenetic and anti-cancer activities against P388 murine leukemia cells. Compounds containing a disulfide bond including gliotoxin G, 5a,6-didehydrogliotoxin and gliotoxin showed potent *in vitro* inhibitory activity against the recombinant H3K9 histone methyl transferase G9a. The presence of a disulfide bond is usually accompanied by distinct toxic effects that limit the therapeutic usage of this compound group. Here, the Ascomycete *Dichotomomyces cejpii*, isolated from the marine sponge *Callyspongia* cf. *C. flammea*, allowed isolation of new gliotoxin derivatives devoid of a disulfide bridge. Along with the likewise isolated polyketide heveadride these compounds were investigated as anti-inflammatory, cytotoxic or cytostatic agents [47].

Several gliotoxins have been identified as potent inhibitors of cancer associated inflammatory signaling pathways [48]. One of the crucial pathways linking

cancer and inflammation is nuclear factor kappa B (NF-κB). Growing evidence indicates the involvement of this transcription factor in many inflammatory diseases and cancer progression. NF-κB became a promising therapeutic target of both hematological malignancies and solid tumors [49]. Many risk factors related to life style activate inflammatory pathways via NF-κB. Aberrantly activated NF-κB leads to expression of target genes involved in all steps of tumorigenesis. Moreover, constitutively active NF-κB serves as a useful prognostic indicator.

NF-κB is an inducible factor that acts as a dimer of pair-wise combinations of proteins from the Rel family [7]. This family comprises five members, RelA (p65), Rel (c-Rel), RelB, NF-κB1 (p105/p50) and NF-κB2 (p100/p52), which require dimerization prior to activation. Preferential dimer-binding is conditional for DNA affinity. In comparison to most eukaryotic transcription factors, the p50/p65 heterodimer presents a particularly high DNA affinity, which is why this dimer interacts with DNA more frequently than other NF-κB dimers [50]. Upon pathway activation through ligand binding, the natural inhibitor of kappa B (IκB), which is sequestering the inactive p50/p65 dimer in the cytoplasm, is phosphorylated, ubiquitinated and degraded by the proteasome. Active dimer translocates to the nucleus, binds to corresponding DNA sequences in promoter or enhancer regions and is responsible for the expression of pro-inflammatory genes [51].

In the present study we investigated the inhibitory effect of newly isolated natural epipolythiodiketopiperazines on anti-proliferative mechanisms via TNFα-induced p50/p65 NF-κB activity to understand cytostatic effects of these marine-derived drug candidates.

2.3. Materials and methods

2.3.1. Cell culture

K562 (human chronic myeloid leukemia) and Jurkat (T-cell leukemia) cells (DSMZ) were cultured in RPMI 1640 medium (Lonza, Belgium) supplemented with 10 % (v/v) fetal calf serum (Lonza, Belgium) and 1 % (v/v) antibiotic-antimycotic (Bio-Whittaker, Belgium) at 37 °C and 5 % CO2, humidified atmosphere. Cells were harvested every 3 days.

2.3.2. Transient transfection and luciferase reporter gene assay

K562 cells were transiently transfected as described previously [28]. For each electroporation, we used 5 µg of a luciferase reporter gene construct containing 5 repeats of a consensus NF-κB site (Stratagene, Genomics Agilent, Diegem, Belgium) and 5 µg of a Renilla luciferase plasmid (Promega, Leiden, Netherlands). The ICAM-1 LUC reporter plasmid was a generous gift from Prof. Wim Vanden Berghe (University of Antwerp, Belgium). The full-length ICAM-

1 promoter construct contains approximately 1.4 kb of ICAM-1 5′-flanking DNA linked to the firefly luciferase (LUC) gene. Promoter sequences between 393 and 176 bp upstream of the gene, containing binding sites for C/EBP and NF-κB. After electroporation, cells were re-suspended in RPMI 1640 culture medium, 10 % FCS, 1% AB and cultured at 37 °C and 5 % CO2 for 24 h. Afterwards, cells were harvested and re-suspended in fresh growth medium (RPMI 1640, 0.1 % FCS, 1 % AB) to a final concentration of 1x106 cells/mL and pre-treated for 2 h with 6-acetylmonodethiogliotoxin at indicated concentrations, followed by TNFα activation (20 ng/mL) for 6 h. After incubation, 75 µL of Dual-GloTM Luciferase Reagent (Promega, Leiden, Netherlands) was added to 75 µL of the cellular suspension for a 10 min at 22 °C before luciferase activity measurement. Subsequently, 75 µL of Dual-GloTM Stop&Glo® Reagent (Promega, Leiden, Netherlands) was added for 10 min at 22 °C to the cell suspension to measure Renilla activity. An Orion microplate luminometer (Berthold) was used to measure luciferase and Renilla activity. The results are expressed as a ratio of arbitrary units of firefly luciferase activity to Renilla luciferase activity.

2.3.3. Cell viability assessment

To assess percentage of viable K562 cells within sample and to determinate K562 cells proliferation trypan blue exclusion test was used. Trypan blue is a

vital stain that belongs to the family of azo compounds. It is a selective dye that stains only dead cells, passing through their plasma membrane. Viable cells are unstained as they can actively extrude this dye. Briefly, 20 µL of cell suspension was mixed with 20 µL of trypan blue solution and evaluated by Malassez cell counting chamber. In order to assess the cell viability, the percentage of unstained cells to the total amount of cells within the sample was calculated and normalized to 100% of control cells viability. In order to assess cell proliferation the concentration of unstained cells was determined and normalized to 100% of control cells concentration.

2.3.4. Extraction of cellular proteins

After the indicated incubation times with 6-acetylmonodethiogliotoxin and TNFα, Jurkat cells were lysed, and the nuclear and cytoplasmic extracts were prepared according to Duvoix et al. [28]. Briefly, cell pellets (10^7 cells per sample) were suspended in ice-cold hypotonic lysis buffer containing protease inhibitor cocktail (Complete®, Roche, Luxembourg) and incubated on ice for 15 min. After incubation, 10% Igepal was added to the cell suspension and each microcentrifuge tube was vigorously mixed by Vortex for 10 seconds to lyse cells followed by centrifugation in refrigerated microcentrifuge tube at 18,000 rcf for 1 min. The cytoplasmic extract (supernatant) was aliquoted and stored at -80 °C until use. Cell pellets were additionally washed with 100 µL of hypotonic

lysis buffer and after centrifugation at 4 °C, 18 000 rcf for 2 min the supernatant was removed. The ice-cold nuclear extraction buffer was added to each pellet and the cell suspension was gently mixed on an orbital shaker for 15 min at 4 °C following centrifugation at 10 500 rcf for 7 min at 4 °C. Then nuclear extracts (supernatant) were transferred to pre-chilled microcentrifuge tubes and stored at -80 °C until use. Protein content was determined for each sample using the Bradford assay (Bio-Rad protein Assay, Biorad, Nazareth, Belgium).

2.3.5. Western Blot analysis

Proteins of nuclear and cytoplasmic extracts were separated by size using sodium dodecyl sulfate polyacrylamide gel electrophoresis (SDS-PAGE, 10 %), transferred onto nitrocellulose membranes and blocked with 5 % non-fat milk in phosphate buffered saline (PBS)-Tween overnight. Blots were then incubated with primary antibodies: anti-IκBα (1/500 Santa Cruz SC-371, Tebu-Bio, Boechout, Belgium), anti-p50 (1/5000, Santa Cruz SC-7178X), anti-p65 (1/5000, Santa Cruz SC-8008), anti-α-tubulin (1/5000, Calbiochem CP06, VWR, Leuven, Belgium) or anti-lamin B (1/1000, Santa Cruz SC-6216). All antibodies were diluted in a PBS-Tween solution containing 5 % bovine serum albumin (BSA) or 5 % milk according to the providers' protocols. After incubation with primary antibodies, membranes were washed 3 x 10 min with PBS-Tween followed by an incubation of 1 h at RT with the corresponding secondary (HRP-conjugated)

antibodies. After washing 3 x 10 min with PBS-Tween, specific immunoreactive proteins were visualized by autoradiography using the ECL Plus Western Blotting Detection System Kit ® (GE Healthcare, Roosendaal, Netherlands). Lamin B for cytoplasmic extracts and α-tubulin for nuclear extracts, were used as loading controls.

2.3.6. TransAM assay

Jurkat cells were seeded at concentration 3 x 105 cells/mL and 107 cells were treated with Alterporriol E for 4 hour followed by activation with TNFα (20ng/mL) for 30 minutes. Subsequently, nuclear proteins were extracted from the cells according to manufacturer's protocol (Active motif, Nuclear extract kit, USA). Nuclear protein extracts were submitted for TransAM assay, which was conducted according to the manufacturer' instruction (Active motif, TransAM NFκB family, USA) and luminescent signal was measured by Luminometer (Berthold technologies, CentroLB 960, Germany).

2.3.7. Statistical analysis

Data are expressed as mean ± S.D. Significance was determined by the Student's T-tests. P-values below 0.05 were considered as statistically significant. IC50 values were calculated using XY scatter dependency chart. The 50 %

inhibition activity on NF-κB expression was established by using the best fitting model and calculated by trend formulas. The average value of at least 3 independent experiments was applied. Data are expressed as mean ± S.D. Significance was determined by the Student's T-tests. P-values below 0.05 were considered as statistically significant.

2.4. Results

2.4.1. Epipolythiodiketopiperazines dose-dependently inhibit TNF alpha-induced NF-κB activation

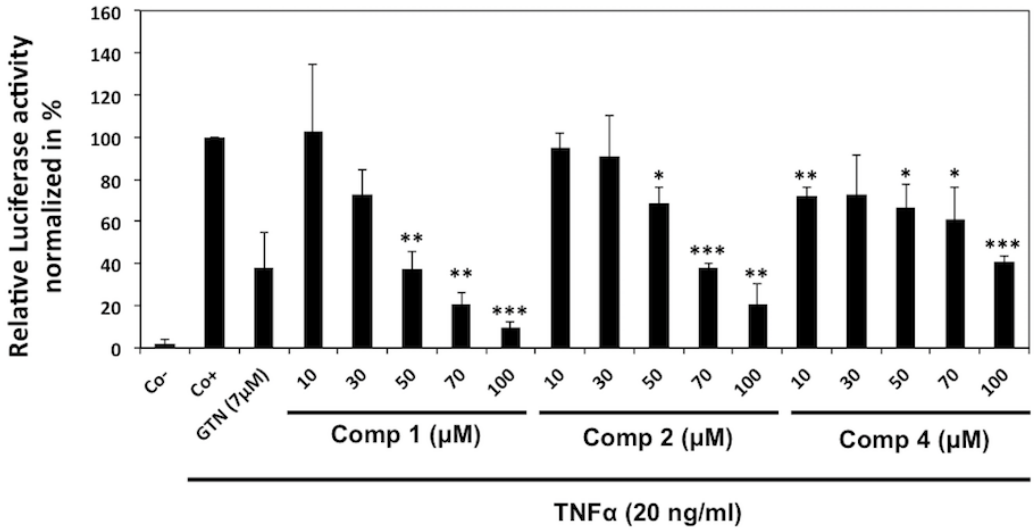

Figure 2.1. Inhibition of TNF alpha-induced NF-κB activation by pre-treatment with epipolythiodiketopiperazines. K562 cells were transiently transfected with both, firefly luciferase vector (NF-κB pGL4) and ph-RG-tk *Renilla* plasmid for 24 hours. After transfection, K562 cells were treated with

compound **1** (6-acetylmonodethiogliotoxin), **2** (6-acetylbisdethiobis (methylthio)gliotoxin) or **4** (heveadride) at indicated concentrations for 2 hours followed by a TNFα-treatment (20 ng/mL) during 6 hours. The cells were assayed for Luciferase activity. Each value is a mean ± SD of three independent experiments. Negative control (Co-) corresponds to DMSO treated cells, without TNFα activation, positive control (Co+) corresponds to DMSO treated cells activated by TNFα. Goniothalamin (GTN) at concentration 7µM was used as a positive inhibitory control. Asterisks indicate a significant difference between untreated and 6-acetylmonodethiogliotoxin-treated cells as analyzed by t-test (*$p < 0.05$; **$p < 0.01$; ***$p < 0.001$).

Compounds **1**, **2** and **4** were analyzed in order to assess their inhibitory potential on TNFα-induced NF-κB activity in K562 cells. Considering the low amount of compound 3 available, we were unable to include this compound in biological assays. We determined compounds inhibition potential on TNFα-induced activation of a luciferase gene under the control of canonical NF-κB response elements. We treated transiently transfected K562 cells at different concentrations of compounds **1**, **2** and **4,** respectively, followed by the stimulation with TNFα. Results show that TNFα-induced NF-κB reporter gene activity was dose-dependently decreased by compounds **1**, **2** and **4** compared to control with IC_{50} values of 38.5 ± 1.2 µM (compound **1)**, 65.7 ± 2.0 µM

(compound **2**) and 82.7 ± 11.3 µM (compound **4**) (Fig 2.1). IC_{50} values were calculated using XY scatter dependency chart. The 50 % inhibition activity on NF-κB expression was established by using the best fitting model and calculated by trend formulas. The average value of at least 3 independent experiments was applied. Molecular mechanism of compound 1 (6-acetylmonodethiogliotoxin) was investigated in more detail.

2.4.2. 6-Acetylmonodethiogliotoxin down-regulates the expression of NF-κB target genes

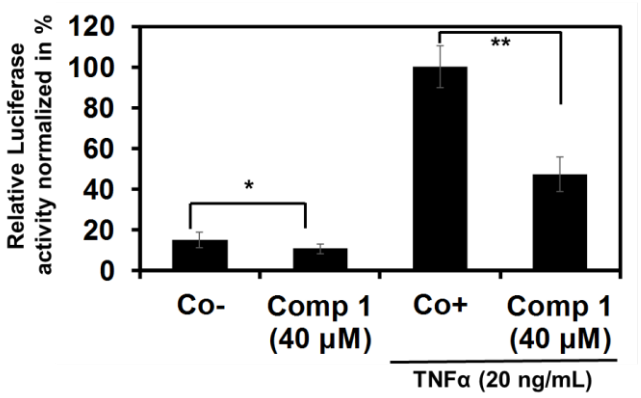

Figure 2.2. 6-acetylmonodethiogliotoxin inhibits TNFα-induced NF-κB-dependent ICAM-1 gene expression. 6-acetylmonodethiogliotoxin (Comp 1) inhibits NF-κB-dependent ICAM-1 genes expression. K562 cells were transiently transfected with ICAM-1 along with ph-RG-tk *Renilla* plasmid for 24 hours. After transfection, K562 cells were treated or not with 6-acetylmonodethiogliotoxin at IC_{50} concentrations for two hours followed by a TNFα-treatment (20 ng/mL) during 6 hours. The cells were assayed for

Luciferase activity. Each value is a mean ± SD of three determinations. Asterisks indicate a significant difference compared to control positive as analyzed by t-test (*$p < 0.05$; **$p < 0.01$; ***$p < 0.001$). Negative control (Co-) corresponds to transfected and DMSO only treated cells, without TNFα activation, positive control (Co+) corresponds to transfected and DMSO treated cells activated by TNFα.

NF-κB signaling results in activation of a large battery of target genes. Many of these genes have been associated with different steps of tumorigenesis [52]. In order to further validate the previously observed inhibition of NF-kB reporter gene activity we investigated whether 6-acetylmonodethiogliotoxin affects ICAM-1 gene transcription. K562 cells were transiently transfected with ICAM-1 plasmid followed by treatment with 6-acetylmonodethiogliotoxin at IC_{50} concentration, and then exposed to TNFα. Our results show that TNFα induced ICAM-1 promoter-driven reporter gene activity and 6-acetylmonodethiogliotoxin significantly inhibited this induction by 53% compared to control (Fig 2.2).

2.4.3. 6-acetylmonodethiogliotoxin mediated downstream inhibition of NF-κB signaling by preventing binding of p65 to DNA

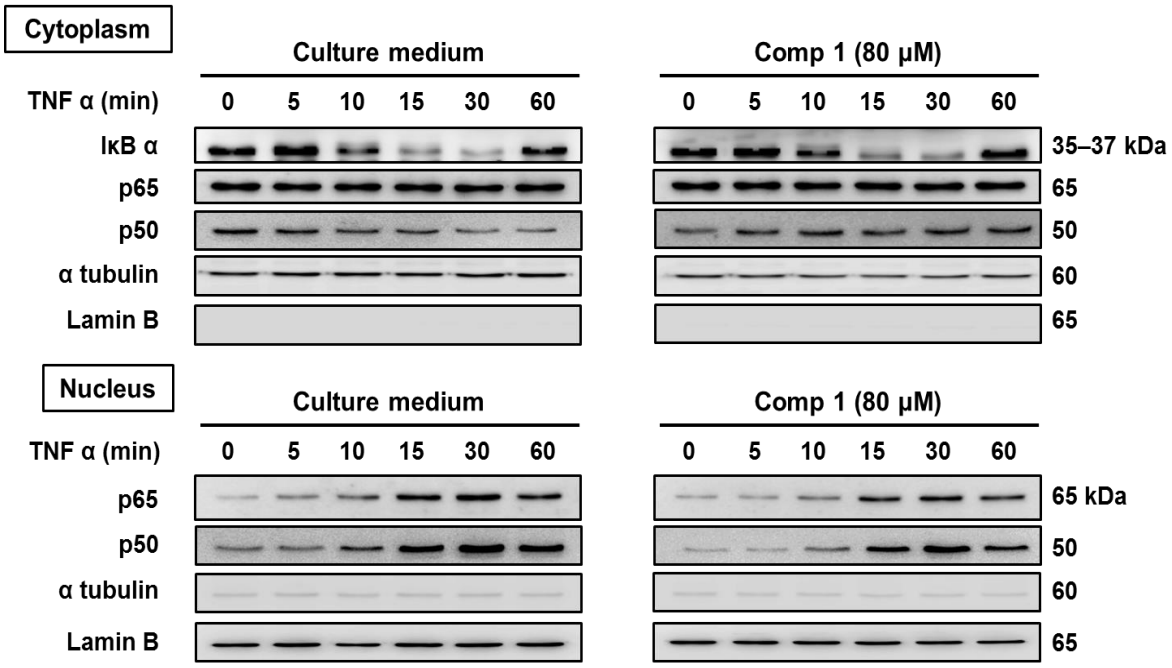

Figure 2.3. Effect of 6-acetylmonodethiogliotoxin on the degradation of IκBα and translocation of p65 and p50 to the nucleus. Jurkat cells were pre-treated with 6-acetylmonodethiogliotoxin (Compound **1**) at 80 μM for 2 hours followed by activation with TNFα (20 ng/mL) for indicated time periods. Cytoplasmic and nuclear extracts were tested for IκBα, pIκBα, p50 and p65. Protein loading and purity of extracts were verified by lamin B and α-tubulin Western blots.

We further analyzed the molecular mechanism underlying the inhibition potential of 6-acetylmonodethiogliotoxin on TNFα-induced NF-κB activation. Here, we focused on degradation of IκBα, the natural inhibitor of NF-κB as well

as on translocation of p50 and p65 subunits to the nucleus. As shown in Figure 2.3, 6-acetylmonodethiogliotoxin did neither prevent IκBα degradation, nor p50/p65 nuclear translocation. These results indicate that 6-acetylmonodethiogliotoxin mediated downstream inhibition of NF-κB pathway. As both subunits p50 and p65 translocated to the nucleus, 6-acetylmonodethiogliotoxin could either prevent their binding to DNA or abrogate NF-κB transcriptional activity.

In order to validate our hypothesis we investigated whether 6-acetylmonodethiogliotoxin is able to interfere with the binding affinity of NF-κB to its consensus response element. Figure 2.4 showed that 6-acetylmonodethiogliotoxin at IC_{50} concentrations significantly decreased binding affinity of p65 to the NF-κB consensus and this effect was further more pronounced at the higher concentration, whereas p50 was not affected by 6-acetylmonodethiogliotoxin treatment (data not shown). Altogether, these results provide evidence that 6-acetylmonodethiogliotoxin acts as a downstream inhibitor of NF-κB pathway altering binding of p65 to DNA.

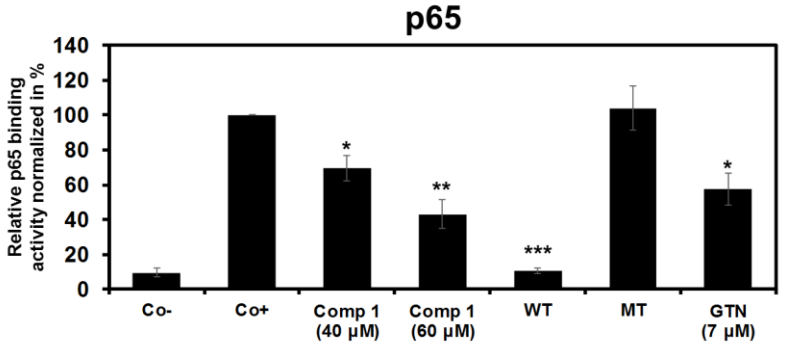

Figure 2.4. 6-acetylmonodethiogliotoxin (1) reduces binding affinity of p65 to DNA in a dose dependent manner. Dose-dependent effects of 6-acetylmonodethiogliotoxin (Comp 1) on p65 binding affinity to DNA. Jurkat cells were pre-incubated with 6-acetylmonodethiogliotoxin at indicated concentrations for 4 hours and treated with TNFα (20 ng/mL) for 30 minutes, and then subjected to TransAM assay. Negative control (Co-) corresponds to nuclear extracts of DMSO treated cells, without TNFα activation, positive control (Co+) corresponds to nuclear extracts of DMSO treated cells activated by TNFα, wild-type (WT) and mutated type (MT) corresponds to nuclear extracts of DMSO treated cells activated by TNFα loaded on plate comprising wild-type or mutated consensus oligonucleotide, respectively. Goniothalamin (GTN) at concentration 7μM was used as a positive inhibitory control. Shown data are mean ± SD of three independent experiments. Asterisks indicate a significant difference compared to control positive as analyzed by t-test (*$p < 0.05$; **$p < 0.01$; ***$p < 0.001$).

As the NF-κB pathway is known to regulate a large battery of genes involved in cell proliferation and survival, we investigated the effects of compound 1 (6-acetylmonodethiogliotoxin) (Fig 2.5A, 5B), compound 2 (6-acetylbisdethiobis (methylthio)gliotoxin) (Fig 2.5C, 5D) and compound 4 (heveadride) (Fig 2.5E, 5F) on K562 cell viability and proliferation.

Importantly, any of the tested compounds decreased cancer cell viability after 8 hours of treatment used for the investigation of NF-κB mechanisms, reflecting that down-regulation of NF-κB activation was not due to cell death induction. At later time points (24h, 48h and 72h), 6-acetylmonodethiogliotoxin dose-dependently inhibited cancer cell proliferation (Fig. 2.5B). At 50 μM, compound 1 (6-acetylmonodethiogliotoxin) induced cytostatic effects and at higher concentrations of 70 μM and 100 μM a moderate cytotoxicity was observed reaching a maximum of 20% and 30% at 72h, respectively. These observations could be the secondary consequences of early NF-κB inhibition.

However, compound 2 (6-acetylbisdethiobis(methylthio)gliotoxin) and compound 4 (heveadride), are weaker NF-κB inhibitors compared to compound 1 (6-acetylmonodethiogliotoxin) and did not significantly decrease K562 cell viability at any concentration or measured time point (Fig. 2.5C and 2.5E, respectively). On the other hand, 100 μM of both compounds reduced K562 proliferation compared to control. Whether these effects could be directly linked to the observed NF-κB down-regulation will be object of future studies.

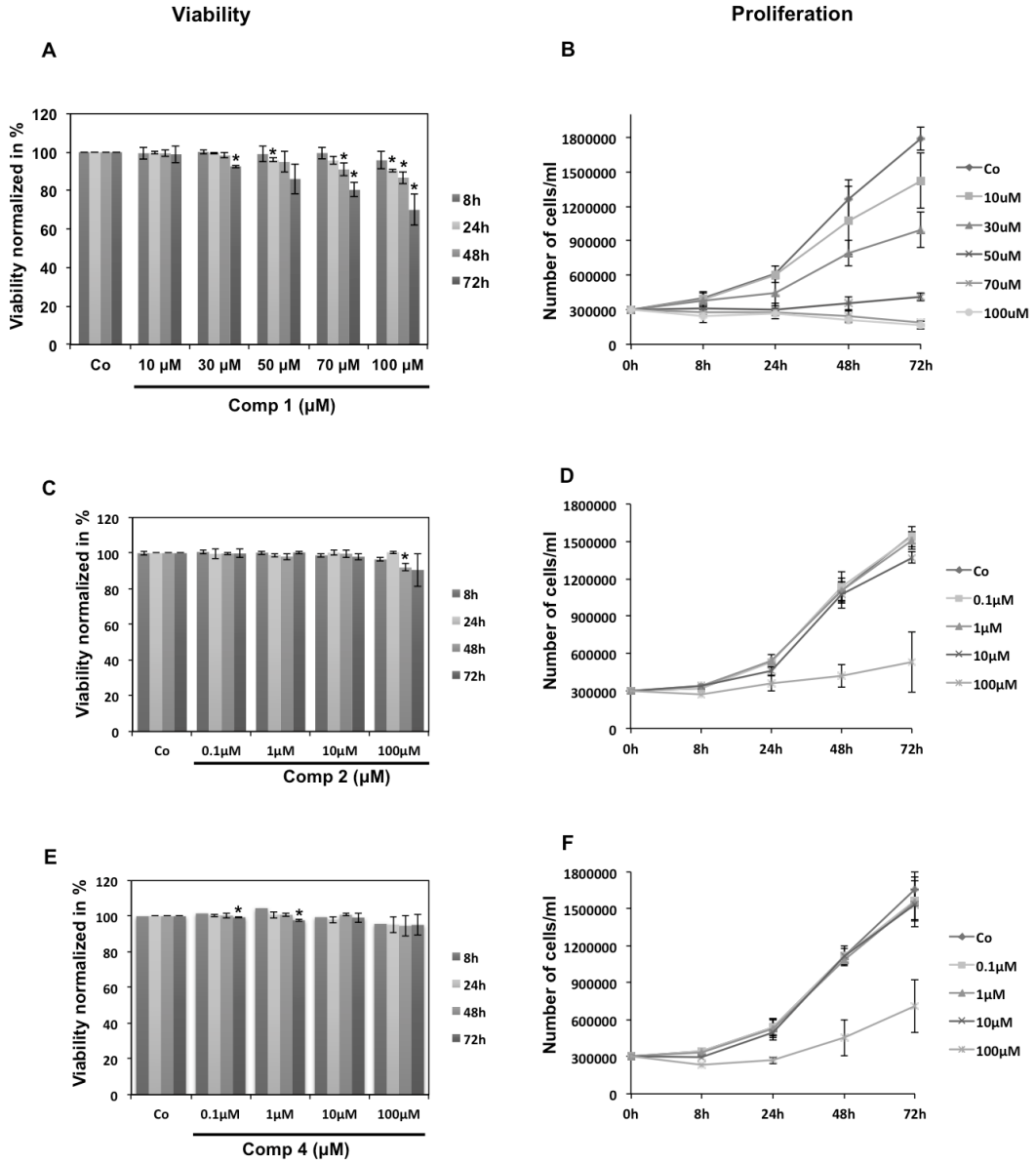

Figure 2.5. Effects of epipolythiodiketopiperazines on cancer cells viability and proliferation. Effects of compound **1** (6-acetylmonodethiogliotoxin) (2.5A, 5B), compound **2** (6-acetylbisdethiobis(methylthio)gliotoxin) (2.5C, 5D) and compound **4** (heveadride) (2.5E, 5F) at the indicated concentrations on K562

cells viability and proliferation respectively, analyzed after 8, 24, 48 and 72 hours. Control (Co) corresponds to untreated cells. Each value is a mean ± SD of three determinations. The asterisk indicates a significant difference compared to the control as analyzed by t-test (*$p < 0.05$)

2.5. Discussion

Our data indicate strong anti-proliferative potential on chronic myeloid leukemia cells, as 6-acetylmonodethiogliotoxin dose- and time-dependently inhibited K562 cell proliferation.

Importance of inflammation in cancer initiation and progression is nowadays well established. Many epidemiological, experimental and clinical studies strengthen the tight relationship between cancer and inflammation [53]. During past decades, NF-κB, as a crucial player in inflammatory signaling, became a popular target in cancer therapy. Abnormal NF-κB signaling can be detected in as much as 95% of all cancer cases and is responsible for aberrant expression of huge battery of genes involved in cancer onset and progression [52]. Natural compounds have been shown to counteract with NF-κB signaling and down-regulate its activity, thus acting as potent agents in both, cancer prevention and treatment [48, 54-58].

A transannular sulfur bridge as present in compound **1** seems to be essential for the observed NF-κB pathway interfering activity, as the related compound **2** without this feature did not display any activity. The finding of 6-

acetylmonodethiogliotoxin with a monosulfide bridge is of importance, as this compound may serve as lead for the development of more potent and selective ligands for this therapeutically interesting drug target.

It is interesting to note, that monosulfides of gliotoxin derivatives have been obtained semi-synthetically from disulfid gliotoxin derivatives by reaction with tervalent phosphorus compounds, e.g. triphenylphosphine [59]. The investigated marine derived strain of Dichotomomyces cejpii however constantly produced 6-acetylmonodethiogliotoxin (1) under different cultivation conditions that was isolated directly from the fungal extract as a natural product. To our knowledge there are only sirodesmin H, isolated from the fungus Phoma lingam and emestrin-G, isolated from the fungus Armillaria tabescens, respectively, where such a bridged monosulfid was obtained directly by isolation as a natural product [60, 61]. However these compounds solely possess the same epimonothiodioxopiperazine moiety while the rest of the structural backbone is quite different.

CHAPTER 3

The dialkyl resorcinol stemphol disrupts calcium homeostasis to trigger programmed immunogenic necrosis in leukemia

3.1. Abstract

Stemphol (STP) is a novel druggable phytotoxin triggering mixed apoptotic and non-apoptotic necrotic-like cell death in human acute myeloid leukemia (AML). Use of several chemical inhibitors highlighted that STP-induced non-canonical programmed cell death was Ca^{2+}-dependent but independent of caspases, poly (ADP-ribose) polymerase-1, cathepsin, or calpains. Similar to thapsigargin, STP led to increased cytosolic Ca^{2+} levels and computational docking confirmed binding of STP within the thapsigargin binding pocket of the sarco/endoplasmic reticulum (ER) Ca^{2+}-ATPase (SERCA). Moreover, the inositol 1,4,5-trisphosphate receptor is implicated in STP-modulated cytosolic Ca^{2+} accumulation leading to ER stress and mitochondrial swelling associated with collapsed cristae as observed by electron microscopy. Confocal fluorescent microscopy allowed identifying mitochondrial Ca^{2+} overload as initiator of STP-induced cell death insensitive to necrostatin-1 or cycloheximide. Finally, we observed that STP-induced necrosis is dependent of mitochondrial permeability transition pore (mPTP) opening. Importantly, the translational immunogenic potential of STP was validated by HMGB1 release of STP-treated AML patient cells. STP reduced colony and *in vivo* tumor forming potential and impaired the development of AML patient-derived xenografts in zebrafish.

Keywords: calcium; caspase-independent apoptosis; programmed necrosis; leukemia; cancer

3.2. Introduction

Even though apoptosis is the most investigated cell death modality, many cancer cells were described to develop resistance mechanisms by inactivating, mutating or overexpressing selected genes of the anti-apoptotic signaling cascades [62]. Accordingly, recent research efforts investigated alternative cell death modalities relying on caspase-independent pathways including necroptosis, parthanatos or paraptosis, amongst others [63]. Key common determinants of these cell death modalities are a dysregulation of reactive oxygen species (ROS) and Ca^{2+} homeostasis [64] leading to cell demise [18, 65]. Drug-induced Ca^{2+} uptake or cellular redistribution from endoplasmic reticulum (ER) to cytoplasm and mitochondria are critical factors in health and disease [65]. Disruption of the physiological levels of Ca^{2+} in mitochondria and ER were shown to trigger necrosis by opening of mitochondrial permeability transition pore (mPTP) [66] or paraptosis [28]. Autophagy, as well as mitophagy, preceded or not by ER stress was shown to be triggered as a defense mechanism when Ca^{2+} homeostasis is lost [67, 68].

Immune cells are essential components of the tumor microenvironment, and recent research focused on chemotherapy-induced activation of the immune reaction. Immunogenic cell death (ICD) is an emerging cell death modality stimulating the immune response against cancer cells by activation of macrophages and dendritic cells in the tumor microenvironment [69]. ICD is characterized by exposure of calreticulin (CRT) and heat shock proteins as well

as the release of ATP and high mobility group box (HMGB)1 [70]. ER stress is considered as a major ICD activation pathway after perturbation of Ca^{2+} homeostasis and ROS generation [70].

Stemphol (STP), a natural dialkyl resorcinol, is a phytotoxin extracted from *Stemphylium globuliferum* with potent antimicrobial activities against fungi (*Mucor hiemalis*), yeast (*Schizosaccharomyces pombe*), Gram-positive bacteria (*Bacillus subtilis* and *Staphylococcus aureus*) and was also described as a self-inhibitor in *Pleospora herbarum* [71]. Despite its significant bioactivity, so far, the anti-tumor potential of STP was never investigated.

Since the interplay between different cell death and cell stress modalities became an interesting pharmacological target, for this study, we investigated the cytotoxic effect of STP on Ca^{2+} homeostasis. We demonstrate for the first time *in vivo* and *in vitro* anticancer potential of STP. From a mechanistic point of view, we used a multi-parametric approach to document how a Ca^{2+} flux from ER to cytosol eventually culminating in mitochondrial Ca^{2+} overload triggers non-canonical cell death *via* mPTP opening.

3.3. Materials and methods

3.3.1. Compound

Stemphol (50982-33-7) was extracted from the endophytic fungal strain Stemphylium globuliferum (Fig 3.1A).

3.3.2. Cell culture

Human histiocytic lymphoma U-937, chronic myelogenous leukemia K-562, T-cell leukemia Jurkat and Burkitt lymphoma RAJI were obtained from the American Type Culture Collection (ATCC, Manassas, USA). Monocyte THP-1 and promyeloblast HL-60 were obtained from Korean cell line Bank (KCLB, Seoul, South Korea). All cells were cultured according to standard procedures.

3.3.3. Cell viability and cell death assessment

Trypan blue exclusion assay (Biowhittaker, Geneclone, Seoul, South Korea) was used to assess cell viability. The mode of cell death was determined and quantified after determination of the nuclear morphology by Hoechst 33342 (Sigma-Aldrich, Geneclone, Seoul, South Korea) and propidium iodide staining (Sigma-Aldrich, Geneclone, Seoul, South Korea). Cells were observed by fluorescence microscopy (Nikon Eclipse Ti-U, Nikon Instruments Korea, South Korea). Caspase 3/7 activity was assessed by Caspase-Glo 3/7 Assay (Promega, Cosmogenetech, Seoul, South Korea), and intracellular ATP levels were measured by CellTiter-Glo Luminescent Cell Viability Assay (Promega, Cosmogenetech, Seoul, South Korea).

3.3.4. Colony formation assays

U-937, THP-1 (both at 10^3 cells/mL) and HL-60 (3 x 10^3 cells/mL) cells were seeded into semisolid methylcellulose medium (Methocult H4230, StemCell

Technologies Inc., Canada) treated with indicated concentrations of STP, and grown for 10 days at 37°C and 5% CO_2. Colonies were detected with an ImageQuant LAS 4000 mini camera (GE Healthcare Life Sciences, South Korea), after adding 1 mg/mL of 3-(4,5-dimethylthiazol-2-yl)-2,5-diphenyltetrazoliumbromide (MTT) reagent (Sigma-Aldrich, Geneclone, Seoul, South Korea), and were quantified by Image J software (version 1.47t) (U.S. National Institute of Health, Bethesda, MD, USA).

3.3.5. Zebrafish xenograft assays

All procedures were conducted according to our previous study [72]. Wild-type zebrafish (*Danio rerio*) were obtained from the Zebrafish International Resource Center (ZIRC, University of Oregon, OR), and maintained according to SNU guidelines at 28.5 °C with 10 hrs dark/4 h light cycles. For cancer xenograft assays, after mating, fertilized eggs were incubated in Danieau's solution with 0.003 % of phenylthiourea (PTU) at 28.5 °C for 48 hrs. Micropipettes for injection and anesthesia were generated from a 1.0 mm glass capillary (World Precision Instruments, FL, USA) by using a micropipette puller (Shutter Instrument, USA). 48 hrs post fertilization (hpf), zebrafish were anesthetized in 0.02 % tricaine (Sigma, Geneclone, Seoul, South Korea) and immobilized on an agar plate. 200 U-937 cells or 400 patient cells were stained for 2 hrs by 4 μM of Cell tracker CM-Dil dye (Invitrogen, Geneclone, Seoul, South Korea), then treated STP at indicated concentrations for 8 hrs. Cells were then injected into

the yolk sac by microinjection (PV820 microinjector, World Precision Instruments, FL, USA). Subsequently, zebrafish were incubated in 96-well plates containing Danieau's solution with 0.003 % phenylthiourea (PTU) at 28.5 °C for 72 hrs. Fishes were then immobilized in a drop of 3 % methylcellulose in Danieau's solution on a glass slide. Pictures were taken by fluorescence microscopy (Leica DE/DM 5000B). Areas of fluorescent tumors were quantified by Image J software.

3.3.6. Investigation of cellular morphology

For Giemsa staining, cells were pretreated with STP then spun onto a glass slide for 5 minutes at 800 *g* using a cytopad with caps (Elitech biomedical systems, Geneclone, Seoul, South Korea). Cells were then fixed and stained with the Diff-Quik staining kit (Dade Behring S.A., Geneclone, Seoul, South Korea) according to the manufacture's protocol and pictures were taken (Nikon Eclipse Ti-U, Nikon Instruments Korea, South Korea). A total of 50 cells were counted in one area, and three independent areas were counted for each set of three independent experiments.

For transmission electron microscopy (TEM), cells were pelleted and fixed in 2.5 % glutaraldehyde (Electron Microscopy Sciences, Geneclone, Seoul, South Korea) diluted in 0.1 M sodium cacodylate buffer, pH 7.2 (Electron Microscopy Sciences, Geneclone, Seoul, South Korea) overnight. Cells were then rinsed with sodium cacodylate buffer twice and postfixed in 2 % osmium tetroxide for two

h at room temperature. Samples were washed with distilled water and then stained with 0. 5% uranyl acetate at 4 °C for overnight. After 24 hrs, samples were dehydrated through a graded series of ethanol solutions to water followed by propylene oxide, and then infiltrated in 1:1 propylene oxide/Spurr's resin. Samples were kept overnight embedded in Spurr's resin, mounted in molds and left to polymerize in an oven at 56 °C for 48h. Ultrathin sections (70–90 nm) were obtained with ultramicrotome, EM UC7 (Leica, Germany). Sections were stained with uranyl acetate and lead citrate and subsequently examined with a JEM1010 transmission electron microscope (JEOL, Japan).

3.3.7. Measurement of cytosolic and mitochondrial calcium levels

Experiments were conducted based on published procedures with modifications [73]. Experiments were based on published procedures with modifications. Cells were stained with 500 nM Fluo-3-AM (Thermo Fisher Scientific, Geneclone, Seoul, South Korea) in the dark for 25 minutes at 37 °C after indicated times of STP (30 μM) treatment. After 15 minutes at room temperature, cytosolic Ca^{2+} levels were assessed by flow cytometry (FACS Calibur, Becton Dickinson, San Jose, CA, USA). Thapsigargin (TSG, 1 μM, 30 minutes) was used to increase intracellular calcium levels. To block the influx of extracellular Ca^{2+}, cells were treated with 650 mM EGTA for 2 minutes before/concomitantly to TSG (10 nM), and cytosolic Ca^{2+} levels were quantified every 15 seconds. To investigate the effect of 2-APB and dantrolene, cells were treated with STP (30 μM) for 1 hr

with or without inhibitor pretreatment at indicated concentrations before Ca^{2+} quantification. For the mitochondrial Ca^{2+} measurement, cells were stained with 2.5 μM Rhod2-AM (Thermo Fisher Scientific, Geneclone, Seoul, South Korea) in the dark for 15 minutes at 4 °C. After washing with HBSS, cells were stained with 100 nM MitoTracker Green (Thermo Fisher Scientific, Geneclone, Seoul, South Korea) and Hoechst (Sigma, Geneclone, Seoul, South Korea) in the dark for 20 minutes at 37 °C. The fluorescent cell were visualized by the confocal microscopy using Leica Confocal system TCS SP8.

3.3.8. Detection of the mitochondrial permeability transition pore (mPTP) opening

The opening of mPTP was investigated using calcein-AM staining (Thermo Fisher Scientific, Geneclone, Seoul, South Korea) combined with $CoCl_2$ to detect mitochondrial calcein fluorescence. At the end of treatment, cells were washed with Hanks' Balanced Salt Solution (HBSS) (containing Ca^{2+} and Mg^{2+}) and added 10 nM Calcein-AM and 300 μM $CoCl_2$ at 37 °C for 15 minutes. After incubation, the fluorescence of mitochondrial calcein was analyzed by flow cytometry.

3.3.9. Quantification of reactive oxygen species

Treated or untreated cells were stained with 10 μM of 2',7'-dichlorodihydrofluorescein diacetate (H_2DCFDA) (LifeTechnologies,

Geneclone, Seoul, South Korea) for 20 minutes at 37 °C in the dark. Fluorescence intensity was assessed using by FACSCalibur (Becton Dickinson, San Jose, CA, USA) and H_2O_2 (50 μM, 30 minutes) was used as a control positive.

3.3.10. Western blotting

Proteins were extracted from STP-treated and control cells, and 40 μg were loaded on a 10 – 15 % SDS-PAGE gel. Proteins were transferred to a 0.2 or 0.4 μm PVDF membrane (GE Healthcare Life Science, Geneclone, Seoul, South Korea) and hybridized with an LC3 antibody (Cell Signaling Technology, #2775, USA), eIF2a (Phospho-Ser51)(Signalway antibody, #11279, Geneclone, Seoul, South Korea), eIF2α (Cell signaling technology, #9722, Geneclone, Seoul, South Korea), ATF4 (Cell signaling technology, #11815, Geneclone, Seoul, South Korea), Bip / GRP78 (Cell signaling technology, #C50B12, Geneclone, Seoul, South Korea), CHOP (Cell signaling technology, #L63F7, Geneclone, Seoul, South Korea) and β-actin (Sigma, Clone AC-74, Geneclone, Seoul, South Korea). Bands were acquired using an Amersham Imager 600 (GE Healthcare Life Science, USA) and quantified by ImageJ (version 1.47t) (U.S. National Institute of Health, Bethesda, MD, USA).

3.3.11. Docking studies

AutoDock Vina software (The Scripps Research Institute, CA, USA) was used for the docking simulations. Crystal structures of SERCA were obtained from the Protein Data Bank (PDB ID: 5A3Q) and coordination for STP was generated using the GlycoBioChem PRODRG2 Server [74]. For docking simulation, all ligands and water molecules were removed from the templates and the size of the docking grids were set to cover the entire structure of the proteins. Figures were generated using PyMol Molecular Graphics System. (DeLano, W. L., 2002)

3.3.12. Analysis of the lysosomal mass

Cells plated at 3×10^5 cells/well after indicated treatments were harvested, washed and incubated at 37 °C for 15 minutes with 20 nM LysoTracker Red (Molecular Probes, Invitrogen, Geneclone, Seoul, South Korea). Lysosomal mass changes were quantified by Operetta High-Content Imaging System (Perkin Elmer, USA).

3.3.13. Quantification of HMGB1 release

Human patient samples were seeded in 1 mL of medium at 5×10^5 cells/mL. After 24 hrs, cells were centrifuged, the supernatant was collected and immediately stored at -80 °C. Quantification of HMGB1 release in the supernatants was assessed by enzyme-linked immunosorbent assay kit from Shino-Test-Corporation (Jinbocho, Chiyoda-ku, Tokyo, Japan) according to the manufacturer's instructions.

3.3.14. *In silico* drug-likeness properties

The Lipinski's 'rule-of-five' and other parameters for drug-likeness and oral bioavailability were evaluated by using the SCFBio website [http://www.scfbio-iitd.res.in/] and the Molinspiration property engine v2016.10. [http://www.molinspiration.com]. In silico absorption, distribution, metabolism, excretion (ADME) and toxicity of STP were evaluated by preADMET software ver. 1.0 [https://preadmet.bmdrc.kr/].

3.3.15. Human primary samples

Human leukemia samples were obtained from the Seoul National University Children's Hospital. The Institutional Review Board (IRB) of Seoul National University Hospital (IRB No. H-1609-133-797) reviewed and approved the study protocol, and exempted the study from the obligation to obtain informed consent. This study was performed following World Medical Association's Declaration of Helsinki.

3.3.16. Statistical analysis

Data are expressed as mean ± S.E.M., and significance was estimated by using one-way or two-way ANOVA tests. Post-hoc analyses were performed using Prism 7 software, GraphPad Software (La Jolla, CA, USA). P-values below 0.05

were considered as significant and expressed as *P≤0.05; **P≤0.01; ***P≤0.001; ****P≤0.0001.

3.4. Results

3.4.1. Stemphol inhibits viability, proliferation and colony formation capacity of human leukemia cells

To assess the anti-cancer effect of STP on human leukemia cells, we treated four different leukemia cell lines with STP in a time- and dose-dependent manner. STP impaired viability and proliferation starting at 30 µM (Fig 3.1B) and showed a similar range of IC_{50} for all four leukemia cells at each time point (Table 3.1). Stemphol also induced cytotoxicity in A549 and MCF-7 solid tumor cell lines (Fig 3.1C) but at higher concentrations compared to leukemia cells (Table 3.1). We treated peripheral blood mononuclear cells (PBMCs) from healthy donors with increasing concentrations of STP (Fig 3.1D) to confirm differential toxicity of STP at concentrations of 30, 50, 70 and 100 µM after 8, 24 and 48 hours of treatment (Fig 3.1D, E).

To generalize our findings and to validate initial results, we used a 3D colony formation assay (CFA) with three AML cell lines. Our results showed a significant inhibition of colony formation at 30 µM in U-937 and HL-60 cells and 50 µM in THP-1 (Fig 3.1F) for both number and the total area of colonies. To validate the colony formation approach in an *in vivo* setting, we demonstrated

that STP significantly inhibited the tumor-forming ability of U-937 at 30 mM of STP by using a zebrafish xenograft approach thus validating *in cellulo* results (Fig 3.1G).

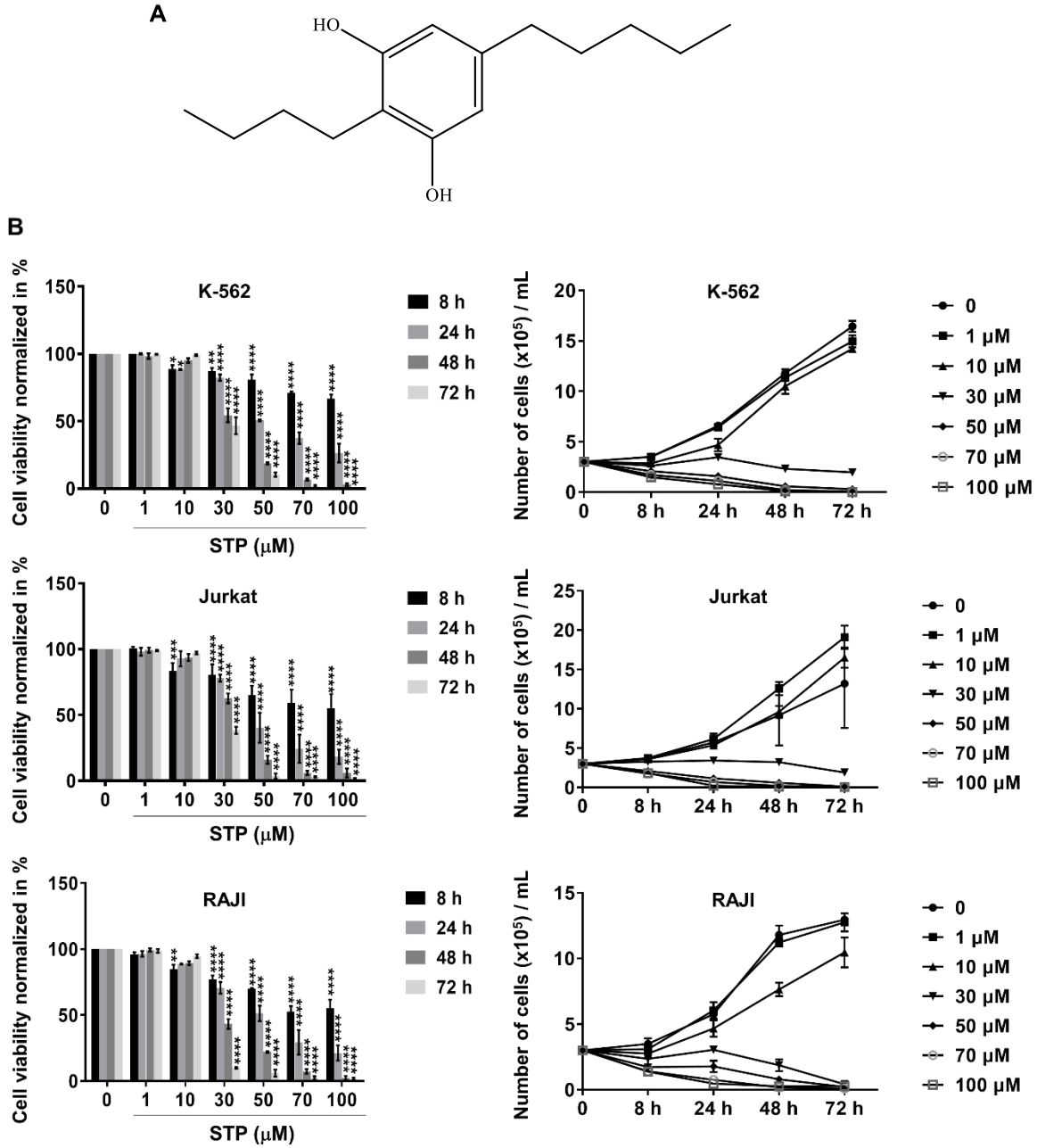

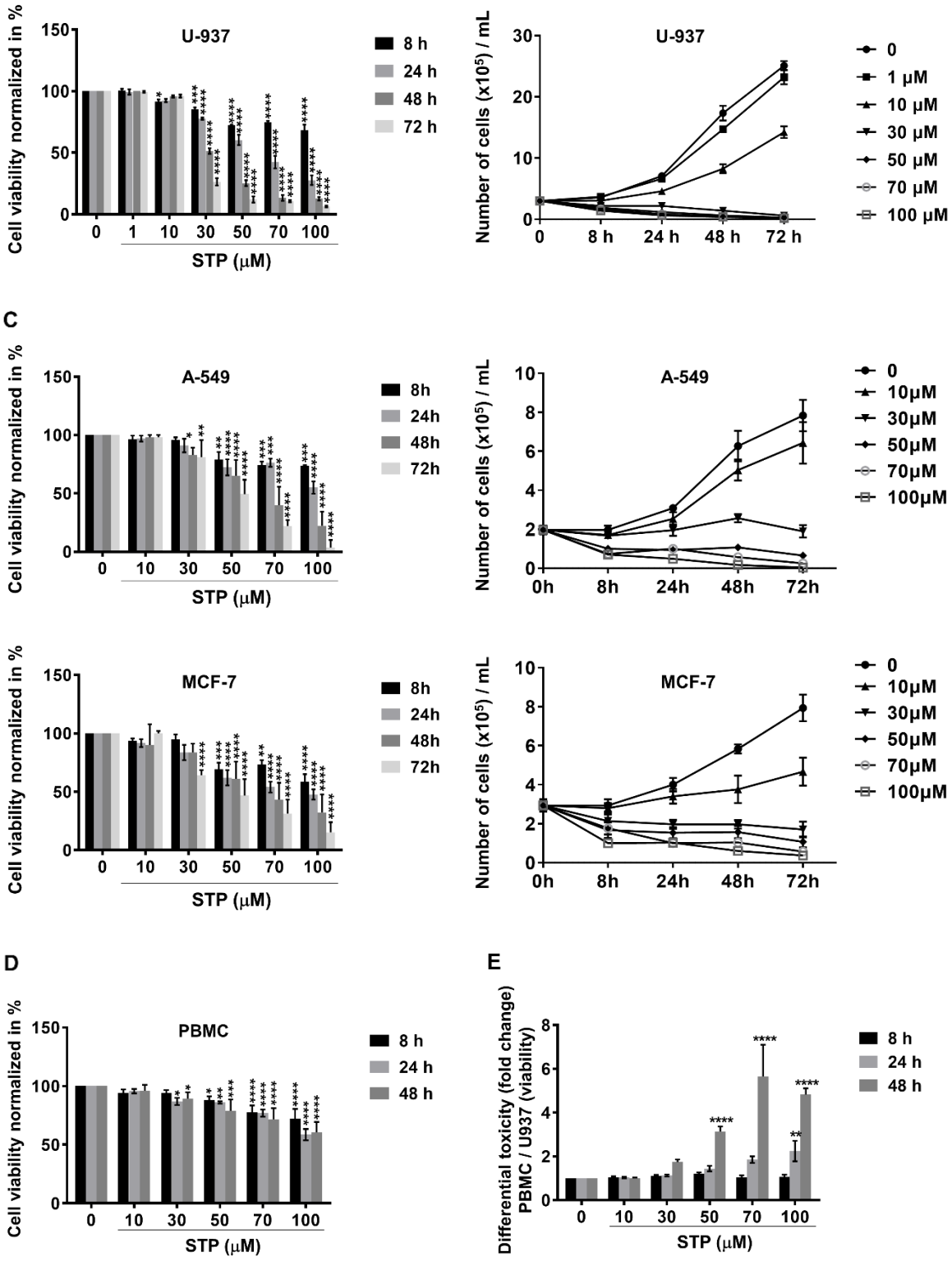
U-937
Cell viability normalized in %
STP (μM)
8 h
24 h
48 h
72 h
Number of cells (x10⁵) / mL
0
1 μM
10 μM
30 μM
50 μM
70 μM
100 μM
C
A-549
8h
24h
48h
72h
0h
10μM
30μM
50μM
70μM
100μM
MCF-7
D
PBMC
E
Differential toxicity (fold change)
PBMC / U937 (viability)

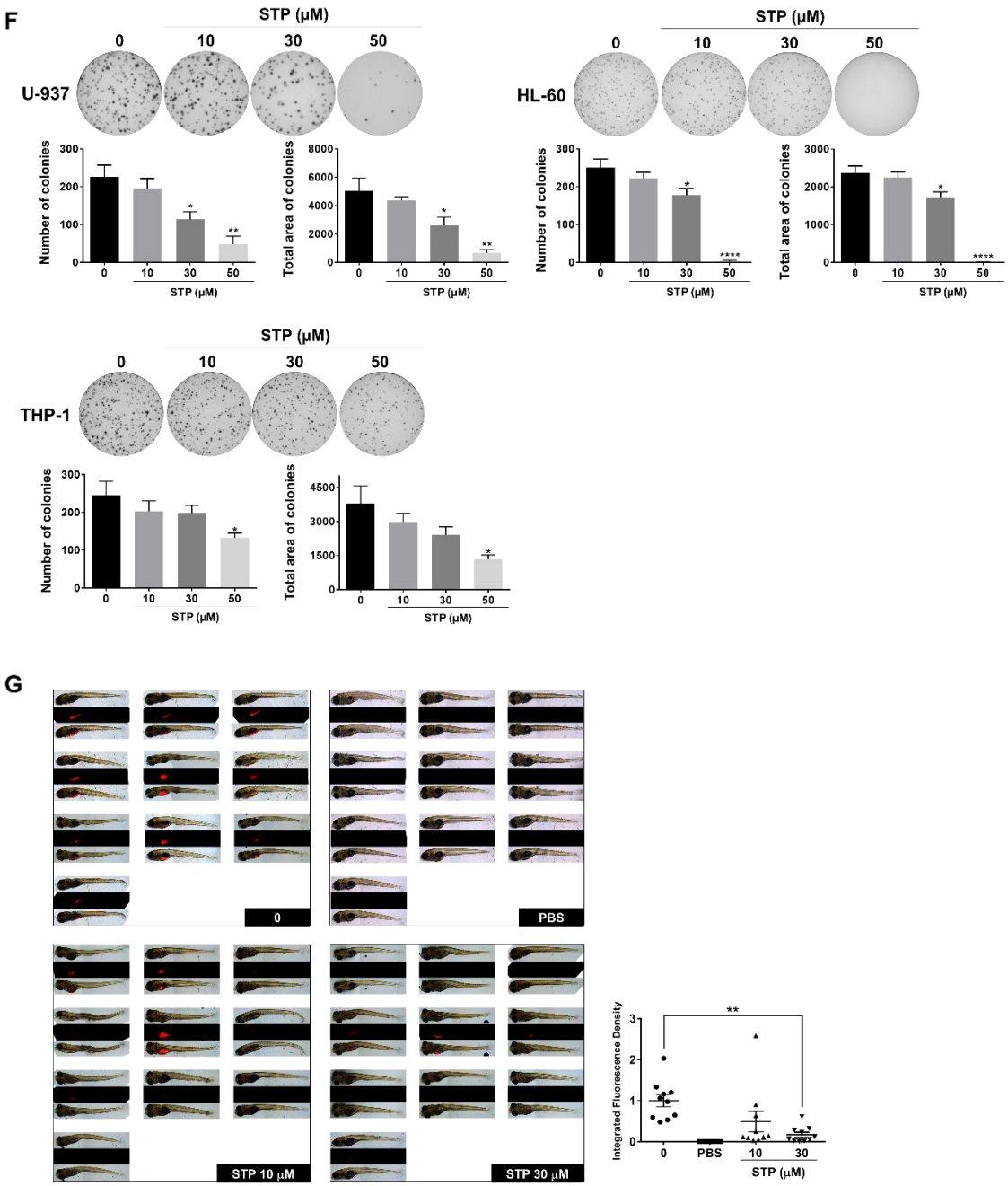

Figure 3.1. Stemphol induces cytotoxicity in human leukemia cells *in vitro* and *in vivo*. (A) Chemical structure of stemphol (2-butyl-5-pentylbenzene-1,3-diol; STP). Time- and dose-dependent effect of STP on cytotoxicity and

proliferation were assessed in **(B)** human leukemia, **(C)** A549 and MCF-7 cells by trypan blue exclusion assay. **(D)** Cytotoxicity of STP on human peripheral blood mononuclear cells (PBMCs) and **(E)** differential toxicity in PBMCs and U-937. **(F)** Inhibitory effect of increasing concentrations of STP on colony formation. **(G)** *In vivo* antitumor forming ability by STP was evaluated by zebrafish xenografts. Top: bright field, middle: CM-Dil, bottom: merge. All data represent the mean ± S.E.M. of three independent experiments. Statistical significance was assessed as *P≤0.05; **P≤0.01; ***P≤0.001; ****P≤0.0001.

Table 3.1. IC_{50} of STP on human leukemia cell lines. IC_{50} values were evaluated after indicated time point of STP treatment.

		IC_{50} (μM)			
	Cell line	**8 h**	**24 h**	**48 h**	**72 h**
Leukemia	**K-562**	> 100	54.9 ± 2.8	31.5 ± 0.8	29.1 ± 0.7
	Jurkat	> 100	45.6 ± 2.2	33.9 ± 1.0	27 ± 0.5
	RAJI	> 100	47.4 ± 3.3	26.7 ± 0.9	18.7 ± 0.8
	U-937	> 100	60.1 ± 2.4	31.3 ± 1.0	22.6 ± 1.2
Lung carcinoma	**A549**	> 100	> 100	60.92 ± 3.2	48.2 ± 1.9
Breast adenocarcinoma	**MCF7**	> 100	85.3 ± 8.5	64.2 ± 5.6	44.6 ± 2.7

3.4.2. Stemphol induces differential cell death modalities

Since STP decreased the viability of cancer cell lines, we then investigated STP-induced cell death modalities. As a first approach, we quantified the morphological changes of STP-treated U-937 nuclei after Hoechst and propidium iodide (PI) staining. Results showed that STP-induced both apoptosis characterized by nuclear condensation and fragmentation as well as PI-positive necrosis-like cellular demise from 30 µM at 8 hours (Fig 3.2A), quantified by trypan blue staining and colony forming assays. Interestingly, STP triggered apoptosis in a caspase-independent manner as pretreatment by zVAD did not prevent apoptosis. Further luminescent caspase 3/7 assays ascertained this observation as STP did not induce significant caspase 3/7 activation compared to etoposide used as a *bona fide* control for the induction of caspase-dependent apoptosis (Fig 3.2B). In agreement with the onset of a non-apoptotic type cell death, STP significantly and dose-dependently decreased intracellular ATP levels (Fig 3.2C).

We next investigated the mechanism involved in caspase-independent cell death (CICD) by using specific inhibitors. Our results showed that the poly [ADP-ribose] polymerase 1 (PARP-1) inhibitor 3-aminobenzamide (3-AB) did not significantly recover STP-induced cell death, excluding a PARP-1-dependent cell death mechanism (Fig 3.2D). In the absence of caspase involvement, we assessed the effect of two different cathepsin inhibitors, E64D for cysteine and pepstatin A for aspartyl cathepsins, which were also unable to rescue STP-triggered cell death (Fig 3.2E, F).

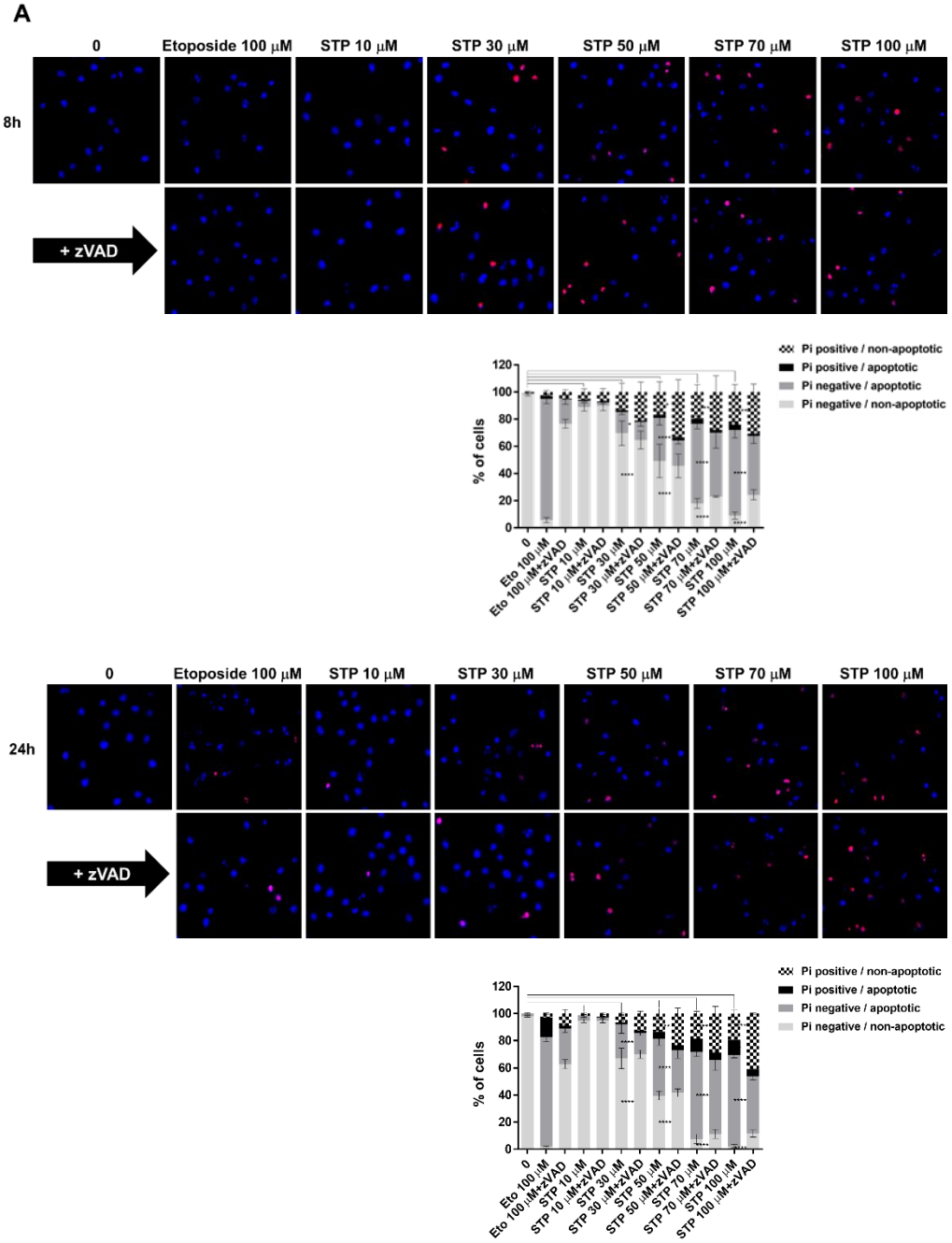
A
0
Etoposide 100 μM
STP 10 μM
STP 30 μM
STP 50 μM
STP 70 μM
STP 100 μM
8h
+ zVAD
Pi positive / non-apoptotic
Pi positive / apoptotic
Pi negative / apoptotic
Pi negative / non-apoptotic
% of cells
0
Eto 100 μM
Eto 100 μM+zVAD
STP 10 μM
STP 10 μM+zVAD
STP 30 μM
STP 30 μM+zVAD
STP 50 μM
STP 50 μM+zVAD
STP 70 μM
STP 70 μM+zVAD
STP 100 μM
STP 100 μM+zVAD
24h

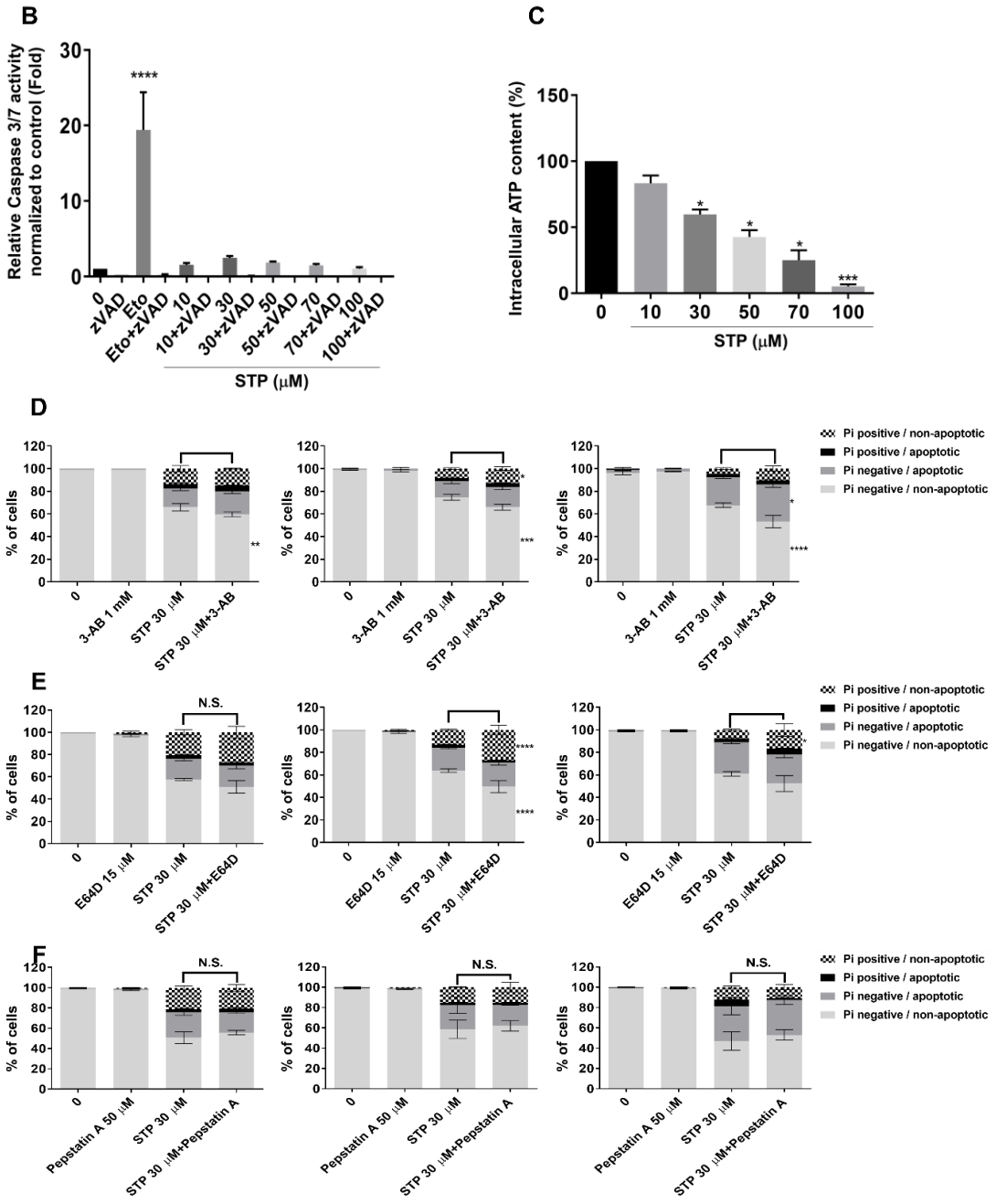

Figure 3.2. Stemphol induces different cell death modalities. (A) Cell death modalities triggered by STP were identified by Hoechst/PI staining. Etoposide (Eto) was used as a positive control for apoptosis induction. U-937 cells were treated with STP with or without 50 μM zVAD for 8 hours, and the effect of

STP was assessed on **(B)** caspase 3/7 activity and **(C)** intracellular ATP levels. Time-dependent effect of a pretreatment by selected inhibitors prior to 8 (left), 12 (middle) and 24 hours (right) STP (30 μM) treatment: **(D)** 3-AB (1 mM), **(E)** E64D (15 μM) and **(F)** pepstatin A (50 μM). All data represent the mean ± S.E.M. of three independent experiments. Statistical significance was assessed as *P≤0.05; **P≤0.01; ***P≤0.001; ****P≤0.0001 and N.S. is for non-significant.

3.4.3. Stemphol induces apoptosis by increasing cytosolic calcium levels

Since selected anticancer compounds were shown to trigger CICD by perturbation of Ca^{2+} homeostasis [75], we first assessed the effect of STP on intracellular Ca^{2+} accumulation. By using Fluo-3-AM as a probe, our results showed a 2- to 4-fold increase of cytosolic Ca^{2+} levels in AML cell lines triggered by STP at 30 μM as early as 30 minutes after the treatment. This induction is comparable to the effect of TSG, used as a positive control for increased intracellular calcium (Fig 3.3A), thus implying that Ca^{2+} movements are potentially involved in STP-triggered cell demise.

To further ascertain our results and to determine the origin of the Ca^{2+} accumulating in STP-treated cells, we used EGTA as an extracellular Ca^{2+} chelator to block extracellular Ca^{2+} influx (Fig 3.3B). Any changes in cellular Ca^{2+} levels would then be caused by intracellular Ca^{2+} movements. As expected,

TSG alone led to a rapid increase in intracellular Ca^{2+} levels due to inhibition of SERCA. On the other hand, when we used cells pretreated with STP for 30 to 120 minutes, TSG was unable to trigger any cytosolic Ca^{2+} accumulation, most likely due to a complete STP-induced depletion of Ca^{2+} from the endoplasmic reticulum (Fig 3B). Acute treatment with STP in the presence of EGTA showed that STP increased cytosolic Ca^{2+} at levels comparable to those obtained with TSG reaching a plateau after 90 seconds, implying that STP-activated ER Ca^{2+} release is an immediate response (Fig 3.3C).

As both inositol 1, 4, 5-trisphosphate receptor (IP_3R) and ryanodine receptor (RyR) Ca^{2+} release channels could potentially be involved in cytosolic Ca^{2+} accumulation triggered by STP, we assessed the effect of 2-aminoethoxydiphenyl borate (2-APB), an IP_3R inhibitor and dantrolene, a RyR inhibitor on cytosolic Ca^{2+} accumulation. Our results show that 2-APB significantly reduced cytosolic Ca^{2+} levels induced by STP from 30 mM (Fig 3.3D), whereas dantrolene showed only a weak but significant effect at 100 mM (Fig 3.3E). Altogether, we concluded that STP facilitated Ca^{2+} release from ER to cytosol essentially through IP_3R.

We further investigated ER stress and unfolded protein response (UPR) triggered by luminal ER calcium depletion [76]. Stemphol rapidly increased activating transcription factor (ATF)-4 protein levels between 30 and 60 minutes to reach a 14-fold induction after 2 hours, while glucose-regulated protein, 78 kDa

(GRP78) and CHOP expression did not change up to 8 hours (Fig 3.3F). Moreover, we observed rapidly increased levels of eukaryotic translation initiation factor (eIF2a) phosphorylation from 15 minutes to reach a 9-fold increase at 30 minutes.

Since STP was shown to induce ER Ca^{2+} release at levels comparable to those obtained with TSG, we hypothesized that STP could undergo a direct interaction with SERCA triggering Ca^{2+} release. To validate our hypothesis, we conducted a docking simulation using Autodock Vina (version 1.1.2) software [77]. Crystal structure of SERCA in complex with TSG (Protein Data Bank ID: 5A3Q), [78] was used as a template of docking and predicted binding affinity energy was -8.7 kcal/mol. Based on docking simulation, STP was located at the same site as TSG on SERCA with the binding energy of -6.0 kcal/mol. In details, STP is predicted to bind to hydrophobic pocket of SERCA formed by transmembrane helices numbered in M3, M5 and M7 near the cytoplasmic surface of the membrane. Two hydroxyl groups of STP is expected to have polar interaction with amine groups of Ile829 and Phe256 (Fig 3.3G) which are important sites of SERCA for Ca^{2+} regulation. Once TSG binds to those spots, SERCA becomes fixed in a form analogous to E2 state, thus blocking conformational change for the influx of Ca^{2+} [79]. Based on the docking simulation, we suggest that STP acts as a SERCA inhibitor comparable to TSG.

Next, to link the onset of CICD to the observed Ca^{2+} changes, we decided to assess the effect of STP on cell death induction in the presence of a cytosolic Ca^{2+} chelator, BAPTA-AM. BAPTA-AM significantly induced apoptosis in U-937 cells alone (5 μM) underlining the essential role of Ca^{2+} homeostasis in the survival of U-937 cells (data not shown) or in combination with STP (30 μM) (Fig 3.3H). To disentangle the pro-apoptotic effect of BAPTA-AM from STP-induced CICD, we co-treated U-937 cells with zVAD and BAPTA-AM, which abrogated the pro-apoptotic caspase-dependent effect of the Ca^{2+} chelator alone so that remaining cell death modulation by STP was essentially due to CICD. Our results showed that a treatment by zVAD and BAPTA-AM reduced STP-triggered CICD (Fig 3.3I), which was completely blocked when EGTA, an extracellular Ca^{2+} chelator, was added (Fig 3.3J). Altogether, our approach validated that the STP-induced CICD was most likely caused by cytosolic Ca^{2+} accumulation. Residual levels of necrosis (Fig 3.3I, J) could nevertheless not be prevented by this approach.

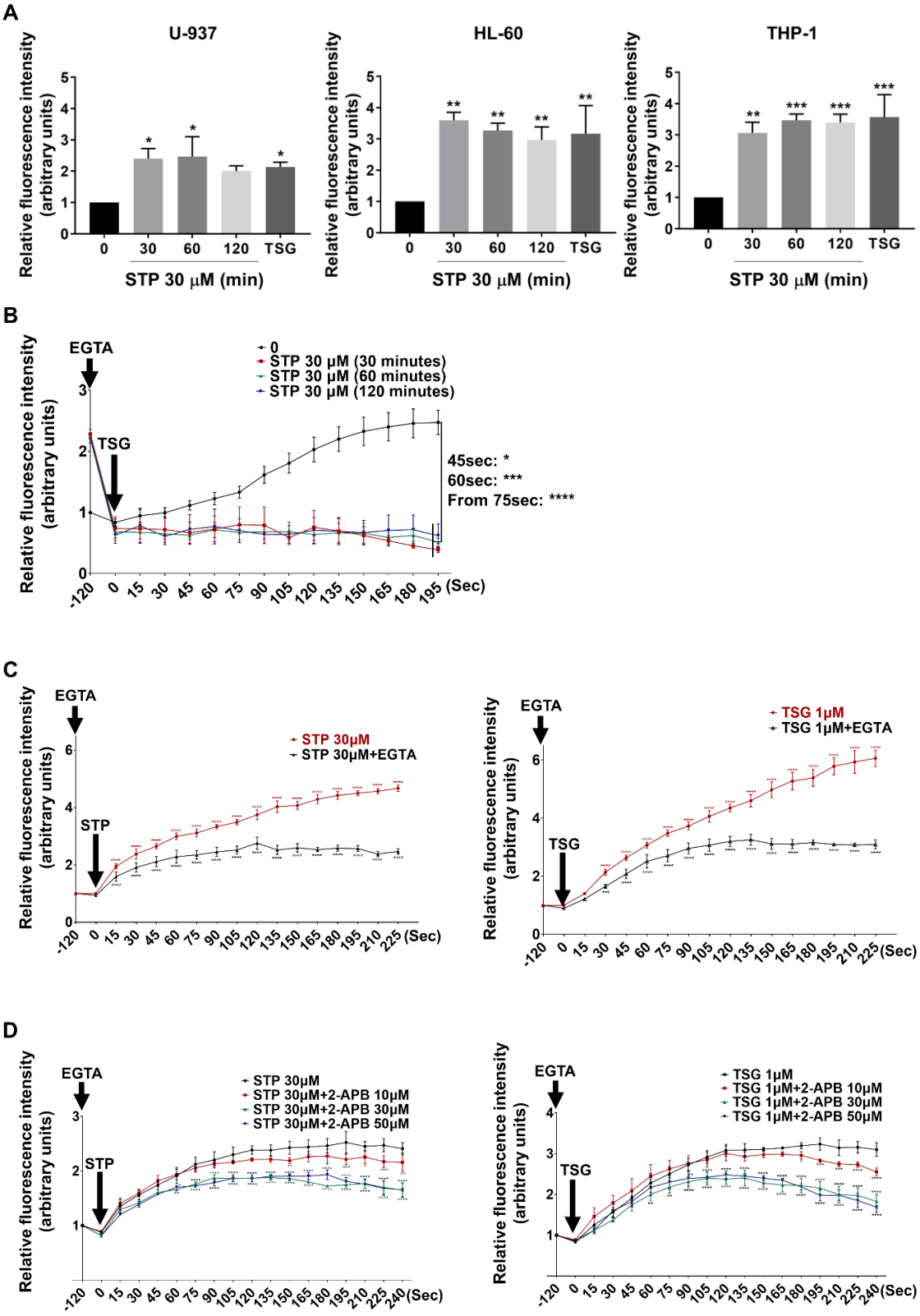
A
U-937
HL-60
THP-1
Relative fluorescence intensity (arbitrary units)
0
30
60
120
TSG
STP 30 μM (min)
B
EGTA
TSG
0
STP 30 μM (30 minutes)
STP 30 μM (60 minutes)
STP 30 μM (120 minutes)
45sec: *
60sec: ***
From 75sec: ****
(Sec)
C
EGTA
STP
STP 30μM
STP 30μM+EGTA
TSG
TSG 1μM
TSG 1μM+EGTA
D
STP 30μM
STP 30μM+2-APB 10μM
STP 30μM+2-APB 30μM
STP 30μM+2-APB 50μM
TSG 1μM
TSG 1μM+2-APB 10μM
TSG 1μM+2-APB 30μM
TSG 1μM+2-APB 50μM

E

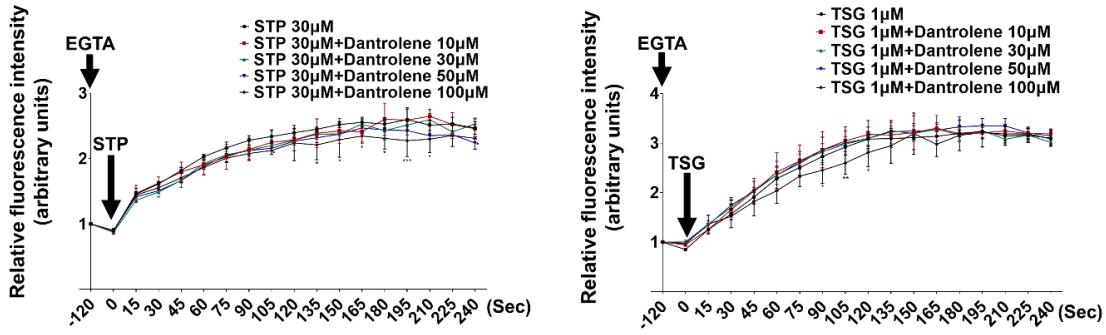
EGTA
STP
STP 30μM
STP 30μM+Dantrolene 10μM
STP 30μM+Dantrolene 30μM
STP 30μM+Dantrolene 50μM
STP 30μM+Dantrolene 100μM
Relative fluorescence intensity (arbitrary units)
(Sec)
EGTA
TSG
TSG 1μM
TSG 1μM+Dantrolene 10μM
TSG 1μM+Dantrolene 30μM
TSG 1μM+Dantrolene 50μM
TSG 1μM+Dantrolene 100μM
Relative fluorescence intensity (arbitrary units)
(Sec)

F

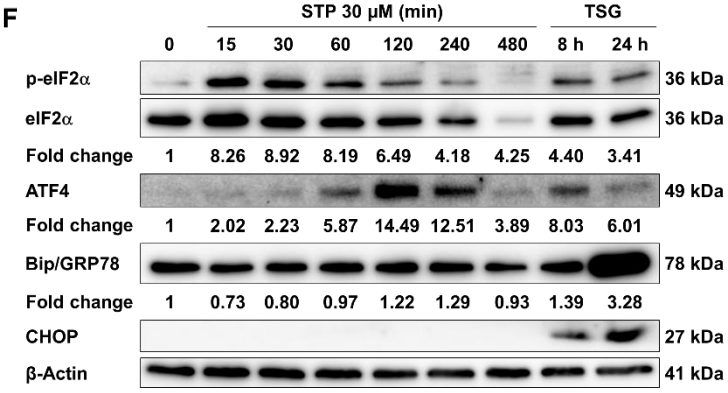
STP 30 μM (min)
TSG
0 15 30 60 120 240 480 8 h 24 h
p-eIF2α
36 kDa
eIF2α
36 kDa
Fold change 1 8.26 8.92 8.19 6.49 4.18 4.25 4.40 3.41
ATF4
49 kDa
Fold change 1 2.02 2.23 5.87 14.49 12.51 3.89 8.03 6.01
Bip/GRP78
78 kDa
Fold change 1 0.73 0.80 0.97 1.22 1.29 0.93 1.39 3.28
CHOP
27 kDa
β-Actin
41 kDa

G

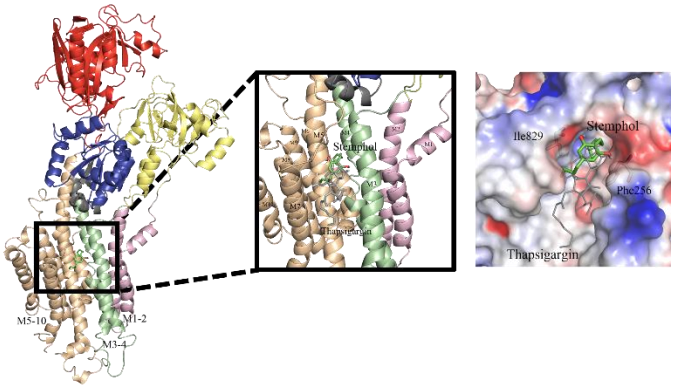
Stemphol
Thapsigargin
M5-10
M1-2
M3-4
Ile829
Stemphol
Phe256
Thapsigargin

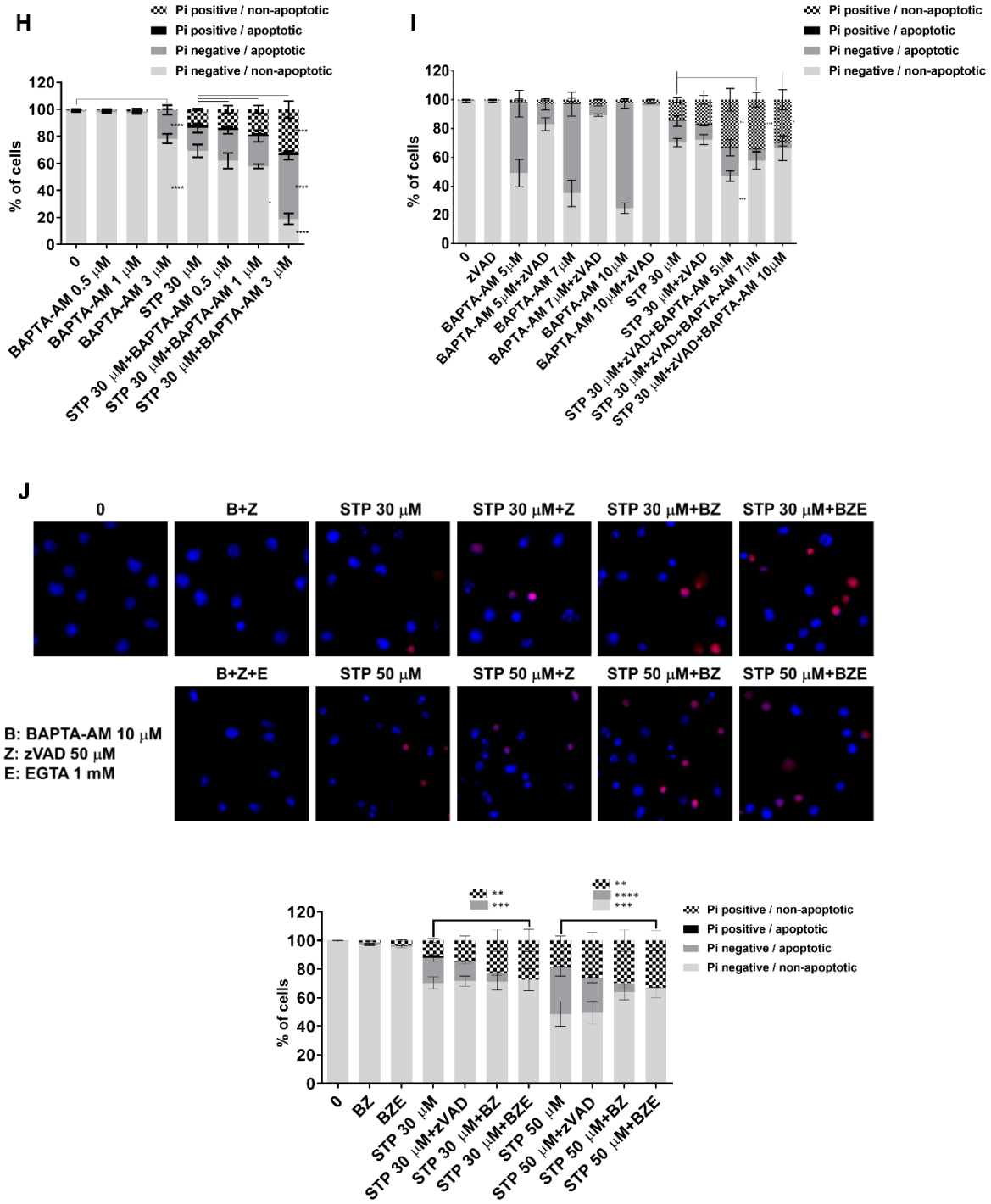

Figure 3.3. Stemphol induces caspase-independent apoptosis by facilitating endoplasmic reticulum Ca^{2+} release. (A) U-937, HL-60 and THP-1 cells were

treated with STP (30 μM) for indicated time points, and cytosolic Ca2+ levels were measured by Fluo-3-AM. Thapsigargin (TSG; 1 μM, 30 minutes) was used as a positive control intracellular calcium accumulation. In the presence of 650 μM EGTA, cytosolic Ca2+ levels were measured every 15 seconds in **(B)** STP-pretreated cells and **(C)** STP acute-treated cells. U-937 cells were treated with 650 μM EGTA and the indicated concentration of **(D)** 2-APB or **(E)** dantrolene, and cytosolic Ca2+ levels were measured every 15 seconds in STP acute-treated cells. All data represent the mean ± S.E.M. of three independent experiments. **(F)** ER stress-related proteins were detected by western blot. β-actin was used as a loading control. After quantification of the bands, p-eIF2α levels were normalized to total eIF2α and all other proteins were normalized to β-actin. **(G)** Full length structure of SERCA protein is represented as a cartoon model with a different color for each domain. STP is shown as a stick model in green (carbon) and red (oxygen). Right figures show close-up images of SERCA shown as cartoon and electrostatic potential surface with STP and TSG (stick in grey) occupying the same binding site. Calculated electrostatic potential surface is represented as positively and negatively charged surfaces in blue and red, respectively. **(H)** Low (0.5, 1 and 3 μM) concentrations of BAPTA-AM were used to pretreat U-937 cells before 8 hours of STP (30 μM) treatment, and its effect was evaluated on STP-induced cell death modalities. **(I)** Combined effect of zVAD (50 μM) and BAPTA-AM (10 μM) pretreatment (1 hour). **(J)** Effect on STP-induced cell death modalities by BAPTA-AM (10 μM), EGTA (1 mM) and

zVAD (50 μM) pretreatment (1 hour) and its effect was evaluated on STP-induced cell death modalities. Statistical significance was assessed as *P≤0.05; **P≤0.01; ***P≤0.001; ****P≤0.0001.

3.4.4. Stemphol-induced necrosis-like cell death is due to mitochondrial calcium overload

To further determine the origin of STP-induced necrosis, we first pretreated cells for 1 hour with necrostatin-1 (Nec-1) and necrosulfonamide (NSA), inhibitors of receptor interacting serine/threonine kinase (RIPK)1 and mixed lineage kinase domain like pseudokinase (MLKL), respectively which failed to prevent STP-induced necrosis (Fig 3.4A, B). Moreover, zVAD did not significantly modulate the effect of STP-induced necrosis (Fig 3.4A, B). Considering the extensive cytoplasmic vacuolization observed after Diff-quick staining of STP-treated U-937 cells (Fig 3.4C) we assessed the effect of paraptosis inhibitors cycloheximide and mitogen-activated protein kinase (MAPK) inhibitors which did not affect necrosis triggered by STP (Fig 3.4D, E).

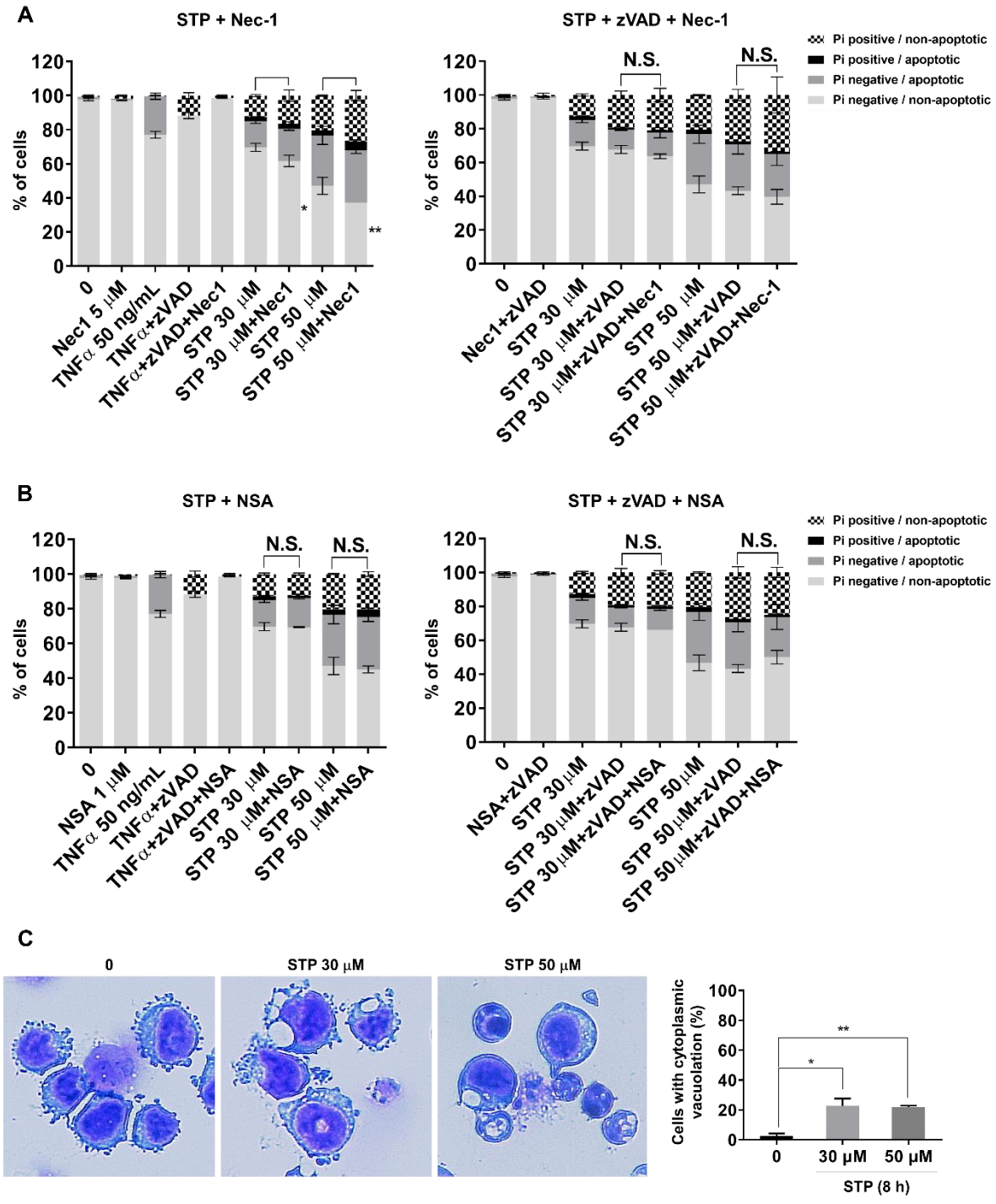
A
STP + Nec-1
STP + zVAD + Nec-1
% of cells
Pi positive / non-apoptotic
Pi positive / apoptotic
Pi negative / apoptotic
Pi negative / non-apoptotic
N.S.
0
Nec1 5 μM
TNFα 50 ng/mL
TNFα+zVAD
TNFα+zVAD+Nec1
STP 30 μM
STP 30 μM+Nec1
STP 50 μM
STP 50 μM+Nec1
Nec1+zVAD
STP 30 μM+zVAD
STP 30 μM+zVAD+Nec1
STP 50 μM+zVAD
STP 50 μM+zVAD+Nec-1
B
STP + NSA
STP + zVAD + NSA
NSA 1 μM
TNFα 50 ng/mL
TNFα+zVAD
TNFα+zVAD+NSA
STP 30 μM+NSA
STP 50 μM+NSA
NSA+zVAD
STP 30μM+zVAD
STP 30μM+zVAD+NSA
STP 50μM
STP 50μM+zVAD
STP 50μM+zVAD+NSA
C
0
STP 30 μM
STP 50 μM
Cells with cytoplasmic vacuolation (%)
30 μM
50 μM
STP (8 h)

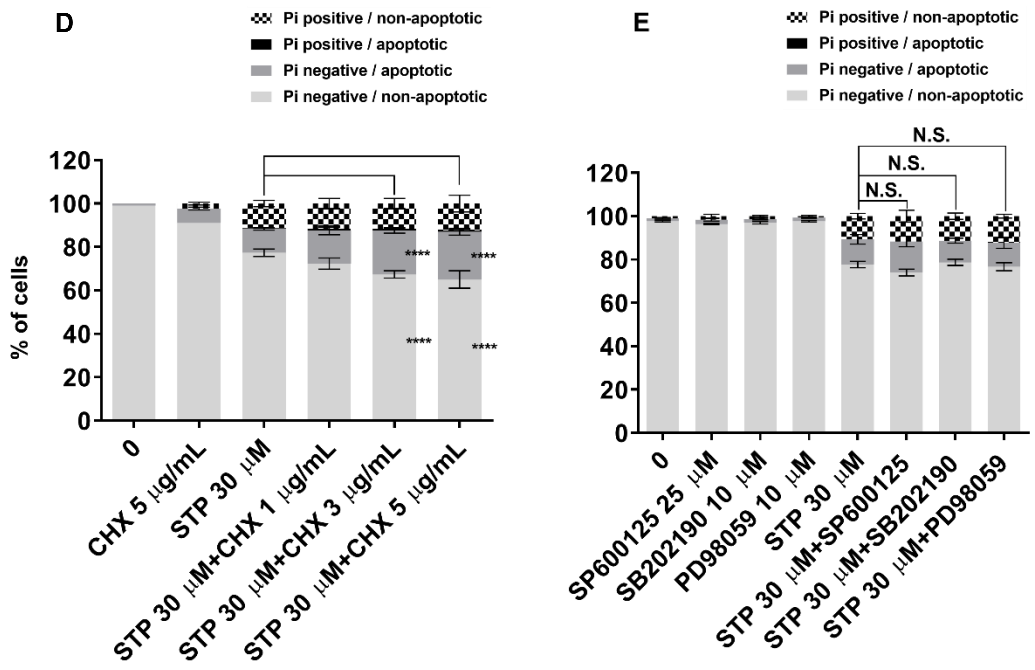

Figure 3.4. Characterization of stemphol-induced regulated necrosis. U-937 cells were pretreated with **(A)** Nec-1 or **(B)** NSA with or without zVAD and effects on STP-induced necrosis were quantified by Hoechst/PI staining. **(C)** Stemphol-triggered cytoplasmic vacuoles were evaluated by Diff-Quik staining. Cells with vacuoles were quantified. Cells were pretreated with paraptosis inhibitors **(D)** CHX, and **(E)** MAPK inhibitors and STP-induced necrosis was assessed. All data represent the mean ± S.E.M. of three independent experiments. Statistical significance was assessed as *P≤0.05; **P≤0.01; ***P≤0.001; ****P≤0.0001 and N.S. is for non-significant.

Transmission electron microscopy (TEM) revealed that STP treatment led to an irregular morphology of mitochondria with swollen and collapsed cristae at 30

mM (Fig 3.5A). As such morphological alterations of mitochondria could also be caused by Ca^{2+} overload [80], we measured Ca^{2+} levels in mitochondria by using Rhod2-AM, a fluorescent mitochondrial Ca^{2+} probe (Fig 3.5B). We used confocal laser microscopy for a quantitative analysis of the co-localization of Rhod2-AM and MitoTracker Green. Results clearly indicated that STP significantly induced Ca^{2+} overload in mitochondria from 4 hours by around 50 %. Etoposide, a common inducer of caspase-dependent apoptosis, did not increase Ca^{2+} in mitochondria. Pretreatment by Ru360, an inhibitor of the mitochondrial Ca^{2+} uniporter (MCU) significantly inhibited STP-induced cell death from 2 hours by 50 %, and it showed a preferential inhibitory effect on necrosis (Fig 3.5C). These results implied that STP-induced Ca^{2+} overload in mitochondria occurred through MCU, eventually causing necrosis.

For the next step of our investigation, we tempted to ascertain the origin of the mitochondrial overload by STP. As previously demonstrated (Fig 3.3I, J), STP triggered necrosis even in the presence of intra- and extracellular Ca^{2+} chelators like BAPTA-AM and EGTA. These results exclude a direct transfer of Ca^{2+} from the cytosol or the extracellular medium into the mitochondria. Moreover, our data showed that pretreatment by BAPTA-AM did not alter the STP-induced co-localization of MitoTracker Green and Rhod2-AM, further strengthening our hypothesis that the origin of the STP-induced Ca^{2+} is not cytosolic (Fig 3.5D). On the other hand, unlike BAPTA-AM, 2-APB and Ru360 significantly reduced co-localization, implying that IP_3R and MCU are crucial regulators of STP-

induced mitochondrial Ca^{2+} overload. As mitochondrial Ca^{2+} overload leads to opening of mPTP, finally triggering necrosis, we used cyclosporine A (CsA), which is a potent inhibitor of mPTP opening. CsA did not inhibit STP-induced necrosis alone (Fig 3.5E). In contrast, CsA significantly inhibited approximately 50 % of STP-induced necrosis by a combination treatment with MCU inhibitor Ru360 (5 μM), which has no inhibitory effect on STP-induced necrosis alone (Fig 3.5F). Calcein/cobalt assays confirmed this result and showed that STP triggered mPTP opening in a time-dependent manner in various AML cell lines including U-937, HL-60 and THP-1 (Fig 3.5G, H, I). Interestingly, a combination of CsA and Ru360 significantly reduced the number of cells with mPTP opening (Fig 3.5J). Besides Ca^{2+}, ROS are well known as secondary messengers of necrosis. As mitochondria are sites of intense ROS production, we additionally investigated changes of ROS levels after STP treatment. Results showed that STP significantly decreased ROS levels from 10 mM after 4 hours of treatment and from 30 μM after 30 minutes (Fig 3.5K). Besides, STP significantly decreased the oxygen consumption rate (OCR) of basal respiration, maximal respiration and ATP production (Fig 3.5L). The result implied that STP decreased mitochondrial bioenergetics, in agreement with our TEM observations of damaged mitochondrial morphologies.

Altogether, in addition to its effect on SERCA, we concluded here that STP induced an ROS-independent type of mPTP opening-dependent necrosis by

facilitating Ca^{2+} transfer from ER to mitochondria, essentially through IP_3R and MCU.

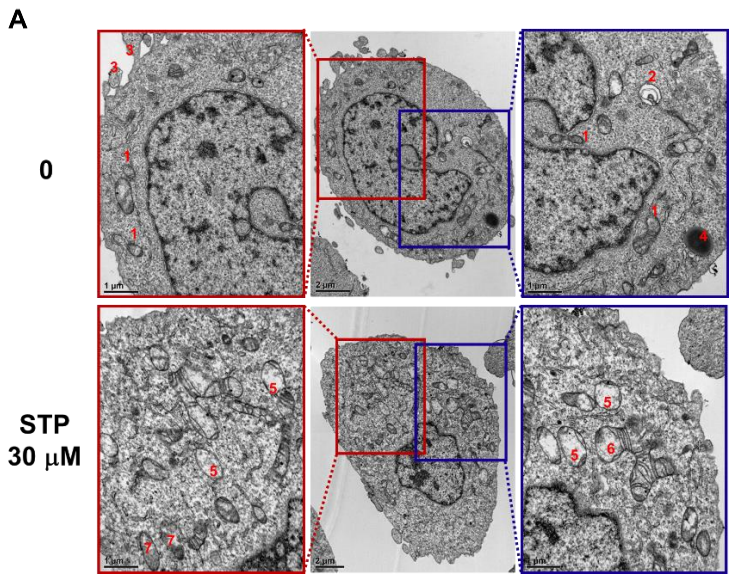

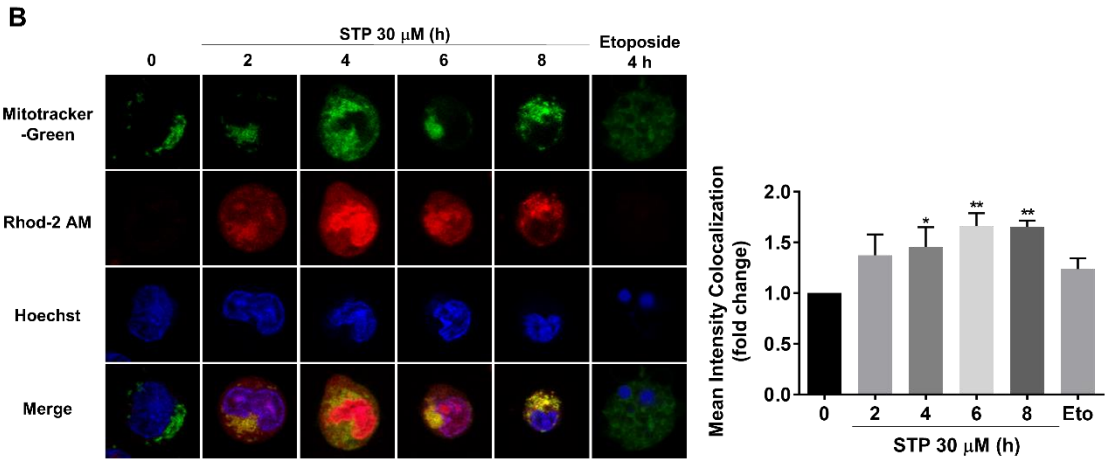

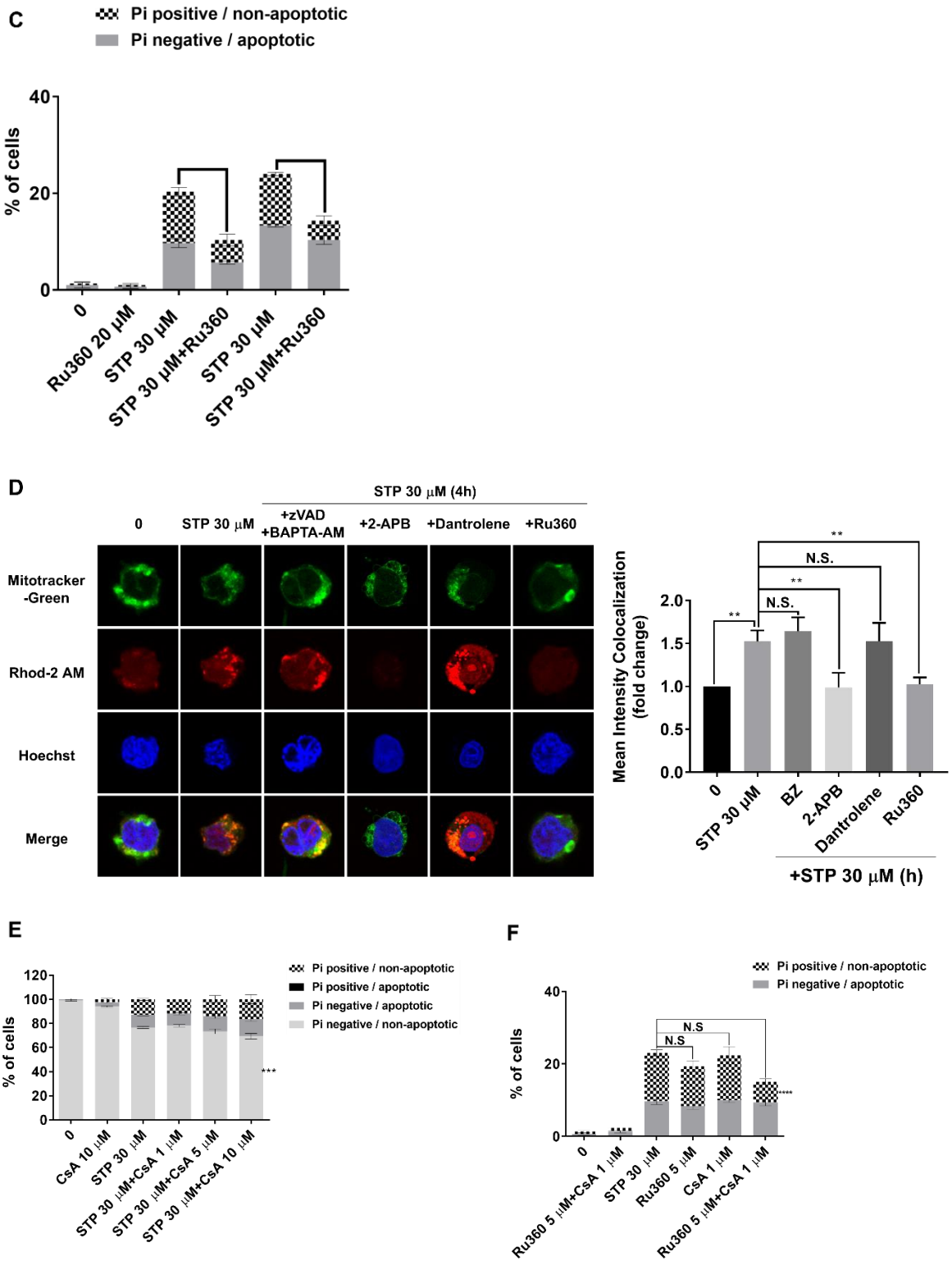
C
Pi positive / non-apoptotic
Pi negative / apoptotic
% of cells
40
20
0
0
Ru360 20 μM
STP 30 μM
STP 30 μM+Ru360
STP 30 μM
STP 30 μM+Ru360
D
STP 30 μM (4h)
0
STP 30 μM
+zVAD
+BAPTA-AM
+2-APB
+Dantrolene
+Ru360
Mitotracker
-Green
Rhod-2 AM
Hoechst
Merge
Mean Intensity Colocalization
(fold change)
2.0
1.5
1.0
0.5
0.0
**
N.S.
**
N.S.
**
0
STP 30 μM
BZ
2-APB
Dantrolene
Ru360
+STP 30 μM (h)
E
Pi positive / non-apoptotic
Pi positive / apoptotic
Pi negative / apoptotic
Pi negative / non-apoptotic
% of cells
120
100
80
60
40
20
0
***
0
CsA 10 μM
STP 30 μM
STP 30 μM+CsA 1 μM
STP 30 μM+CsA 5 μM
STP 30 μM+CsA 10 μM
F
Pi positive / non-apoptotic
Pi negative / apoptotic
% of cells
40
20
0
N.S
N.S
****
0
Ru360 5 μM+CsA 1 μM
STP 30 μM
Ru360 5 μM
CsA 1 μM
Ru360 5 μM+CsA 1 μM

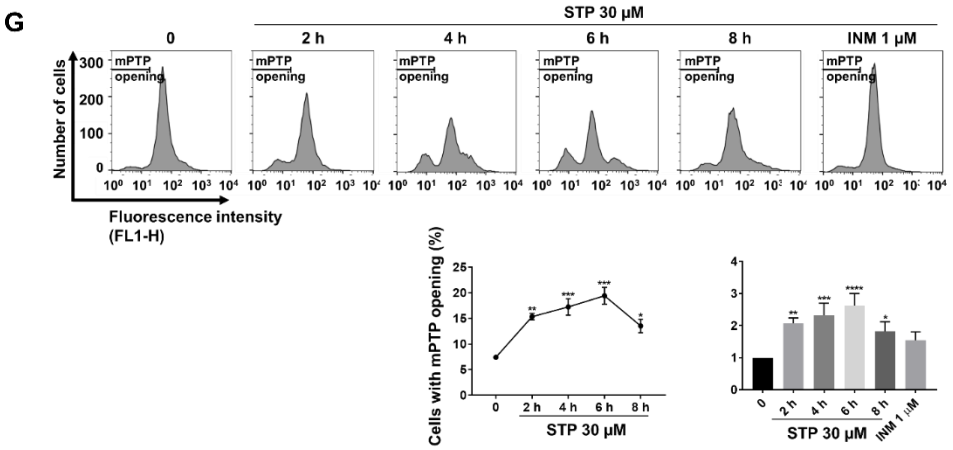
G
STP 30 μM
0
2 h
4 h
6 h
8 h
INM 1 μM
mPTP opening
Number of cells
Fluorescence intensity (FL1-H)
Cells with mPTP opening (%)
STP 30 μM
Relative level of mPTP opening (fold change)
INM 1 μM

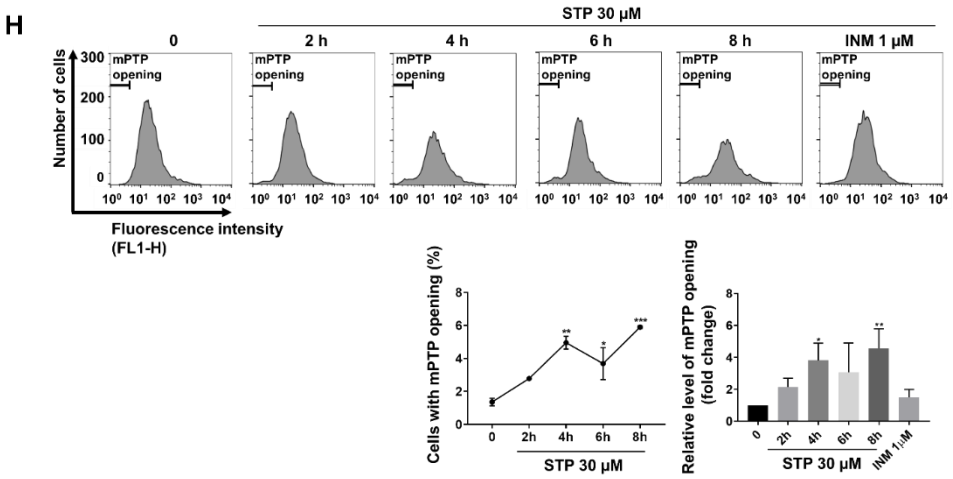
H
STP 30 μM
0
2 h
4 h
6 h
8 h
INM 1 μM
mPTP opening
Number of cells
Fluorescence intensity (FL1-H)
Cells with mPTP opening (%)
STP 30 μM
Relative level of mPTP opening (fold change)
INM 1 μM

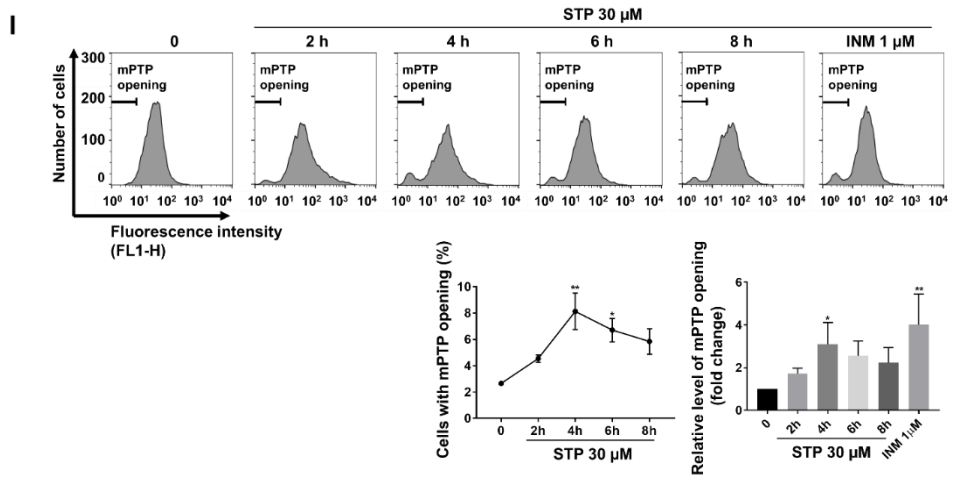
I
STP 30 μM
0
2 h
4 h
6 h
8 h
INM 1 μM
mPTP opening
Number of cells
Fluorescence intensity (FL1-H)
Cells with mPTP opening (%)
STP 30 μM
Relative level of mPTP opening (fold change)
INM 1 μM

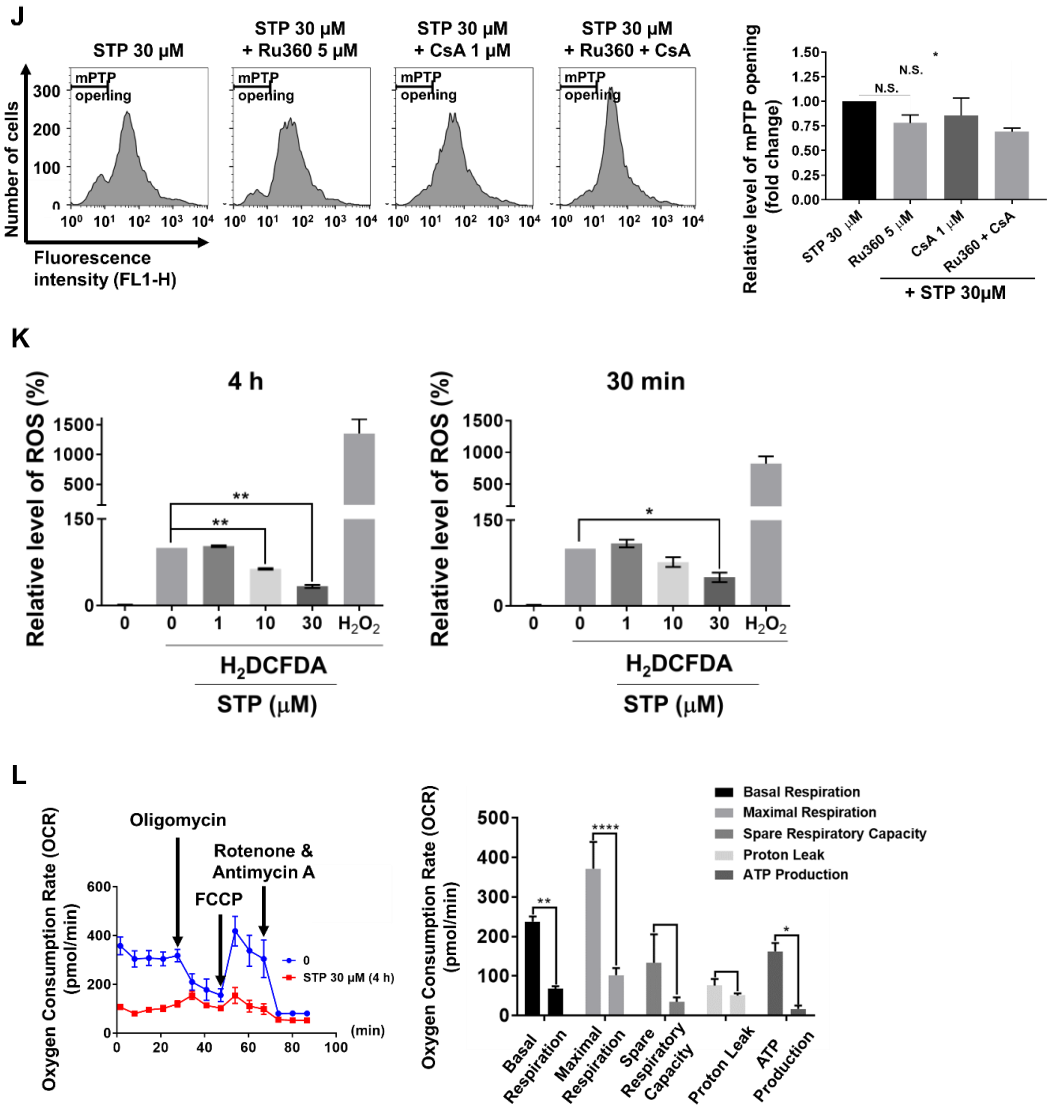

Figure 3.5. Stemphol-triggered mitochondrial Ca^{2+} overload is causing programmed necrosis. (A) U-937 cells were treated with STP and investigated by TEM at 12.000x and 25.000x magnification: (1) normal mitochondria; (2) autophagolysosome; (3) blebs; (4) lysosome; (5) edematous mitochondria; (6) mega-mitochondria and (7) mitochondrial microautophagy. **(B)** Cells were

treated with 30 μM of STP at indicated time points and observed by confocal immunofluorescence microscopy after staining with MitoTracker Green, Rhod2-AM, and Hoechst. The intensity of the Rhod2-AM signal was quantified in the region also stained with MitoTracker Green by Leica LAS-X software platform. **(C)** U-937 cells were pretreated with Ru360 for 1 hour followed by STP treatment at indicated time points followed by quantification after Hoechst/PI staining. **(D)** U-937 cells were pretreated for 1 hour with zVAD, BAPTA-AM, 2-APB, dantrolene or Ru360 and treated by STP for 8 hours. Staining and quantification were performed as in (B). **(E)** U-937 cells were pretreated for 1 hour with cyclosporin A, and then treated by STP for 4 hours. Cells were quantified after Hoechst/PI staining according to the type of cell death. **(F)** Cells were pretreated for 1 hour with Ru360 or/and cyclosporin A, and then treated by STP for 4 hours. Cells were quantified after Hoechst/PI staining according to the type of cell death. **(G)** U-937, (H) HL-60 and (I) THP-1 cells were treated by STP for the indicated time course followed by staining with calcein-AM and quenching by $CoCl_2$. Mitochondrial permeability transition pore opening was measured using flow cytometry. 1 μM of ionomycin (INM) (8 hours) is used as a positive control for mPTP induction. **(J)** U-937 cells were pretreated for 1 hour with Ru360 or/and cyclosporine A, and treated by STP for 4 hours. After stained with calcein-AM and quenching by $CoCl_2$, the mPTP opening was measured using flow cytometry. **(K)** U-937 cells treated with STP at indicated time points were stained with H_2DCFDA and then quantified by FACSCalibur. H_2O_2 was

used as a positive control. **(L)** U-937 cells were treated with 30 μM of STP for 4 hours and oxygen consumption rate (OCR) was measured by Seahorse XFp analyzer. All data represent the mean ± S.E.M. of three independent experiments. Statistical significance was assessed as *P≤0.05; **P≤0.01; ***P≤0.001; ****P≤0.0001 and N.S. is for non-significant.

3.4.5. Inhibition of autophagy potentialized STP-triggered anticancer effect

Cytoplasmic vacuolization observed after Diff-Quik staining and TEM could also witness autophagy, a stress resistance mechanism. Furthermore, TEM observations clearly showed autophagosome formation in STP-treated cells (Fig 3.6A). As STP significantly increased LC3 I-II conversion (Fig 3.6B) and a LysoTracker Red signal witnessing an increase in lysosomal mass (Fig 3.6C), we concluded that STP could activate autophagy and thus potentially contribute in part to resistance against this compound. To validate this hypothesis, we treated cells with 30 and 50 μM STP with an autophagy inhibitor Bafilomycin A (Baf-A1) to inhibit autophagy which significantly potentialized STP-induced cell demise (Fig 3.6D).

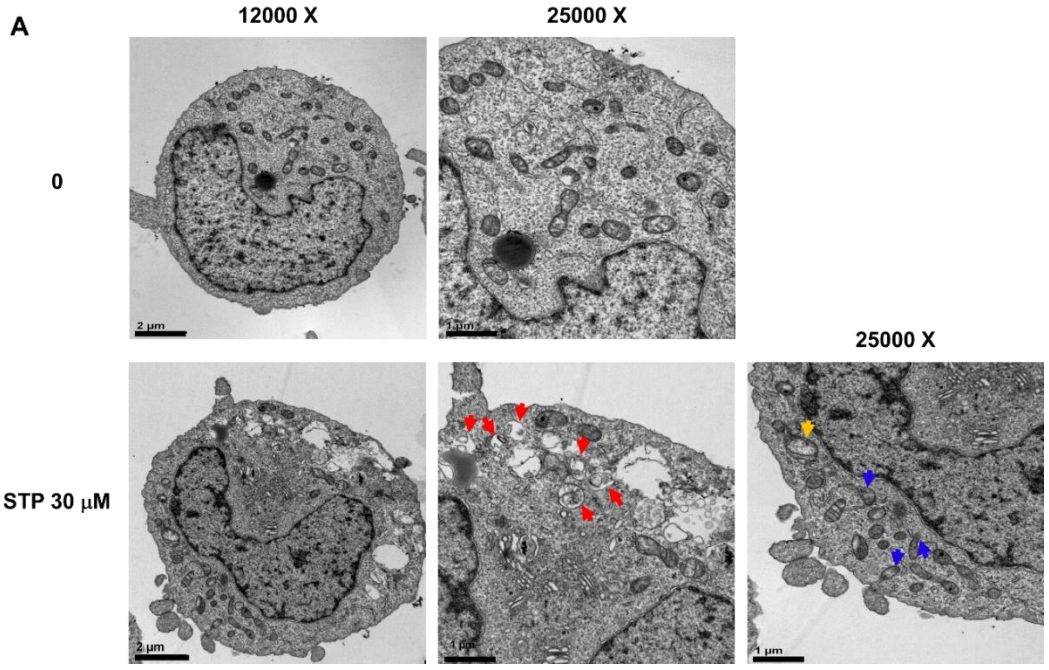
A
12000 X
25000 X
0
25000 X
STP 30 μM
2 μm
1 μm

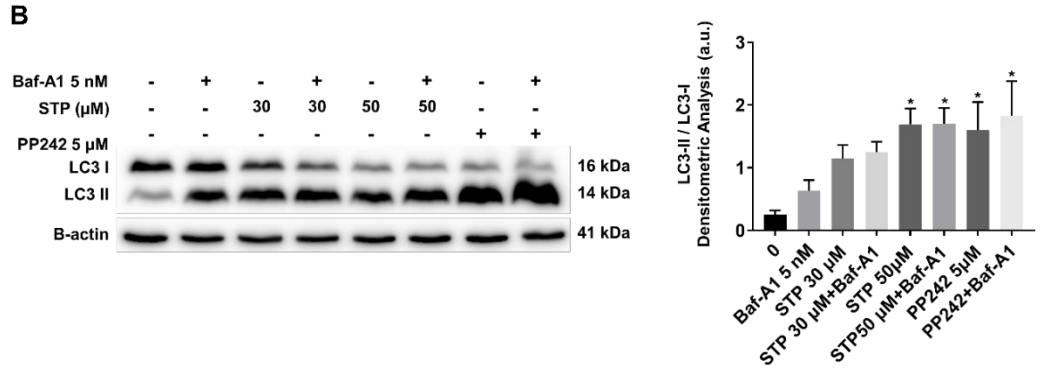
B
Baf-A1 5 nM
STP (μM)
PP242 5 μM
LC3 I
LC3 II
B-actin
16 kDa
14 kDa
41 kDa
LC3-II / LC3-I Densitometric Analysis (a.u.)
0
Baf-A1 5 nM
STP 30 μM
STP 30 μM+Baf-A1
STP 50μM
STP50 μM+Baf-A1
PP242 5μM
PP242+Baf-A1

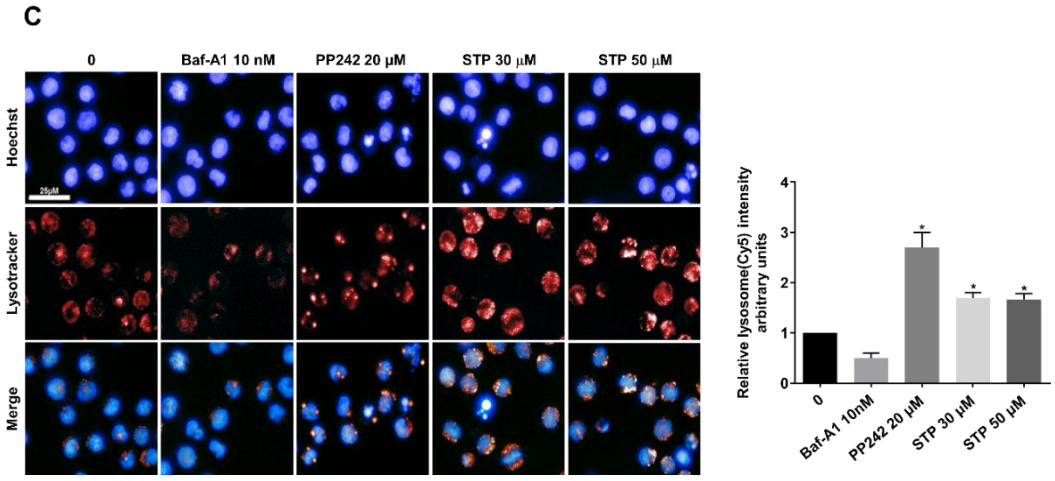
C
0
Baf-A1 10 nM
PP242 20 μM
STP 30 μM
STP 50 μM
Hoechst
Lysotracker
Merge
Relative lysosome(Cy5) intensity arbitrary units
0
Baf-A1 10nM
PP242 20 μM
STP 30 μM
STP 50 μM

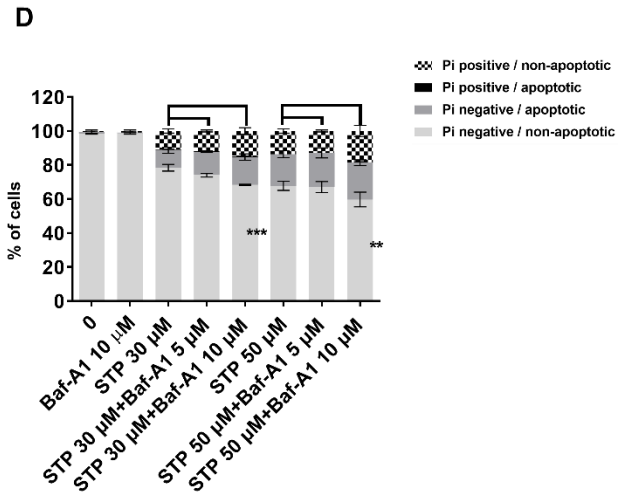

Figure 3.6. Stemphol triggered autophagy as a protective mode. (A) U-937 cells were treated with STP for 8 hours and pictures were taken by TEM at 12.000x and 25.000x magnification. Red, blue and yellow arrows indicate autophagolysosomes, mitochondrial microautophagy, and autophagosomes, respectively. **(B)** U-937 cells were pretreated with Baf-A1 for two h before the end of an 8 hours STP treatment. Protein were extracted, and LC3 proteins were detected by western blot. β-actin was used as a loading control. After quantification of the bands, LC3-II levels were normalized to LC3-I. PP242 (8 hours) was used as a positive control for autophagy induction. **(C)** After treatment of STP for 8 hours, U-937 cells were stained with Hoechst and LysoTracker Red. LysoTracker Red intensity was quantified by Operetta High-Content Imaging System. Baf-A1 (8 hours) and PP242 (8 hours) were used as a negative and positive control for autophagy inhibition and induction, respectively. **(D)** U-937 cells were pretreated with Baf-A1 for 1 hour and

subsequently treated with STP at 30 and 50 μM for 8 hours. After Hoechst/PI staining, STP-induced cell death modalities were quantified. All data represent the mean ± S.E.M. of three independent experiments. Statistical significance was assessed as *P≤0.05; **P≤0.01; ***P≤0.001; ****P≤0.0001.

3.4.6. Translational potential of stemphol in human leukemia

Considering that colony formation was strongly reduced when AML cell lines were treated with STP (Fig 3.1), we validated the effect of STP on cells freshly isolated from AML and ALL patients. In extension of CFAs with different cell lines (Fig 3.1C), our results showed that tumor mass formation in zebrafish was completely abrogated or significantly reduced by STP treatment (30 μM) (Fig 3.7A). Moreover, considering the ATP loss observed in cell lines and the immunogenic potential of Ca^{2+} reduction in the endoplasmic reticulum, we also validated that STP can trigger HMGB1 release in 3 out of 4 patients tested so far, further increasing the translational potential of STP (Fig 3.7B).

Finally, we used *in silico* approaches to further investigate the drug-likeness of STP. Interestingly, *in silico* approaches showed that STP has potential drug-likeness as it perfectly follows Lipinski's 'rule of five' [81] (Table 3.2). Stemphol has adequate molecular mass, high lipophilicity (LogP less than 5) and two hydrogen bond donors and acceptors, which enable efficient interaction with the hydrogen bonding groups of putative receptors.

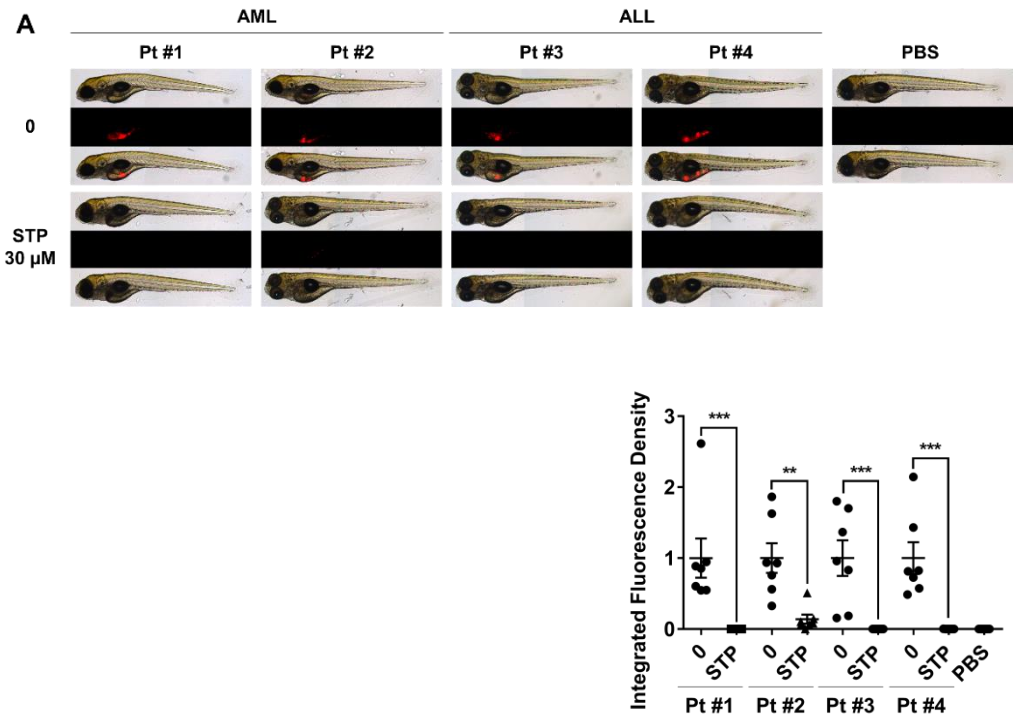
A
AML
ALL
Pt #1
Pt #2
Pt #3
Pt #4
PBS
0
STP
30 µM
Integrated Fluorescence Density
***
**
***
***
0
STP
0
STP
0
STP
0
STP
PBS
Pt #1
Pt #2
Pt #3
Pt #4
B
HMGB1 (ng/mL)
****
**
****
0
STP 30 µM
Pt #1
Pt #2
Pt #3
Pt #4
AML
ALL

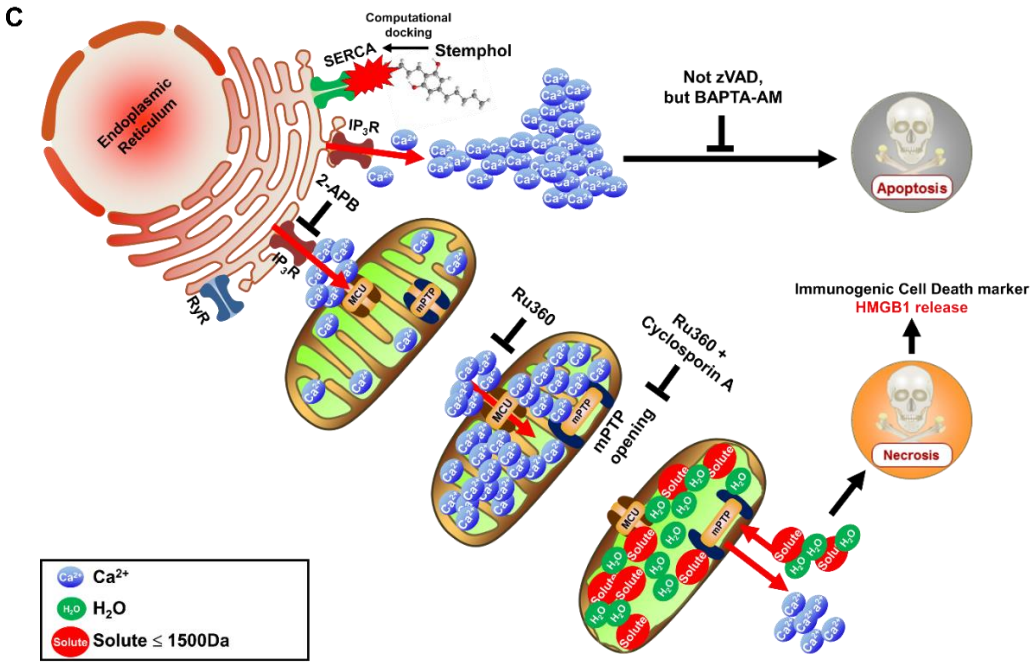

Figure 3.7. Translational potential of stemphol. (A) *In vivo* antitumor forming ability by STP was assessed in patient-derived xenograft in zebrafish. Top: bright field, middle: CM-Dil, bottom: merge. Seven zebrafish were used per condition. **(B)** HMGB1 release induced by STP. Four different patient samples were assessed for HMGB1 release, and statistical significance was assessed as *P≤0.05; **P≤0.01; ***P≤0.001; ****P≤0.0001. **(C)** Mechanism of action of stemphol in human leukemia. STP is the first resorcinol derivative able to disrupt Ca^{2+} homeostasis in ER, cytosol, and mitochondria, triggering non-canonical cell death and HMGB1 release. Arrows indicate activation and bars indicate inhibition.

2-APB, 2-aminoethoxydiphenyl borate; **BAPTA-AM**, 1,2-Bis(2-aminophenoxy) ethane-N,N,N',N'-tetraacetic acid tetrakis(acetoxymethyl

ester); **HMGB1**, high mobility group box 1; **IP$_3$R**, inositol 1,4,5-trisphosphate receptor; **MCU**, mitochondrial calcium uniporter; **mPTP**, mitochondrial permeability transition pore; **RyR**, ryanodine receptor; **SERCA**, sarco/endoplasmic reticulum Ca^{2+}-ATPase; **zVAD**, carbobenzoxy-valyl-alanyl-aspartyl-[O-methyl]-fluoromethylketone

Table 3.2. *In silico* prediction for the drug-likeness and oral bioavailability of stemphol compared to thapsigargin. Drug-likeness for STP was calculated and interpreted based on Lipinski's 'rule of five' [81].

	Stemphol	**Thapsigargin**
Drug-likeness		
Mass	236	650
Hydrogen bond donor	2	2
Hydrogen bond acceptors	2	12
LogP	4.173099	3.927899
Molar Refractivity	71.612572	163.786789

3.5. Discussion

Even though the investigation of caspase-dependent apoptotic cell death has so far largely contributed to advancing cytotoxic drug development, anti-apoptotic resistance mechanisms by appearing in basically all types of cancer requires the development of new anticancer agents acting at on non-canonical cell death

pathways [82]. Our results show that STP triggers CICD, a potential advantage in apoptosis-resistant cancer types. Accordingly, we report here that STP induces two different cell death modalities in leukemia cells, in a caspase-independent manner confirmed by the use of different pharmaceutical inhibitors. PARP-1 (3-AB) and cysteine cathepsin inhibitor (E64D) strengthened STP-induced cell death underlining the potential protective effect of PARP-1 and cysteine cathepsins, involved in autophagy.

Moreover, our results show that STP-induced caspase-independent apoptosis and necrosis by disrupting Ca^{2+} homeostasis of ER, cytosol and mitochondria in U-937 AML cells. As we further observed HMGB1 release from the patients with AML and ALL, these results provide a proof of concept that STP leads to release of ICD markers, an essential feature of efficient chemotherapeutic compounds [70, 83] (Fig 3.7C).

Considering that intracellular Ca^{2+} chelator BAPTA-AM completely blocked STP-induced apoptosis, cytosolic Ca^{2+} must be a key player in the cell death triggered by STP. We further identified ER as the origin of the Ca^{2+} release towards the cytosol. Nevertheless, in the presence of EGTA, STP-released Ca^{2+} is immediately depleted from the cytosol due to the temporary gradient that is established between cytosol and Ca^{2+}-chelated extracellular medium (Fig 3C). Mitochondrial Ca^{2+} overload and ROS accumulation then trigger the opening of mPTP and allow solutes of 1.5 kDa or smaller to enter mitochondria [84] leading

to mitochondrial swelling and rupture, finally inducing regulated necrosis. Cyclophilin D (CYPD) is a positive regulator of mPTP opening [85] and a pharmacological inhibitor of CYPD, CsA is used to investigate mPTP-mediated necrosis [86]. Despite this inhibitory effect on mPTP opening, CsA is also reported to have only limited effects in mitochondria with elevated Ca^{2+} concentrations [87]. When intra -mitochondrial Ca^{2+} was reduced by the MCU inhibitor Ru360, CsA became able to significantly inhibit STP-induced mPTP opening and necrosis, showing that STP contributed to mPTP-mediated necrotic cell death. This combinatory strategy allows to identify the mPTP-mediated necrosis in a situation that CsA alone is insensitive due to high Ca^{2+} concentrations. A combinatory inhibition of MCU and mPTP could potentially allow to reduce cardiac ischemia-reperfusion injury (IRI), a clinical side effect induced by persistent mPTP opening.

Besides Ca^{2+}, ROS are a critically involved in regulated necrosis, but in hematopoietic cells like Jurkat and U-937 as well as colon carcinoma HT-29 cells, programmed necrosis still occurs *via* mPTP opening in the presence of ROS scavengers [88]. These observations are in agreement with our data indicating that STP-induced cell death is independent of ROS production. Our results rather showed a decrease of ROS levels after STP treatment. Indeed, considering that mitochondria generate ROS even under physiological conditions, the STP-induced reduction of mitochondrial structure and function, as shown by TEM and OCR analysis, would at the same time lead to reduced

ROS accumulation. For this reason, we believe that Ca^{2+} modulators, able to induce programmed necrosis, could be more efficient anticancer drug candidates in leukemia, compared to ROS modulators.

Both activators and inhibitors of Ca^{2+} pumps or channels could be considered as potential anticancer agents [21]. Furthermore, despite a preferential sensitivity of cancer to Ca^{2+} modulators compared to healthy cells, extensive research efforts are required to explore unexpected side effects. SERCA is a pump that transports Ca^{2+} from the cytosol into the sarcoplasmic/endoplasmic reticulum so, inhibition of SERCA increases cytosolic Ca^{2+} levels as shown in our experiment. Therefore, SERCA appears as a potential target for anti-cancer therapy. In this context, the SERCA inhibitor G-202 (mipsagargin), a TSG derivative, already completed a dose-escalation phase I clinical trial (NCT01056029) for the treatment of advanced solid tumors. The authors used G-202 (mipsagargin), a soluble prodrug of the cytotoxic analog of TSG, 8-O-(12Aminododecanoyl)-8-O debutanoylthapsigargin (12-ADT). Results showed that the carboxypeptidase prostate-specific membrane antigen membrane antigen (PSMA) cleaves this prodrug to release TSG thus allowing specific targeting of prostate cancer [30]. Another type of TSG prodrug, G-115 is cleaved by serine protease prostate specific antigen (PSA) and allows targeted treatment of prostate cancer [31]. Considering docking results suggesting binding of STP within the TSG binding pocket of SERCA and the comparable effect of STP on Ca^{2+} release, we hypothesize here that STP could be used efficiently to target cancer. Potential

side effects of STP could also be reduced by selective targeting of cancer whether by pro-drug synthesis or targeted nano-encapsidation.

ICD is a newly proposed concept to kill cancer cells mediated by immune system activation. ICD is mediated by ′damage-associated molecular patterns' (DAMPs), and previous studies described that DAMPs trigger an efficient immune response in AML and significantly correlate with improved relapse-free survival [89]. High mobility group box 1 (HMGB1) is one representative DAMP that is released from cells undergoing mostly necrotic cell death [83, 90]. Here we reported for the first time chemotherapeutic compound-induced HMGB1 release in patients with AML and ALL. Furthermore, Ca^{2+} leakage from the ER is strongly believed to be required for ER stress, subsequent CRT exposure and ICD [91-94]. Among ER stress-related proteins, phosphorylation of eIF2α is essential for translocation of ER-resident CRT to the cell surface [95, 96] and this ecto-CRT is associated with better prognosis in AML patients by enhancing cellular immune response against tumor antigens [97].

ATF4 is an important regulator of ER stress response but it was recently identified to be activated also upon ER stress-independent mitochondrial stress [98]. Since we considered that STP induced mitochondrial stress, which subsequently triggers necrosis; ATF4 induction following STP exposure could be associated with mitochondrial stress response protein. The list of DAMPs is rapidly increasing and it recently included mitochondrial DNA and transcription

factor A [99]. Thus, mitochondrial-derived DAMPs have an excellent potential to act as potent ICD inducers and ATF4 can be used as a reliable marker for mitochondrial stress leading to ICD in the future.

Unlike TSG that was shown to induce HMGB1 release only in combination with cisplatin [100], STP was able to trigger HMGB1 release independently of any co-treatment. Considering STP-induced upregulation of phospho-eIF2α and ATF4 as well as HMGB1 release, STP could act as an excellent ICD inducer, which will be investigated in detail in future studies.

Finally, the *in silico* analysis suggested that STP has advantageous properties for drug development compared to TSG, so far only used as a prodrug. Indeed, STP complied better with Lipinski's 'rule of five', a well-known tool for the investigation of drug-likeness.

STP is a so far undescribed *in vitro* and *in vivo* Ca^{2+} modulator able to trigger non-canonical Ca^{2+}-dependent cell death modalities in cancer. The differential Ca^{2+} sensitivity of tumors and normal cells enable Ca^{2+} modulators to specifically target cancer and non-canonical cell death modalities induced by STP are advantageous to overcome apoptosis-resistant cancer types alone or in combination with other chemotherapeutic compounds.

References

[1] D. Hanahan, R.A. Weinberg, Hallmarks of cancer: the next generation, Cell, 144 (2011) 646-674.

[2] J.C. Barrett, Mechanisms of multistep carcinogenesis and carcinogen risk assessment, Environmental health perspectives, 100 (1993) 9-20.

[3] S. Ji, B. Orlikova, M. Diederich, Non-edible plants as an attractive source of compounds with chemopreventive potential, J Cancer Prev, 19 (2014) 1-6.

[4] D.J. Newman, G.M. Cragg, Natural products as sources of new drugs over the 30 years from 1981 to 2010, Journal of natural products, 75 (2012) 311-335.

[5] L.M. Coussens, Z. Werb, Inflammation and cancer, Nature, 420 (2002) 860-867.

[6] S. Ghosh, M. Karin, Missing pieces in the NF-kappaB puzzle, Cell, 109 Suppl (2002) S81-96.

[7] M. Karin, Y. Ben-Neriah, Phosphorylation meets ubiquitination: the control of NF-[kappa]B activity, Annu Rev Immunol, 18 (2000) 621-663.

[8] T. Lawrence, The nuclear factor NF-kappaB pathway in inflammation, Cold Spring Harb Perspect Biol, 1 (2009) a001651.

[9] T.D. Gilmore, Introduction to NF-kappaB: players, pathways, perspectives, Oncogene, 25 (2006) 6680-6684.

[10] P.J. Jost, J. Ruland, Aberrant NF-kappaB signaling in lymphoma: mechanisms, consequences, and therapeutic implications, Blood, 109 (2007) 2700-2707.

[11] J.P. Monk, G. Phillips, R. Waite, J. Kuhn, L.J. Schaaf, G.A. Otterson, D. Guttridge, C. Rhoades, M. Shah, T. Criswell, M.A. Caligiuri, M.A. Villalona-Calero, Assessment of tumor necrosis factor alpha blockade as an intervention to improve tolerability of dose-intensive chemotherapy in cancer patients, J Clin Oncol, 24 (2006) 1852-1859.

[12] M.A. Calzado, S. Bacher, M.L. Schmitz, NF-kappaB inhibitors for the treatment of inflammatory diseases and cancer, Curr Med Chem, 14 (2007) 367-376.

[13] T.D. Gilmore, M. Herscovitch, Inhibitors of NF-kappaB signaling: 785 and counting, Oncogene, 25 (2006) 6887-6899.

[14] E. Niederberger, G. Geisslinger, The IKK-NF-kappaB pathway: a source for novel molecular drug targets in pain therapy?, FASEB J, 22 (2008) 3432-3442.

[15] M. Karin, Y. Yamamoto, Q.M. Wang, The IKK NF-kappa B system: a treasure trove for drug development, Nat Rev Drug Discov, 3 (2004) 17-26.

[16] K.W. McIntyre, D.J. Shuster, K.M. Gillooly, D.M. Dambach, M.A. Pattoli, P. Lu, X.D. Zhou, Y. Qiu, F.C. Zusi, J.R. Burke, A highly selective inhibitor of I kappa B kinase, BMS-345541, blocks both joint inflammation and destruction in collagen-induced arthritis in mice, Arthritis Rheum, 48 (2003) 2652-2659.

[17] A. Field-Smith, G.J. Morgan, F.E. Davies, Bortezomib (Velcadetrade mark) in the Treatment of Multiple Myeloma, Ther Clin Risk Manag, 2 (2006) 271-279.

[18] M. Brini, T. Cali, D. Ottolini, E. Carafoli, Intracellular calcium homeostasis and signaling, Met Ions Life Sci, 12 (2013) 119-168.

[19] F. Bronner, Extracellular and intracellular regulation of calcium homeostasis, ScientificWorldJournal, 1 (2001) 919-925.

[20] M. Brini, D. Ottolini, T. Cali, E. Carafoli, Calcium in health and disease, Met Ions Life Sci, 13 (2013) 81-137.

[21] G.R. Monteith, D. McAndrew, H.M. Faddy, S.J. Roberts-Thomson, Calcium and cancer: targeting Ca2+ transport, Nat Rev Cancer, 7 (2007) 519-530.

[22] B.L. Schwab, D. Guerini, C. Didszun, D. Bano, E. Ferrando-May, E. Fava, J. Tam, D. Xu, S. Xanthoudakis, D.W. Nicholson, E. Carafoli, P. Nicotera, Cleavage of plasma membrane calcium pumps by caspases: a link between apoptosis and necrosis, Cell Death Differ, 9 (2002) 818-831.

[23] P. Pinton, R. Rizzuto, Bcl-2 and Ca2+ homeostasis in the endoplasmic reticulum, Cell Death Differ, 13 (2006) 1409-1418.

[24] F. Zhong, M.C. Davis, K.S. McColl, C.W. Distelhorst, Bcl-2 differentially regulates Ca2+ signals according to the strength of T cell receptor activation, J Cell Biol, 172 (2006) 127-137.

[25] V. Prasad, G.P. Boivin, M.L. Miller, L.H. Liu, C.R. Erwin, B.W. Warner, G.E. Shull, Haploinsufficiency of Atp2a2, encoding the sarco(endo)plasmic reticulum Ca2+-ATPase isoform 2 Ca2+ pump, predisposes mice to squamous

cell tumors via a novel mode of cancer susceptibility, Cancer Res, 65 (2005) 8655-8661.

[26] N. Gomez-Ospina, F. Tsuruta, O. Barreto-Chang, L. Hu, R. Dolmetsch, The C terminus of the L-type voltage-gated calcium channel Ca(V)1.2 encodes a transcription factor, Cell, 127 (2006) 591-606.

[27] T. Vanden Berghe, A. Linkermann, S. Jouan-Lanhouet, H. Walczak, P. Vandenabeele, Regulated necrosis: the expanding network of non-apoptotic cell death pathways, Nat Rev Mol Cell Biol, 15 (2014) 135-147.

[28] D. Lee, I.Y. Kim, S. Saha, K.S. Choi, Paraptosis in the anti-cancer arsenal of natural products, Pharmacol Ther, 162 (2016) 120-133.

[29] W.J. Lee, S.J. Roberts-Thomson, G.R. Monteith, Plasma membrane calcium-ATPase 2 and 4 in human breast cancer cell lines, Biochem Biophys Res Commun, 337 (2005) 779-783.

[30] S.R. Denmeade, A.M. Mhaka, D.M. Rosen, W.N. Brennen, S. Dalrymple, I. Dach, C. Olesen, B. Gurel, A.M. Demarzo, G. Wilding, M.A. Carducci, C.A. Dionne, J.V. Moller, P. Nissen, S.B. Christensen, J.T. Isaacs, Engineering a prostate-specific membrane antigen-activated tumor endothelial cell prodrug for cancer therapy, Sci Transl Med, 4 (2012) 140ra186.

[31] S.R. Denmeade, C.M. Jakobsen, S. Janssen, S.R. Khan, E.S. Garrett, H. Lilja, S.B. Christensen, J.T. Isaacs, Prostate-specific antigen-activated thapsigargin prodrug as targeted therapy for prostate cancer, J Natl Cancer Inst, 95 (2003) 990-1000.

[32] C. Cardenas, M. Muller, A. McNeal, A. Lovy, F. Jana, G. Bustos, F. Urra, N. Smith, J. Molgo, J.A. Diehl, T.W. Ridky, J.K. Foskett, Selective Vulnerability of Cancer Cells by Inhibition of Ca(2+) Transfer from Endoplasmic Reticulum to Mitochondria, Cell Rep, 14 (2016) 2313-2324.

[33] E.R. Fearon, B. Vogelstein, A genetic model for colorectal tumorigenesis, Cell, 61 (1990) 759-767.

[34] T. Dorai, B.B. Aggarwal, Role of chemopreventive agents in cancer therapy, Cancer letters, 215 (2004) 129-140.

[35] M. Karin, B. Mintz, Receptor-mediated endocytosis of transferrin in developmentally totipotent mouse teratocarcinoma stem cells, The Journal of biological chemistry, 256 (1981) 3245-3252.

[36] H. Lai, N.P. Singh, Oral artemisinin prevents and delays the development of 7,12-dimethylbenz[a]anthracene (DMBA)-induced breast cancer in the rat, Cancer letters, 231 (2006) 43-48.

[37] S.K. Manna, Y.P. Gad, A. Mukhopadhyay, B.B. Aggarwal, Suppression of tumor necrosis factor-activated nuclear transcription factor-kappaB, activator protein-1, c-Jun N-terminal kinase, and apoptosis by beta-lapachone, Biochemical pharmacology, 57 (1999) 763-774.

[38] P.A. Jones, S.B. Baylin, The epigenomics of cancer, Cell, 128 (2007) 683-692.

[39] Y. Cui, C. Lu, L. Liu, D. Sun, N. Yao, S. Tan, S. Bai, X. Ma, Reactivation of methylation-silenced tumor suppressor gene p16INK4a by

nordihydroguaiaretic acid and its implication in G1 cell cycle arrest, Life sciences, 82 (2008) 247-255.

[40] H.M. Byun, S.H. Choi, P.W. Laird, B. Trinh, M.A. Siddiqui, V.E. Marquez, A.S. Yang, 2'-Deoxy-N4-[2-(4-nitrophenyl)ethoxycarbonyl]-5-azacytidine: a novel inhibitor of DNA methyltransferase that requires activation by human carboxylesterase 1, Cancer letters, 266 (2008) 238-248.

[41] N.K. Sah, Z. Khan, G.J. Khan, P.S. Bisen, Structural, functional and therapeutic biology of survivin, Cancer letters, 244 (2006) 164-171.

[42] O. Warburg, On the origin of cancer cells, Science, 123 (1956) 309-314.

[43] W. Li, J. Liu, Y. Zhao, PKM2 inhibitor shikonin suppresses TPA-induced mitochondrial malfunction and proliferation of skin epidermal JB6 cells, Molecular carcinogenesis, (2012).

[44] G. Aviello, B. Romano, F. Borrelli, R. Capasso, L. Gallo, F. Piscitelli, V. Di Marzo, A.A. Izzo, Chemopreventive effect of the non-psychotropic phytocannabinoid cannabidiol on experimental colon cancer, Journal of molecular medicine, 90 (2012) 925-934.

[45] X. Wu, S. Patterson, E. Hawk, Chemoprevention--history and general principles, Best practice & research. Clinical gastroenterology, 25 (2011) 445-459.

[46] G.M. König, S. Kehraus, S.F. Seibert, A. Abdel-Lateff, D. Müller, Natural products from marine organisms and their associated microbes, ChemBioChem, 7 (2006) 229-238.

[47] M. Schnekenburger, M. Dicato, M. Diederich, Epigenetic modulators from “The Big Blue”: A treasure to fight against cancer, Cancer letters, 351 (2014) 182-197.

[48] A.H. Aly, A. Debbab, C. Clements, R. Edrada-Ebel, B. Orlikova, M. Diederich, V. Wray, W. Lin, P. Proksch, NF kappa B inhibitors and antitrypanosomal metabolites from endophytic fungus Penicillium sp. isolated from Limonium tubiflorum, Bioorganic & medicinal chemistry, 19 (2011) 414-421.

[49] A. Panwalkar, S. Verstovsek, F. Giles, Nuclear factor-kappaB modulation as a therapeutic approach in hematologic malignancies, Cancer, 100 (2004) 1578-1589.

[50] F.E. Chen, D.B. Huang, Y.Q. Chen, G. Ghosh, Crystal structure of p50/p65 heterodimer of transcription factor NF-kappaB bound to DNA, Nature, 391 (1998) 410-413.

[51] B. Orlikova, D. Tasdemir, F. Golais, M. Dicato, M. Diederich, The aromatic ketone 4'-hydroxychalcone inhibits TNFalpha-induced NF-kappaB activation via proteasome inhibition, Biochemical pharmacology, 82 (2011) 620-631.

[52] B.B. Aggarwal, P. Gehlot, Inflammation and cancer: how friendly is the relationship for cancer patients?, Current opinion in pharmacology, 9 (2009) 351-369.

[53] A. Mantovani, P. Allavena, A. Sica, F. Balkwill, Cancer-related inflammation, Nature, 454 (2008) 436-444.

[54] S. Hajjouli, S. Chateauvieux, M.H. Teiten, B. Orlikova, M. Schumacher, M. Dicato, C.Y. Choo, M. Diederich, Eurycomanone and eurycomanol from Eurycoma longifolia Jack as regulators of signaling pathways involved in proliferation, cell death and inflammation, Molecules (Basel, Switzerland), 19 (2014) 14649-14666.

[55] B. Orlikova, N. Legrand, J. Panning, M. Dicato, M. Diederich, Anti-inflammatory and anticancer drugs from nature, Cancer treatment and research, 159 (2014) 123-143.

[56] I.E. Orhan, M. Kartal, A.R. Gulpinar, G. Yetkin, B. Orlikova, M. Diederich, D. Tasdemir, Inhibitory effect of St. Johns Wort oil macerates on TNFalpha-induced NF-kappaB activation and their fatty acid composition, Journal of ethnopharmacology, 155 (2014) 1086-1092.

[57] B. Orlikova, M. Schumacher, T. Juncker, C.C. Yan, S.H. Inayat-Hussain, S. Hajjouli, C. Cerella, M. Dicato, M. Diederich, Styryl-lactone goniothalamin inhibits TNF-alpha-induced NF-kappaB activation, Food and chemical toxicology : an international journal published for the British Industrial Biological Research Association, 59 (2013) 572-578.

[58] W. Ebrahim, A.H. Aly, V. Wray, A. Mandi, M.H. Teiten, F. Gaascht, B. Orlikova, M.U. Kassack, W. Lin, M. Diederich, T. Kurtan, A. Debbab, P. Proksch, Embellicines A and B: absolute configuration and NF-kappaB transcriptional inhibitory activity, Journal of medicinal chemistry, 56 (2013) 2991-2999.

[59] S. Safe, A. Taylor, Sporidesmins. Part XI. The reaction of triphenylphosphine with epipolythiodioxopiperazines, Journal of the Chemical Society C: Organic, (1971) 1189-1192.

[60] M.S.C. Pedras, S.R. Abrams, G. Séguin-Swartz, Isolation of the first naturally occurring epimonothiodioxopiperazine, a fungal toxin produced by phoma lingam, Tetrahedron Letters, 29 (1988) 3471-3474.

[61] H.M. Herath, M. Jacob, A.D. Wilson, H.K. Abbas, N.P. Nanayakkara, New secondary metabolites from bioactive extracts of the fungus Armillaria tabescens, Nat Prod Res, 27 (2013) 1562-1568.

[62] F.H. Igney, P.H. Krammer, Death and anti-death: tumour resistance to apoptosis, Nat Rev Cancer, 2 (2002) 277-288.

[63] M. Diederich, C. Cerella, Non-canonical programmed cell death mechanisms triggered by natural compounds, Semin Cancer Biol, 40-41 (2016) 4-34.

[64] W.X. Zong, C.B. Thompson, Necrotic death as a cell fate, Genes Dev, 20 (2006) 1-15.

[65] C. Cerella, M. Diederich, L. Ghibelli, The dual role of calcium as messenger and stressor in cell damage, death, and survival, Int J Cell Biol, 2010 (2010) 546163.

[66] A. Halestrap, Biochemistry: a pore way to die, Nature, 434 (2005) 578-579.

[67] M.W. Harr, C.W. Distelhorst, Apoptosis and autophagy: decoding calcium signals that mediate life or death, Cold Spring Harb Perspect Biol, 2 (2010) a005579.

[68] E. Kania, B. Pajak, A. Orzechowski, Calcium homeostasis and ER stress in control of autophagy in cancer cells, Biomed Res Int, 2015 (2015) 352794.

[69] D.R. Green, T. Ferguson, L. Zitvogel, G. Kroemer, Immunogenic and tolerogenic cell death, Nat Rev Immunol, 9 (2009) 353-363.

[70] G. Kroemer, L. Galluzzi, O. Kepp, L. Zitvogel, Immunogenic cell death in cancer therapy, Annu Rev Immunol, 31 (2013) 51-72.

[71] S. Marumo, H. Hattori, M. Katayama, Stemphol from Pleospora-Herbarum as a Self-Inhibitor, Agr Biol Chem Tokyo, 49 (1985) 1521-1522.

[72] C. Florean, M. Schnekenburger, J.Y. Lee, K.R. Kim, A. Mazumder, S. Song, J.M. Kim, C. Grandjenette, J.G. Kim, A.Y. Yoon, M. Dicato, K.W. Kim, C. Christov, B.W. Han, P. Proksch, M. Diederich, Discovery and characterization of Isofistularin-3, a marine brominated alkaloid, as a new DNA demethylating agent inducing cell cycle arrest and sensitization to TRAIL in cancer cells, Oncotarget, 7 (2016) 24027-24049.

[73] C. Cerella, S. Cordisco, M.C. Albertini, A. Accorsi, M. Diederich, L. Ghibelli, Magnetic fields promote a pro-survival non-capacitative Ca2+ entry via phospholipase C signaling, Int J Biochem Cell Biol, 43 (2011) 393-400.

[74] A.W. Schuttelkopf, D.M. van Aalten, PRODRG: a tool for high-throughput crystallography of protein-ligand complexes, Acta crystallographica. Section D, Biological crystallography, 60 (2004) 1355-1363.

[75] A. Lemarie, D. Lagadic-Gossmann, C. Morzadec, N. Allain, O. Fardel, L. Vernhet, Cadmium induces caspase-independent apoptosis in liver Hep3B cells: role for calcium in signaling oxidative stress-related impairment of mitochondria and relocation of endonuclease G and apoptosis-inducing factor, Free Radic Biol Med, 36 (2004) 1517-1531.

[76] D. Mekahli, G. Bultynck, J.B. Parys, H. De Smedt, L. Missiaen, Endoplasmic-reticulum calcium depletion and disease, Cold Spring Harb Perspect Biol, 3 (2011).

[77] O. Trott, A.J. Olson, AutoDock Vina: improving the speed and accuracy of docking with a new scoring function, efficient optimization, and multithreading, J Comput Chem, 31 (2010) 455-461.

[78] Y. Sagara, G. Inesi, Inhibition of the sarcoplasmic reticulum Ca2+ transport ATPase by thapsigargin at subnanomolar concentrations, The Journal of biological chemistry, 266 (1991) 13503-13506.

[79] C. Toyoshima, H. Nomura, Structural changes in the calcium pump accompanying the dissociation of calcium, Nature, 418 (2002) 605-611.

[80] O. von Ahsen, C. Renken, G. Perkins, R.M. Kluck, E. Bossy-Wetzel, D.D. Newmeyer, Preservation of mitochondrial structure and function after Bid- or Bax-mediated cytochrome c release, J Cell Biol, 150 (2000) 1027-1036.

[81] C.A. Lipinski, F. Lombardo, B.W. Dominy, P.J. Feeney, Experimental and computational approaches to estimate solubility and permeability in drug discovery and development settings, Adv Drug Deliv Rev, 46 (2001) 3-26.

[82] Y. Pommier, O. Sordet, S. Antony, R.L. Hayward, K.W. Kohn, Apoptosis defects and chemotherapy resistance: molecular interaction maps and networks, Oncogene, 23 (2004) 2934-2949.

[83] L. Galluzzi, A. Buque, O. Kepp, L. Zitvogel, G. Kroemer, Immunogenic cell death in cancer and infectious disease, Nat Rev Immunol, 17 (2017) 97-111.

[84] R.A. Haworth, D.R. Hunter, The Ca2+-induced membrane transition in mitochondria. II. Nature of the Ca2+ trigger site, Arch Biochem Biophys, 195 (1979) 460-467.

[85] T. Miura, M. Tanno, The mPTP and its regulatory proteins: final common targets of signalling pathways for protection against necrosis, Cardiovasc Res, 94 (2012) 181-189.

[86] A.P. Halestrap, C.P. Connern, E.J. Griffiths, P.M. Kerr, Cyclosporin A binding to mitochondrial cyclophilin inhibits the permeability transition pore and protects hearts from ischaemia/reperfusion injury, Mol Cell Biochem, 174 (1997) 167-172.

[87] N. Brustovetsky, J.M. Dubinsky, Limitations of cyclosporin A inhibition of the permeability transition in CNS mitochondria, J Neurosci, 20 (2000) 8229-8237.

[88] D. Moquin, F.K. Chan, The molecular regulation of programmed necrotic cell injury, Trends Biochem Sci, 35 (2010) 434-441.

[89] J. Fucikova, I. Truxova, M. Hensler, E. Becht, L. Kasikova, I. Moserova, S. Vosahlikova, J. Klouckova, S.E. Church, I. Cremer, O. Kepp, G. Kroemer, L. Galluzzi, C. Salek, R. Spisek, Calreticulin exposure by malignant blasts correlates with robust anticancer immunity and improved clinical outcome in AML patients, Blood, 128 (2016) 3113-3124.

[90] O. Krysko, T. Love Aaes, C. Bachert, P. Vandenabeele, D.V. Krysko, Many faces of DAMPs in cancer therapy, Cell Death Dis, 4 (2013) e631.

[91] S. Gebremeskel, B. Johnston, Concepts and mechanisms underlying chemotherapy induced immunogenic cell death: impact on clinical studies and considerations for combined therapies, Oncotarget, 6 (2015) 41600-41619.

[92] A.D. Garg, D.V. Krysko, T. Verfaillie, A. Kaczmarek, G.B. Ferreira, T. Marysael, N. Rubio, M. Firczuk, C. Mathieu, A.J. Roebroek, W. Annaert, J. Golab, P. de Witte, P. Vandenabeele, P. Agostinis, A novel pathway combining calreticulin exposure and ATP secretion in immunogenic cancer cell death, EMBO J, 31 (2012) 1062-1079.

[93] L. Menger, E. Vacchelli, S. Adjemian, I. Martins, Y. Ma, S. Shen, T. Yamazaki, A.Q. Sukkurwala, M. Michaud, G. Mignot, F. Schlemmer, E. Sulpice, C. Locher, X. Gidrol, F. Ghiringhelli, N. Modjtahedi, L. Galluzzi, F. Andre, L. Zitvogel, O. Kepp, G. Kroemer, Cardiac glycosides exert anticancer effects by inducing immunogenic cell death, Sci Transl Med, 4 (2012) 143ra199.

[94] R. Tufi, T. Panaretakis, K. Bianchi, A. Criollo, B. Fazi, F. Di Sano, A. Tesniere, O. Kepp, P. Paterlini-Brechot, L. Zitvogel, M. Piacentini, G. Szabadkai, G. Kroemer, Reduction of endoplasmic reticulum Ca2+ levels favors plasma membrane surface exposure of calreticulin, Cell Death Differ, 15 (2008) 274-282.

[95] T. Panaretakis, N. Joza, N. Modjtahedi, A. Tesniere, I. Vitale, M. Durchschlag, G.M. Fimia, O. Kepp, M. Piacentini, K.U. Froehlich, P. van Endert, L. Zitvogel, F. Madeo, G. Kroemer, The co-translocation of ERp57 and calreticulin determines the immunogenicity of cell death, Cell Death Differ, 15 (2008) 1499-1509.

[96] T. Panaretakis, O. Kepp, U. Brockmeier, A. Tesniere, A.C. Bjorklund, D.C. Chapman, M. Durchschlag, N. Joza, G. Pierron, P. van Endert, J. Yuan, L. Zitvogel, F. Madeo, D.B. Williams, G. Kroemer, Mechanisms of pre-apoptotic calreticulin exposure in immunogenic cell death, EMBO J, 28 (2009) 578-590.

[97] M. Wemeau, O. Kepp, A. Tesniere, T. Panaretakis, C. Flament, S. De Botton, L. Zitvogel, G. Kroemer, N. Chaput, Calreticulin exposure on malignant blasts predicts a cellular anticancer immune response in patients with acute myeloid leukemia, Cell Death Dis, 1 (2010) e104.

[98] P.M. Quiros, M.A. Prado, N. Zamboni, D. D'Amico, R.W. Williams, D. Finley, S.P. Gygi, J. Auwerx, Multi-omics analysis identifies ATF4 as a key regulator of the mitochondrial stress response in mammals, J Cell Biol, 216 (2017) 2027-2045.

[99] W. Hou, Q. Zhang, Z. Yan, R. Chen, H.J. Zeh Iii, R. Kang, M.T. Lotze, D. Tang, Strange attractors: DAMPs and autophagy link tumor cell death and immunity, Cell Death Dis, 4 (2013) e966.

[100] I. Martins, O. Kepp, F. Schlemmer, S. Adjemian, M. Tailler, S. Shen, M. Michaud, L. Menger, A. Gdoura, N. Tajeddine, A. Tesniere, L. Zitvogel, G. Kroemer, Restoration of the immunogenicity of cisplatin-induced cancer cell death by endoplasmic reticulum stress, Oncogene, 30 (2011) 1147-1158.

Abstract in Korean (국문초록)

병원균의 감염이나 상처등이 발생했을 때 chemokine 이나 cytokine 은 leukocyte 의 이동을 유도하여 염증 반응을 일으킨다. 이러한 염증 반응은 외부 유래의 병원균이나 상처등으로부터 우리 몸을 보호하는데 유용한 역할을 하지만 한편으로는 암의 발생과 성장을 촉진하기도 한다. 염증반응은 성장 인자, 항사멸 단백질 (anti-apoptotic factors), extracellular-matrix-modifying enzymes 들을 과발현 시킴으로써 종양 세포의 비정상적인 성장과 전이를 촉진하는 등 종양미세환경을 구축하는데 이바지 한다. 이러한 특징으로 인해, 염증은 종양 발생의 중요한 인자로 인식되고 있다.

NK-kB 는 염증 반응 신호전달의 핵심 조절자이다. 자극 인자의 종류에 따라서 신호 전달 양상에 변화가 생기는데 각기 다른 NK-kB 신호전달 체계에 대해서 심도 있는 연구가 진행되어 왔다. Canonical NK-kB 신호 체계는 미생물 감염이나 IL-1, TNFα와 같은 proinflammatory cytokine 들에 의해서 활성화된다. 신호 전달 체계에 의해서 IKK 복합체와 IκB 의 인산화가 일어나고, 프로테아좀에 의한 IκB 의 분해가 시작된다. 마지막으로 IκB 에 의한 억제가 사라진 p65/p50 복합체는 핵 내로 이동하고

proinflammation과 관련된 많은 인자들을 전사하게 된다. 이에 반해, Alternative NK-kB 신호 체계는 TNFα 대신, lymphotoxin b (TNFSF3), CD40 ligand (CD40L and TNFSF5), cell activating factor (BAFF and TNFSF13B) 등에 의해 활성화되게 된다. 이어서 NIK (NF-κB-inducing kinase)에 의해 IKKα 복합체, p100의 인산화가 순차적으로 일어나고 최종적으로 p52-RelB 복합체가 proinflammation 관련 인자들의 발현에 관여하게 된다.

인간의 몸에서 가장 흔한 미네랄 이온인 칼슘은 인간의 생명 현상을 이어가기 위해서 필요한 다양한 생리학적, 생화학적 반응에 관여한다. 이를테면, secondary messenger로써 근육 수축, 신경 전도, 호르몬 방출, 혈액 응고를 직·간접적으로 조절하는데 필수적인 역할을 수행한다. 따라서, 칼슘 이온은 항상 일정한 농도로 유지되어야 하며 보통 혈장 내 2.5 mM (오차범위≤ 20%), 세포 외 공간 (extracellular space)에 1.2 mM, 세포 내에는 50 에서 100 nM 사이로 항상성을 유지하고 있다.

이렇게 인간의 생명 현상을 위하여 필수적인 역할을 하는 칼슘 이온은 그 항상성이 깨질 경우 신호 전달 체계의 교란을 가져오고 결국 세포 사멸을 일으킨다. 소포체와 미토콘드리아는 세포 내 칼슘 이온을 조절하는데 중추적인 역할을 하는 세포 소기관으로 세포

사멸과 밀접한 관련이 있다. 소포체는 세포 소기관중 가장 큰 칼슘 이온의 저장고 역할을 하며, 평상시 100-500 nM 의 칼슘 농도를 유지하고 있다. 특히 소포체 내 칼슘 이온의 항상성에 문제가 생기면 단백질 접힘에 결함이 발생하고 이는 곧 caspase 와 calpain 의존적인 세포사멸을 일으키게 된다. 특히 최근 연구에 따르면, 소포체 내 칼슘의 불균형은 미토콘드리아의 칼슘 유입에 영향을 주고 그 정도가 심해지게 되면 non-canonical 세포사멸이 일어나게 된다. mPTP (mitochondrial permeability transition pore)-의존적 necrosis 는 미토콘드리아 내 칼슘이온의 과부하로 일어나는 대표적인 non-canonical 세포사멸이다. 그 과정을 간단히 살펴보면, 소포체 스트레스에 의해 소포체의 칼슘 이온이 미토콘드리아의 칼슘 과부하를 촉진하고 mPTP 개방을 유도하게 된다. 개방된 틈 사이로 1.5 kDa 이하의 용질이 유입되면서 미토콘드리아의 물리적 구조가 파괴되고, 결국 programmed necrosis 를 일으키게 되는 것이다. 최근 연구에 의하면, 종양 세포의 미토콘드리아는 정상 세포에 비하여 높은 칼슘 이온 농도를 유지하고 있고 특히 소포체와 미토콘드리아내 활발한 칼슘의 이동이 있음이 규명됨으로써, 종양 세포의 생존과 칼슘 의존성에 관한 흥미로운 연관성을 제공하고 있다.

여러 의·과학의 기술적 진보에도 불구하고, 여전히 암의 완치는 인류가 극복해나가야 난제 중 하나이다. World Cancer Research Fund International 의 보고서에 따르면, 2035 년에는 2 천 4 백만명 정도의 암환자가 발생할 것으로 예상되고 있다. 이와 관련, 본 연구는 효율적인 암 치료 방법을 제시하고 실질적인 항암제 개발에 기여하기 위하여, 종양 세포의 생존에 중요한 역할을 하는 NF-kB 와 칼슘이온을 타겟으로 하는 천연물 유래 물질들의 항암효과와 기전을 연구하였다.

먼저, gliotoxin 의 NF-kB 저해 효과를 규명하였던 기존 연구를 바탕으로 gliotoxin 유도체들의 항 NF-kB 효과를 확인하였다. 4 가지 다른 유도체 중 3 가지에서 효율적인 NF-kB 저해 효과를 확인하였고 가장 강력한 효과를 나타낸 6-acetylmonodethiogliotoxin 을 중심으로 관련 기작을 연구하였다. TNF-α를 이용하여 NF-kB 활성화를 유도하였고, p65 의 DNA binding affinity 저해효과를 관찰함으로써 6-acetylmonodethiogliotoxin 의 target 을 명확히 규명할 수 있었다.

또 다른 천연물인 Stemphol (STP)은 암 세포에 작용하여 apoptosis 및 necrosis 세포 사멸을 동시에 유발하는 식물유래 천연물질이다. 특히 백혈병 중에서 만성 골수성 백혈병 (CML)에 비해 환자의

예후가 좋지 못한 급성 골수성 백혈병 (AML)를 종양 모델로 하여 기작 연구를 진행하였다. 이를 통하여, STP 가 thapsigargin 과 유사하게 세포질 내 Ca^{2+} 레벨을 증가시킴을 관찰하였고, 이는 apoptosis 의 중요한 원인임을 규명하였다. 특히, STP 가 일으키는 또 다른 세포사멸 형태인 necrosis 와 관련하여, 미토콘드리아의 Ca^{2+} 과부하가 그 원인임을 구명하였고, 이는 mitochondrial permeability transition pore (mPTP)의 개방에 의존한다는 것을 입증하였다. 마지막으로, STP 가 처리 된 AML 환자 세포에서 면역원성 세포 사멸의 중요한 지표자인 HMGB1 의 방출을 관찰함으로써 이 천연물의 면역원성 세포사멸 및 중계연구의 가능성을 제시하였다.

본 연구를 통해 NF-kB 와 칼슘 이온이 암 치료의 효과적인 타겟이 될 수 있음을 증명하였고, 연구에 사용된 천연물들의 구조와 기능에 대한 추가적인 연구가 동반된다면 항암제 치료제 개발에 이바지 할 수 있을 것으로 기대된다.

Keywords (주요어)

천연물, 세포 사멸, NF-kB, 칼슘, 암, 백혈병, 면역원성 세포사멸

학 번 : 2013-23471